

**Theoretical Study on
Some Inter- and Intra-Molecular Interactions**

Dissertation

zur Erlangung des Grades eines Doktors
der Naturwissenschaften,

vorgelegt von

Hongjun Fan, M. Sc.

geb. am 21. Juli 1972 in Jiajiang, Sichuan, V. R. China,

eingereicht beim Fachbereich 8

der Universität Siegen,

Siegen 2004

Erster Gutachter: Prof. Dr. W.H.E. Schwarz

Zweiter Gutachter: Prof. Dr. M. Albrecht

Tag der mündlichen Prüfung: September 15, 2004

urn:nbn:de:hbz:467-815

Abstract:

Theoretical studies on some intra- and inter-molecular weak interactions

Ab-initio MP2&CI and DF calculations were used to study some chemical topics that involve inter- and intra-molecular so-called weak interactions. These topics include: i) What is the physical origin of the *single bond rotational barrier*, e.g. of ethane? Our answer is that the kinetic Pauli repulsion between CH bond pairs is much more important than hyperconjugative attraction of CH bond pairs through virtual CH σ^* orbitals. ii) What is the physical origin of the *bond length expansion* of electron-rich main-group molecules, e.g. F₂ etc.? It is here dominantly explained by inter-atomic lone pair repulsion, with possible contributions also from atomic hybridization effects of the bonding AOs. The importance of the tails of the lone pairs is stressed. iii) What is the physical origin of *reduced nonbonded interatomic separations*? We found that most so-called reduced distances in the literature are simply due to the contraction of positively charged atoms. If the ubiquitous charge dependence of effective atomic radii is accounted for, a few really reduced distances survive. They are caused by specific orbital interactions of heavy nonmetal atoms, by specific charge attractions or by clamping bridges. iiiii) What is the origin of the different *orientations of fluorescence of dye molecules in zeolite channels*? Oxonine was studied. We can explain the results of single molecule fluorescence microscopy. Correct van der Waals radii, silica - dye molecule - attractions and rotation of the optical transition moment due to orbital interactions are more important than the electrostatic Stark effect.

Zusammenfassung:

Theoretische Studien an intra- und inter-molekularen Schwachen Wechselwirkungen

Ab-initio-MP2&CI- und DF-Rechnungen wurden zur Untersuchung einiger chemischer Problem benutzt, die mit den sogenannten inter- und intra-molekularen Schwachen Wechselwirkungen zusammenhängen. i) Was ist die physikalische Ursache der *Einfachbindungs-Rotationsbarriere*, z.B. von Ethan? Unsere Antwort ist, dass die kinetische Pauli-Abstoßung zwischen CH-Bindungspaaren viel wichtiger ist als die hyperkonjugative Anziehung von CH-Bindungspaaren über virtuelle CH- σ^* -Orbitale. ii) Was ist die physikalische Ursache der *Bindungslängen-Dehnung* bei elektronenreichen Hauptgruppen-Molekülen wie z.B. F₂ usw.? Wir geben eine begründete Erklärung durch interatomare Abstoßung von Einsamen Paaren, möglicherweise verstärkt durch Hybridisierungseffekte der Bindungs-AOs. Die rückwärtigen Schwänze der Einsamen Paare sind besonders relevant. iii) Was ist die physikalische Ursache der *verkürzten nichtbindenden Atomabstände*? Wir fanden, dass die meisten sogenannten verkürzten Abstände in der Literatur auf Vernachlässigung der Verkleinerung der Radien von positiv geladenen Atomen beruhen. Wenn die generelle Ladungsabhängigkeit der effektiven Atomradien mitberücksichtigt wird, bleiben einige wenige echt verkürzte Abstände übrig. Sie sind durch spezifische Orbitalwechselwirkungen schwerer Nichtmetallatome, durch starke Ladungs-Anziehungen oder durch klammernde Brücken verursacht. iiiii) Was bedingt die unterschiedlichen *Fluoreszenz-Orientierungen von Farbstoffmolekülen in Zeolith-Kanälen*? Oxonin wurde studiert. Wir erklären die Ergebnisse der Einzelmolekül-Fluoreszenzmikroskopie durch Verwendung korrekter van der Waals-Radien, durch Silikat-Farbstoff-Anziehungen und durch die Drehung des optischen Übergangsmoments wegen Orbitalwechselwirkungen. Der Starkeffekt in den Kanälen spielt keine Rolle.

Acknowledgements

First, I want to express my deep gratitude to Prof. Dr. W. H. Eugen Schwarz, my doctor supervisor, for his excellent guidance of my PhD work and his kind help of my life in Siegen.

I am very grateful to Prof. Dr. Shuguang Wang for the very helpful discussions and some collaboration in Shanghai.

I would like to thank Prof. Dr. G. Calzaferri, Prof. Dr. A. J. Meixner, and Dr. C. Debus for the constructive discussions and for the additional experimental and numerical details on the topic of dye molecules in zeolite; I also thank Dr. Jier Schwarz-Niu for the preliminary works on the transition dipole moment of oxonine.

I thank Prof. Dr. B. Engelen and Dr. M. Panthöfer for the helpful discussions and on the experimental details, in particular those prior to publication, on the topic of reduced nonbonded distances.

And I thank Prof. Dr. A. Maercker for the constructive suggestions drawing our attention to the hot topic of the rotational barrier of ethane.

I would like to thank Dr. Holger Poggel for his assistance with the computers and software, and Mrs. Petra Schöppner, Mrs. Doris Spiller and Mrs. Erika Stei for their assistance concerning administrative and bureaucratic affairs.

I gratefully acknowledge financial supports by Universität Siegen and by Deutsche Forschungs-Gemeinschaft.

At last I would like to thank my wife, my parents and all the friends I met in Siegen.

Contents

Acknowledgement

Abstract, Zusammenfassung

Contents

1. Introduction: On Weak Interactions	1
References	4
2. The Rotational Barrier of Ethane	5
2.1. Facts and Interpretations	5
2.2. The Partitioning Strategy	5
2.3. Electronic Relaxation and Nuclear Flexing	6
2.4. The Generally Paradoxical Role of Relaxation	7
2.5. A Simple Formal Model of Relaxation	7
2.6. Quantum Chemical Calculations of Staggered and Eclipsed Ethane	9
2.6.1. Fully frozen internal rotation	10
2.6.2. Electronic relaxation	10
2.6.3. Structural relaxation or flexing	12
2.6.4. Structural and electronic relaxation	12
2.7. Summary	13
References	14
3. Single Bond Length Expansion	17
3.1. Introduction	17
3.2. Bond Length Expansion of Second and Third Row Molecules	18
3.2.1. Definition and general magnitude of the bond length expansion	18
3.2.2. Bond length expansions of F ₂ , OHF, H ₂ O ₂ , NH ₂ F, NH ₂ OH, and N ₂ H ₄	18
3.2.3. Bond length expansion of Cl ₂ , SHCl, H ₂ S ₂ , PH ₂ Cl, PH ₂ SH, and P ₂ H ₄	21
3.3. The Difference of LP and BP Repulsions - Surprises Due to the Difference of Images and Graphic Ciphers	22
3.3.1. Model systems 1a and 1b: H ₂ O···He and NH ₃ ···He	23
3.3.2. Model system 2: H ₂ O ··· NH ₃	25

3.3.3. Model system 3: two F ₂ molecules	27
3.3.4. Pauli repulsion energy changes and bond expansion during frozen structure internal rotation	27
3.4. The Actual Shape of Pair Densities	29
3.5. Additional Facts about the Pair Interactions	30
3.5.1. Calculation of pair overlaps	30
3.5.2. He ... NH ₃ and He ... CH ₄ models	32
3.5.3. Correlation between the number of LP – LP interactions and the bond length expansion	33
3.5.4. Correlation between the number of LP – LP interactions and the bond energy weakening	34
3.5.5. Change of energy components upon bond expansion	35
3.6. Some Problems of the LP Explanation	36
3.7. Hybridization Effects	38
3.8. Summary	40
References	41
Appendix I. Introduction to VSEPR (Valence Shell Electron Pair Repulsion) Model	43
Appendix II. Calculation Details	45
AII.1. Computational methods	45
AII.2. The reliability of these three methods	48
4. Reduced Nonbonded Distances	51
4.1. Introduction	51
4.1.1. The empirical approach	51
4.1.2. Theoretical improvements	52
4.1.3. The phenomenon of reduced distances	52
4.1.4. Outline of the present study	53
4.2. Computational Details	53
4.3. Detailed Results	55
4.3.1. The effective radii of F, Cl, Br, I, and O	55
4.3.2. Radii and atomic charges	55
4.3.3. Angular dependence of the radii	62

4.4. Reduced Nonbonded Distances	65
4.4.1. The F···F interaction	66
4.4.2. The Cl···Cl reduced distances	67
4.4.3. Contacts between XY ₃ (X = I,Cl , Y = F,Cl)	69
4.4.4. Contacts between HClO ₃ and HIO ₃	71
4.5. Summary	74
References	75
5. Dye Molecules in Zeolite Channels	76
5.1. Introduction	76
5.2. Applied Methods	77
5.3. Geometrical Reasoning	79
5.3.1. From where comes the $\alpha \leq 40^\circ$ limitation?	79
5.3.2. Reasonable CH···O, NH···O, N···O and Si···H distances	81
5.4. Oxonine in Zeolite L: Structures and Energies	82
5.4.1. Structure model	82
5.4.2. Thermodynamics: which molecular angles are stable?	83
5.4.3. Kinetics: why is no oxonine found at 90°	84
5.4.4. From the calculated model to the real system	87
5.5. The $\pi\pi^*$ Transition Dipole Moment of Oxonine: the Influence of the Zeolite Channel Environment	88
5.5.1. Oxonine, a first model	88
5.5.2. Second model	89
5.5.3. Third model	89
5.5.4. Explanation of the experimental findings	90
5.6. Summary	90
References	92
6. Brief Summary	94
Curriculum Vitae	

1. Introduction: On Weak Interactions

The interactions between atoms can be more or less strong. Comparatively strong interactions are conventionally called ‘ordinary chemical bonds’. The covalent or ionic or metallic “bonds” are of this kind, and they form one of the most fundamental concepts of chemistry. Less strong interactions, say with bond energies significantly below 100 kJ/mol, are called weak or secondary interactions. Among them are the van der Waals, the polarization, the dispersion interactions, hydrogen bonds, metallophilic bonds and so on. The weak interactions play an important role in chemistry, in particular in modern chemistry such as supramolecular chemistry, crystal engineering, surface science, and biodisciplines. The investigation of the weak interaction has attracted a great deal of interest in recent years. One can get some impression about its popularity by three thematic issues of Chemical Reviews [1,2,3].

The weak interaction can be intra-molecular or inter-molecular. The intramolecular weak interaction is very important to understand the conformations of molecules and deviations from standard structures. Two examples for this topic are: a) Intramolecular hydrogen bonds in organic, inorganic, biological and organometallic compounds, as discussed, for example, in [4]. b) Steric interaction and hyperconjugation in ethane: Their study helps to interpret the rotational barrier of ethane and relaxation phenomena in molecules (we will investigate this hot topic in **chapter 2**). One question under heavy discussion is whether weak attractions or weak repulsions play the dominant role. Weak repulsions are the reason for bond expansion and bond weakening in molecular systems with the F-F, F-O, O-O, N-F, N-O, or N-N units, which will be investigated in **chapter 3**. Attractive inter-molecular weak interactions plays an important role in many fields: molecular packing in crystals, solvent chemistry, supermolecular chemistry, host-guest chemistry, attractions on the surface or in channels of crystals, catalysis, drug-design and biochemistry (for details and examples see [1-3]). In **chapters 4 and 5** some topical examples of weak attractions in molecular packing and of molecules in channels are investigated.

The weak interactions consist of attractive and repulsive forces. The repulsive forces are typically due to closed shell Pauli repulsions, i.e. have their origin in the quantum mechanical electronic kinetic energy, and the attractive forces may be of classical electrostatic (in some cases this can also be repulsive) or of quantum mechanical orbital interaction type. The orbital interactions can be partitioned further into exchange, induction and dispersion interactions.

The past decade has seen an explosive growth in experimental and theoretical studies of van der Waals interactions [5,6]. Considerable progress has been achieved toward understanding the nature of this and other interactions at a fundamental level. Conventional ab initio and DFT theories have played a central role in this progress. The applications of ab initio and DFT techniques to this problem concentrated primarily on two areas: a) Accurate, reliable quantum chemical calculations of total, i.e. measurable, **observable** energies. Recent progress in computational capabilities

enabled the use of sufficiently large one-electron basis sets and of highly many-electron correlated methods. With the background of these advances, the ab initio and DFT theory of intermolecular interactions entered a new quantitative level. b) Partitioning the interaction energy into its fundamental **model** components, such as Pauli repulsion, electrostatic, exchange, induction, and dispersion. The analyses of a large number of model complexes helped to identify and ‘understand’ the origins of weak binding and the sources of anisotropy of these interactions. We will come to both areas in this thesis.

As mentioned above, there are four different but interrelated topics in this work. Two of them concern intra-molecular interactions, the other two concern inter-molecular interactions. Our principle research tool is quantum chemical calculation on carefully designed chemical models. GAUSSIAN [7], TURBOMOLE [8], ADF [9] and GAMESS [10] were used to carry out the calculations in the current research at Siegen and Shanghai. The methods used range from AM1, DFT, B3LYP to MP2, and CCSD(T). Medium and large basis sets (TZVP, TZVPP, 6-311g(d,p), 6-311g(2df,pd) and so on) were used except for very large ‘molecules’ with minimal bases for survey investigations (i.e. for a piece of zeolite crystal structure in chapter 5). Concerning the energy partitioning, we use the ADF [11] and the MOROKUMA [12] partitioning methods.

The following is a brief introduction of these 4 topics.

(1) The origin of the rotational barrier of ethane (chapter 2). In recent years some scientists (Goodman, Weinhold, Schreiner etc.) began to believe that this rotational barrier must not be interpreted as in common textbooks, but that it actually comes from attractive hyperconjugation between the C-H bonds and not from repulsive Pauli repulsion between the C-H bonds. One of our professors of organic chemistry drew our attention to this topical problem. We analyzed the frozen structure rotation and the structure relaxation separately. This supports the original and intuitive viewpoint: The conformation of ethane is mainly determined by steric repulsions between the C-H bonds. Several chemical models were designed to elucidate the steric effects and the hyperconjugation directly, and those results also support our viewpoint. This work was finally extended to discuss the paradox of some relaxation phenomena that are important in many fields of chemistry and for other subjects.

(2) E-E bond length expansion (chapter 3). 2nd and 3rd row molecules with single bonds between atoms, which both carry lone pairs, show the phenomenon of particularly long and weak bonding. With reference to an additive increment scheme, the bond lengths are expanded up to 20 pm or up to 10 %, and the bond energies are weakened up to -400 kJ/mol or 70 %. These effects correlate well with the product of the numbers of lone pairs on the two bonded atoms. The explanation through particularly large LP-LP repulsion has been supported here and it explains, why the effect is large, but why it varies only a little with single bond rotation. An important point in this context is that any localized orbital in a polyatomic molecule has a main lobe and a backside tail. That tail is particularly large for lone pair orbitals. It is a pity that most introductory and advanced textbooks communicate a quite misleading

impression of the shape of localized orbitals: the lobes in the common sketches are significantly too slim, and the tails are painted too small in comparison to the main lobes. The importance of tail-tail interaction has here been proven numerically. In addition we have given hints that the nonlinear two-center dependence of bond length and strength on the hybridization of the bond-forming AOs contribute in the same direction as the LP-LP Pauli repulsion. This is so because lone pairs on an atom significantly affect the hybridization of the bonding AOs.

(3) Reduced nonbonded distances (chapter 4). In some compounds the interatomic distances of atoms, nonbonded according to the Lewis-rules, are significantly shorter than the sum of their van der Waals radii. An experimental group in our department had recently uncovered some very impressive examples. Our theoretical study began with deriving theoretical nonbonded radii. We obtained them by extending and modifying a prescription from the literature, namely probing the occupied localized orbital Pauli repulsion with a He atom. These theoretical nonbonded atomic radii were used to replace the so-called experimental ones that were derived from the arbitrary selection of particularly common compounds. We decided not to neglect the charge and angular dependencies of effective atomic theoretical radii, and we studied these dependencies in detail. Some of the interatomic distances found by experimentalists were examined using the theoretical radii. We found that in quite some cases the distances are not actually reduced, but that the trivial charge dependence of the radii was simply neglected: anions are bigger than cations of the same element. One main reason for really reduced nonbonded distances seems to be the specific sensitivity of heavy nonmetallic atoms.

(4) Oxonine in zeolite L channels (chapter 5). The experimental value for the angle between the transition dipole moment of oxonine and the zeolite channel is deduced from experiments to be about 72 degree, while in the same paper a simple geometric model implies that the channel should only allow the molecule to have angles 0 to 40 degrees. The aim of the present theoretical studies is to find the reason for this discrepancy. The calculated model was cut from a zeolite L channel and the dangling bonds were saturated by H atoms. The geometrical optimization was carried out at the AM1 level to find the best positions and the reaction path for the molecular channel-diffusion motion. Energies of three local minima were identified by DFT calculations. The transition dipole moment was calculated by the TD-DFT method. It is found that the discrepancy comes from several reasons, the larger part from using inappropriate parameters in the geometric model. The quantum calculations reproduce the experimental values reasonably well, and this work also cancels some suspicion concerning the adequacy of the experimental method, namely whether the correlation of structural and optical geometric parameters is perturbed by the guest-host interactions.

References

- [1] J.Michl, R.Zahradnik, ed., *VAN DER WAALS I*, *Chem. Rev.*, **1988**, 6.
- [2] A.W.Castleman, P.Hobza, ed., *VAN DER WAALS II*, *Chem. Rev.*, **1994**, 7.
- [3] B.Brutschy, P.Hobza, ed., *VAN DER WAALS III*, *Chem. Rev.*, **2000**, 11.
- [4] Y.Peng, G.C.Bai, H.J.Fan, D.Vidovic, H.W.Roesky, J.Magull, *Inorg. Chem.*, **2004**, 43, 1219.
- [5] S.Scheiner, ed., *Molecular Interactions from van der Waals to Strongly Bound*, Wiley, Chichester, **1997**.
- [6] D.Hadzi, ed., *Theoretical Treatments of Hydrogen Bonding*, Wiley, Chichester, **1997**.
- [7] M.J.Frisch et al., *GAUSSIAN 98*, Gaussian Inc., Pittsburgh PA, **1998**.
- [8] R.Ahlrichs et al., *TURBOMOLE 5.5*, University of Karlsruhe, Germany, **2002**.
- [9] E.J.Baerends et al., *ADF Program System*, Scientific Computing & Modeling, Vrije Universiteit Amsterdam, **2000**.
- [10] M.W.Schmidt et al., *J. Comput. Chem.*, **1993**, 14, 1347; *GAMESS 6*, Department of Chemistry, Iowa State University, Ames IA, **1999**.
- [11] T.Ziegler, A.Rauk, *Theor. Chim. Acta.*, **1977**, 49, 143; *Inorg. Chem.*, **1979**, 18, 1755.
- [12] K.Morokuma, *J. Chem. Phys.*, **1971**, 55, 1236; b) K.Kitaura, K.Morokuma, *Int. J. Quantum Chem.*, **1976**, 10, 325.

2. The Rotational Barrier of Ethane

2.1. Facts and Interpretations

Lively discussions go on about the origins of many chemical phenomena. Correct and incorrect views in the basic fields of chemical bonding and molecular structure were scholarly evaluated in *Angewandte Chemie* by Gernot Frenking [1] in his review of the recent book on chemical bonding by Gillespie and Popelier [2]. One topic in this field is the barrier of rotation about single bonds, a specific view of which has recently been highlighted, also in *Angewandte Chemie*, this time by P. R. Schreiner [3, see also 4-8], a member of another school of computational chemists.

The barrier heights can nowadays reliably be determined, in fact, experimentally [4e,9,10] as well as theoretically [4,5,10f,11,12]. So the existence and the heights of the barriers may be viewed as **physical facts**. For instance, the **rotational barrier of ethane** is known since the mid 1930s to be about 12 kJ/mol [10]. A different point, however, is **our interpretation** of those facts, which still seems to be controversy. A whole set of different reasons (including also electrostatic attractions, electrostatic repulsions or van der Waals attractions) is more or less specifically specified in the textbooks, see e.g. [14-20]. On the other hand, either the "**Pauli repulsion**" between occupied C-H bond orbitals is counted as the dominant factor in some earlier and later original literature, e.g. [12,13,21,22], while it is "**attractive hyper-conjugation**" between occupied and virtual C-H orbitals in some of the more recent literature, e.g. [3-8]. Of course, different mechanisms may have different importance in different compounds.

Illustrative, visually pleasing, and still well **theory-based interpretations** have two purposes, a pedagogical one and a research-directed one. If one can intuitively understand the origin and the tendencies in a series of facts, they are more easily to learn, and one can more efficiently design new sensible experiments within the framework of established science. While the usefulness of such theoretical models is generally stressed, some scholars simultaneously hold that models are '**not absolutely needed**' for our understanding, e.g. [3], while many other ones hold models '**necessary**', for instance in the synthetic efforts for a successful exploitation of the governing physical mechanisms. We will here not discuss the philosophical question of what understanding of a complex field could mean without reference to simple structural models.

2.2. The Partitioning Strategy

One appropriate pathway and **philosophy towards interpretation** and understanding of a physical phenomenon consists of the following two-step procedure.

- *First*, one approximately reproduces the experimental facts theoretically within the framework of a reasonably general and reasonably accurate abstract model theory. In the field of molecular science this model will often be a higher-level quantum chemical approach, such as SCF-MP2 or DFT, applying sufficiently extended basis sets.

- *Second*, within this (or within a simpler model) approach, one partitions the physically measurable quantities, for instance the energetic height of a rotational barrier, into a set of individual contributions. This partitioning is apparently **arbitrary** to quite some degree. A good guide for an **appropriate partitioning** is the following two-step recipe, which is our basic philosophical starting point:

- (i) a few (say one or two) contributions are defined, which are of the order of the physical effect itself and determine its sign in an evident manner, and which can be estimated, or can at least intuitively be understood at the semi-qualitative level, while
- (ii) all the many other contributions to the total effect, which may individually be of large magnitudes and opposite signs, sum up to a small overall 'correction'.

We note that a similar standpoint is taken by Rüdénberg, Kutzelnigg, Ahlrichs, Baerends and others interested in 'understanding' physics, while this approach is sternly rejected by Weinhold, Goodman et al. for unknown reasons.

We will apply the above suggested interpretation strategy to the problem of the rotational barrier of ethane. Within this partitioning scheme, Pauli repulsion turns out to be more important than orbital interference (such as hyperconjugation), i.e. the more traditional viewpoint is supported. Different credible interpretation strategies may in principle lead to **consistent, though different, i.e. complementary, sometimes paradoxical views**. However, 'unusual' new interpretations can also easily be derived by applying inaccurate theoretical models (e.g. too restricted basis sets, or neglect of important correlations), or by applying logically non-stringent partitioning schemes (e.g. choice of ill-defined reference orbitals).

2.3. Electronic Relaxation and Nuclear Flexing

When the two methyl groups of ethane are rotated against each other, both **the electronic and the nuclear degrees of freedom**, i.e. the molecular orbitals and the molecular geometric structure, change somewhat. At the staggered equilibrium ground state and at the eclipsed barrier state, the total energies, the difference of which is the rotational barrier, are stationary. This means that small changes of the geometric or electronic structures will often have only small effects on the values of the total energies and on their difference (i.e. the barrier height), while individual energy contributions may change a lot. It is general wisdom that significantly more extended basis sets are needed to determine other properties than the total energies and their differences.

By comparing two structurally **frozen** methyl groups in staggered and eclipsed conformation, a reasonable barrier height can be obtained, as shown below. **The origin of the barrier is concisely represented**. The individual energy terms of the rotating, structurally *frozen* methyl groups change in a simple manner. Because of the 'freezing', some energy terms do not change at all, some other ones change only a little upon rotation, while Pauli repulsion (plus orbital interactions) between the two frozen methyl fragments increases from staggered to eclipsed conformation by an amount, which is of the order of the barrier (see below). However, upon *relaxing* both the electronic and the geometric structures, i.e. comparing staggered and eclipsed ethane in their 'real' stationary states, all individual energy contributions change largely, while the calculated total barrier height changes only very slightly. The barrier height is now

described as a small sum of several large contributions of different signs. **The physical effect is thereby represented in an involved manner as a complex interplay of different factors** [4-6]. Small changes of the reference states even can drastically modify the weights of these factors.

2.4. The Generally Paradoxical Role of Relaxation

We stress that the special case of the rotational barrier of ethane is just one example of the general case, where one wants to explain the behavior of a complex system. We mention another example, Rüdénberg's famous explanation of 1962 of covalent bonding in H_2^+ and H_2 [23]. When two atoms approach each other and the two partially occupied atomic orbitals, which are frozen to keep their shapes, begin to overlap in a contragradient manner [24], quantum mechanics tells us that the kinetic energy density *decreases* in the overlap region (where the kinetic energy decrease is of the order of magnitude of the bond energy at this level of approximation), while classical electrostatics tells us that the electrostatic energy will not change very much. Upon relaxing the atomic orbitals in the formed molecule, the potential energy must decrease strongly (by about twice the amount of the bond energy, according to the virial theorem). Simultaneously the kinetic energy must *increase* by a similarly large amount, so that it is finally higher than in the free atoms (namely by the amount of the bond energy). The total molecular energy decreases according to the variation principle, but only a little.

So the **physical mechanism** of covalent bonding is the quantum mechanical **tendency to reduce the kinetic energy of atomic electrons when becoming shared by two atoms**. This is a consequence of Heisenberg's uncertainty principle, as first pointed out by Hellmann in 1933 [25]. The classical/quantum mechanical virial theorems tell us that after relaxation, the electronic kinetic energy must have increased, and the attractive potential energy must have decreased (increased its absolute value). This naturally obtains by moving the valence electrons nearer towards the atomic cores (and not by moving them away from the attractive nuclei towards the bond center, as often speculated erroneously since Slater in 1931 [29]).

This situation is typical not only for the quantum regime (chemical bonding, conformational energies, singlet-triplet splittings, etc.), it also occurs in classical physics and technology (thermodynamics of stars, satellite dynamics), in economic and social systems. Some typical examples are displayed in table 1 at the end of this chapter 2. Since this common situation is in contrast to naive common sense, we here display a simple mathematical model, which can be used to simulate and understand any of those systems.

2.5. A Simple Formal Model of Relaxation

Assume that a stationary property E , such as the minimum equilibrium energy or the maximum entropy, comes about through the interplay of two terms A , B , which depend in different manners on some structural or geometric size parameter R . A rather general model is

$$E = A + B \quad , \quad A = -2 a \cdot R \quad , \quad B = + b \cdot R^2 \quad . \quad (2.1)$$

The optimal physical values of R , A , B , E are given by the stationarity condition $dE/dR = 0$, which yields :

$$R = a/b \quad , \quad A = -2a^2/b \quad , \quad B = +a^2/b \quad , \quad E = -a^2/b \quad . \quad (2.2)$$

We now ask for the change of the physical observables R , A , B , E , when the original system with parameters a , b undergoes some chemical variation. Let us assume, for instance, that a substitution or a conformational modification changes the parameter b by $-b\cdot\eta$ to the value $b \cdot (1-\eta)$. In the frozen- R approximation, $\delta^f R = 0$, the changes of A , B , E can be estimated from eq. (1) as

$$\delta^f A = 0 \quad , \quad \delta^f B = -b\cdot\eta \cdot (a/b)^2 \quad , \quad \delta^f E = \delta B = -\eta \cdot a^2/b \quad . \quad (2.3)$$

At this level of approximation, we predict that E will decrease, namely because the chemical modification of the molecule has reduced the prefactor b of the B -term. However, if we take relaxation into account, the structural value R will change, and therefore also A , B , E will finally take modified relaxed values. From eq. (2) one obtains :

$$\delta R = a/b \cdot [1/(1-\eta) - 1] \approx (\eta + \eta^2 + \dots) \cdot a/b \quad , \quad (2.4a)$$

and

$$\delta E = -a^2/b \cdot [1/(1-\eta) - 1] \approx -(\eta + \eta^2 + \dots) \cdot a^2/b \approx \delta^f E \quad , \quad (2.4b)$$

where

$$\delta A \approx -2\eta \cdot a^2/b \quad , \quad \delta B \approx +\eta \cdot a^2/b \quad . \quad (2.4c)$$

It is remarkable that the approximate change $\delta^f E$ of the total E value from eq. (3) is rather similar to the ‘exact’ relaxed change δE from eq. (4b), since for small changes η the correction η^2 is negligible. However, the individual contributions A and B show completely different behaviors in the approximate frozen description (3) and in the relaxed correct description (4c). δA is no longer zero but significantly negative, and δB is no longer similar to δE , but ‘in reality’ it is of opposite sign. One should interpret this very common situation as follows :

The modification of the system goes along with a reduction of the *expression* of the B -term, proportional to $-\eta$. This is the physical driving power, it is the reason of the decrease of E , and one can understand and explain the decrease of E in these terms. This change, however, requires some ‘subsequent’ relaxation of the partially frozen model system. While the *value* of E (the total energy or entropy of the system, for example) changes only slightly upon relaxation (in many cases at least), the individual contributions (such as potential and kinetic energies; or steric repulsion and hyperconjugation and bond energy of adjacent bonds) may change their *values* drastically and may even change their signs. In order to understand the balance of terms ‘inside’ the system, one must analyze the relaxation in detail. However without any detailed analysis, one can already predict the trend of those changes from some general principles, such as the variation principle and the virial theorem in the case of the H_2 molecule mentioned above.

2.6. Quantum Chemical Calculations of Staggered and Eclipsed Ethane

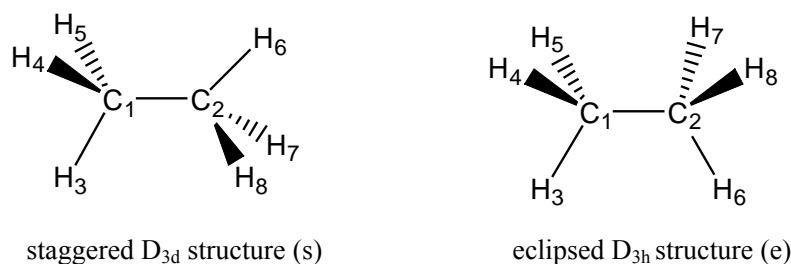


Fig. 1. Conformations of Ethane

Concerning the case of the conformation of ethane (Fig. 1), we have carried out post-Hartree-Fock density functional (DF) calculations using the PW91 DF of Perdew and Wang [26] and a triple-zeta valence (TZV) double polarization basis (2d1f for C and pd for H). The Amsterdam code ADF [27] has been applied. The calculated physical staggered to eclipsed barrier height is 10.7 kJ/mol, which compares reasonably well with the experimental value of 11.4 kJ/mol [10f].

The interaction energies between the two methyl fragments were partitioned according to the scheme of Ziegler and Rauk [28] into three contributions:

$$E = E_{Pau} + E_{el} + E_{orb} = E_{ster} + E_{orb} . \quad (2.5)$$

E_{Pau} is the Pauli repulsion between the frozen *occupied* orbitals of the two interacting methyl fragments. E_{el} is the respective electrostatic interaction. We remember that overlapping electron shells tend to *attract* each other electrostatically because the negative electrons from the one fragment come nearer to the positive nuclei of the other overlapping fragment, and vice versa. The sum $E_{Pau} + E_{el}$ is called the steric interaction E_{ster} . E_{orb} is the orbital relaxation upon interaction, comprising local polarizations and inter-fragment orbital interactions (C-C bonding and H-C··C-H interference).

The basis of this and comparable schemes, such as Morokuma's electronic structure analysis [33] or Weinhold et al.'s so-called "natural" bond orbital analysis (see [5]), is the definition of the intermediate reference states. The results in table 2 are calculated here for two different types of fragments: i) 'atomic' CH₃-like clusters of a real C and 3 real H atoms, and ii) real 'molecular' CH₃ radicals consisting, so to say, of deformed atoms, both with geometric structures as in the optimized staggered or eclipsed ethanes. We explicitly stress that our intermediate reference states are real physical systems, while a large amount of discussion in the literature (e.g. [3-5]) is based on the somewhat basis-set dependent and arbitrarily defined "natural" bond orbitals. Concerning interpretation schemes, one cannot decide beforehand, which choice will yield a simpler, pedagogically preferable or more intuitively convincing approach. This may even depend on the personal taste.

2.6.1. Fully Frozen Internal Rotation

Table 2. Calculated values for ethane, distances in pm, energy differences E in kJ/mol.

Fragments	Structure *)	C-C _{opt}	C-H _{opt}	CCH _{opt}	E_{Pau}	E_{el}	E_{ster}	E_{orb}	E_{tot}
Atomic clusters (C + 3 H)	staggered, optimized **)				-0-	-0-	-0-	-0-	-0-
	eclipsed, frozen at staggered	153.1	109.8	111.4°	+27.1	-1.5	+25.6	-14.5	+11.1
CH ₃ radicals	frozen staggered → eclipsed				+11.1	-1.3	+9.8	+1.3	+11.1
Atomic clusters (C + 3H) difference	staggered, frozen at eclipsed				-46.8	+18.0	-28.8	+29.5	+0.6
	eclipsed, optimized	154.5	109.7	111.9°	-21.8	+16.6	-5.2	+16.0	+10.7
	eclipsed ← staggered				+25.0	-1.4	+23.6	-13.5	+10.1
CH ₃ radicals	frozen eclipsed ← staggered				+10.0	-1.1	+8.9	+1.3	+10.1

*) 'frozen' means structural parameters taken over from the conformation mentioned.

***) reference energy values

The Pauli repulsion (E_{Pau} in table 2) between the occupied bond orbitals *increases* upon rotating the frozen fragments at frozen C-C separation from staggered to eclipsed conformation: concerning methyl radicals of geometric structures as in ethane by 10½ kJ/mol (average of 11.1 and 10.0), which resembles the barrier height quite well; and concerning an assembly of free atoms superimposed at optimized or frozen ethane positions by about 26 kJ/mol (average of 27.1 kJ/mol for staggered frozen methyls, and 46.8 – 21.8 = 25.0 kJ/mol for eclipsed frozen methyls). The electrostatic interaction energy E_{el} changes very little upon frozen rotation, namely by –1 to –1½ kJ/mol. So the steric repulsion E_{ster} between the frozen molecular fragments of deformed atoms *increases* from staggered to eclipsed by 10½ - 1 = 9½ kJ/mol (average of 9.8 and 8.9), which is a little smaller than the actual rotational barrier height. Concerning the frozen fragments of undeformed atoms, the steric barrier is 26 - 1½ = 24½ kJ/mol (average of 25.6 and 23.6), which is about twice the actual barrier. We note that the results are rather similar for both rotated fragments, i.e. whether corresponding to the optimized structures of staggered or of eclipsed ethane. On the other hand the difference between the interactions of independent atomic methyl clusters and those of the molecular methyl radicals is remarkable. So one should not wonder that the use of the artificially deformed reference orbitals from the NBO analysis [4,5] yields the opposite answer. Anyhow we may conclude:

Pauli repulsions of *physical* methyl fragments (molecular, and even more so the atomic ones) definitely favor the staggered conformation.

2.6.2. Electronic Relaxation

Upon internal rotation both the electronic orbitals and the geometric structure of ethane relax because of the increased steric repulsion in the eclipsed conformation. We find empirically in the calculations that relaxing the electronic structure during rotation of structurally frozen

molecular methyl fragments has only a small effect on the barrier, namely an increase of $1\frac{1}{3}$ kJ/mol, yielding a structurally frozen barrier height of $10\frac{1}{2}$ kJ/mol (average of 11.1 and 10.1). On the other hand, the electronic relaxation of the *atomic* methyl fragments reduces the too large steric rotational barrier quite a bit, namely by 14 kJ/mol (average of 14.5 and 13.5), also yielding $10\frac{1}{2}$ kJ/mol.

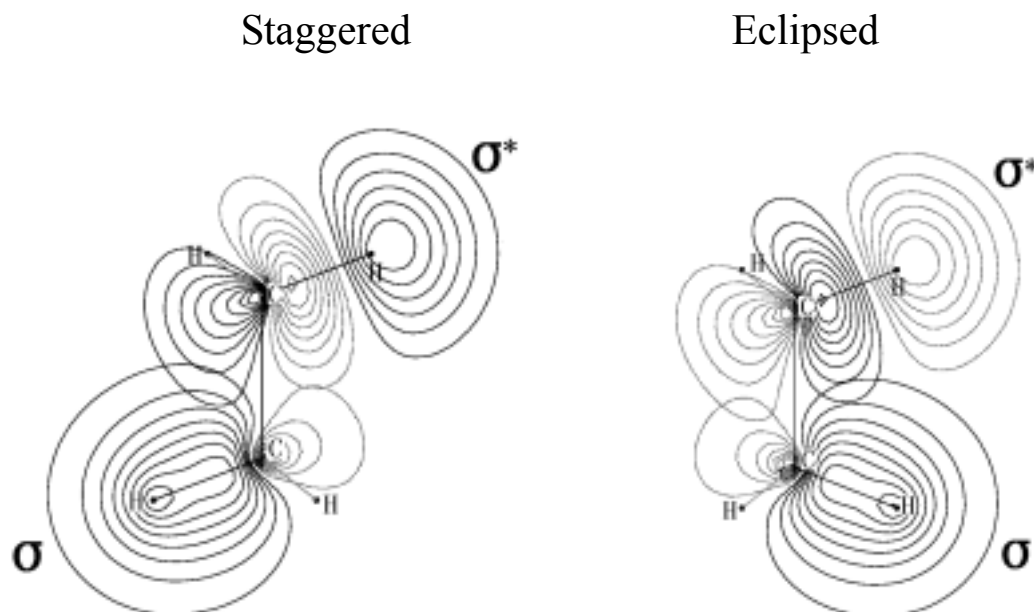


Fig. 2. Superimposed localized C-H σ bonding and σ^* antibonding orbitals of two frozen methyl groups in staggered (left) and eclipsed (right) conformation. Contour lines $\pm n \cdot 0.13 e^{1/2} \text{ \AA}^{-3/2}$

The increased steric repulsions in the eclipsed conformation enforce some orbital deformations inside the fragments. In addition orbital interactions between the fragments (such as hyperconjugation of occupied C-H σ bond orbitals of one fragment with empty C-H σ^* antibonding orbitals of the other fragment) will also change upon rotation. However the $\sigma - \sigma^*$ overlaps are quite similar in the two conformations, see Fig. 2. There, Boys-localized orbitals [30] obtained with the GAMESS code [31] are superimposed. So no big electronic and hyperconjugative effects are to be expected, and only small effects are obtained. Obviously the value of hyperconjugation in the staggered and eclipsed conformations strongly depends on the specific definition of the interacting orbitals. However, large changes were obtained with NBOs as the basis. So:

Orbital relaxations play a minor role for the barrier of rotation of real methyl fragments, but it must be considered in the case of free atomic CH_3 clusters in order to obtain a reasonable numerical value for the barrier height.

2.6.3. Structural Relaxation or Flexing

The relaxation of the geometric structure of the methyl fragments, and in particular of the C-C bond length during internal rotation (structural parameters $\text{H}_3\text{C}-\text{CH}_3$, C-H, C-C-H in table 2), either frozen in the staggered or in the eclipsed conformations, changes the structurally frozen rotational barrier by less than 1 kJ/mol (+0.6 or -0.4 kJ/mol, respectively). The flexing effect is well known for large amplitude internal motions, see e.g. [4-6]. The *individual energy contributions* become completely reorganized thereby. Because of the steric repulsion, the C-C separation increases in the eclipsed conformation by 1.4 pm. This reduces the Pauli repulsion by as much as 48 kJ/mol (average of 46.8 and 48.9), so the Pauli repulsion is now *smaller in the relaxed eclipsed conformation* by $+26 - 48 = -21.8$ kJ/mol. Simultaneously, upon $\text{H}_3\text{C}-\text{CH}_3$ expansion the electrostatic overlap attraction is reduced by 18 kJ/mol (average of 18.0 and 18.1), i.e. there is now a positive electrostatic contribution of $-1/2 + 18 = 16.6$ kJ/mol to the barrier. This yields a steric ‘valley’ of $-21.8 + 16.6 = -5.2$ kJ/mol for the relaxed eclipsed conformation, instead of the $+24\frac{1}{2}$ kJ/mol steric barrier for the structurally frozen case mentioned above.

So: The origin of the barrier of the eclipsed conformation is increased Pauli repulsion of the overlapping frozen methyl groups. As is not uncommon for relaxing systems, the Pauli repulsion becomes, however, smaller for the eclipsed *relaxed* molecule.

2.6.4. Structural and Electronic Relaxation

Table 3. Variation of energy contributions with bond length, in kJ/mol/pm

Molecule	Interactions	dE_{Pau}/dR ^a	dE_{el}/dR	$-dE_{ster}/dR = dE_{orb}/dR$
$\text{H}_3\text{C}-\text{CH}_3$	C-C ^a & $\text{CH}\sigma-\text{CH}\sigma$ ^b & $\text{CH}\sigma^*-\text{CH}\sigma$ ^c	- 34	+ 13	+ 21
F-F	F-F ^a & F(l.p.)-F(l.p.) ^b	- 54	+ 16	+ 39
Cl-Cl	Cl-Cl ^a	- 37	+ 14	+ 23

^a) A-A bonding with $R = \text{A-A}$ distance; ^b) nonbonded pair-pair interaction of σ -CH bond pairs or F-lone pairs ; ^c) virtual-occupied orbital interaction

In order to get an impression of the interplay of electronic relaxation and bond length expansion, we display some calculated physical values of $\text{H}_3\text{C}-\text{CH}_3$, F-F and Cl-Cl in table 3. If the Cl-Cl distance increases around its equilibrium value, the overlap of the bond orbital, the lone pair orbitals and the core orbitals decreases. Accordingly E_{Pau} decreases (by -37 kJ/mol/pm) and E_{el} increases (by 14 units), while the bonding attraction of the atomic $p\sigma$ orbitals is reduced (increasing E_{orb} by 23 units). In contrast to Cl_2 and $(\text{CH}_3)_2$, the bond in F_2 is known to be strained because of exceptionally strong lone pair – lone pair repulsions (see chapter 3). Therefore the variation of E_{Pau} and E_{orb} is larger. The bond – bond repulsion in $(\text{CH}_3)_2$ is weaker again, so the situation is more similar to Cl_2 , also concerning E_{orb} . This is another indication that Pauli repulsion does not play a counterintuitive role, and hyperconjugation not a large role, in ethane, provided the discussion is based on physical (and not the somewhat arbitrary so-called “natural”) reference states.

2.7. Summary

Energy contributions to the rotational barrier of ethane have been calculated. The results are in agreement with literature values. We have here offered a simple ‘explanation’: The Pauli repulsion of electronically and structurally frozen methyl fragments creates a barrier for the eclipsed conformation, which is, however, too high by a factor of about 2. This is brought down to a reasonable value by electronic relaxation, i.e. by some C-H σ bond orbital deformation and hyperconjugation. As is well known, the C-C bond in eclipsed ethane is expanded by about 1½ pm. This flexing, i.e. the structural relaxation accompanying the internal rotation causes a significant modification of the individual electronic energy contributions. On this basis one can develop a quite complex discussion of the rotational barrier. Depending on the definition of occupied and virtual localized orbitals of the methyl fragments, one can also get the impression of basic importance of hyperconjugation for the barrier.

The existence of a simple explanation does not exclude the creation of correct, but complicated explanations. This is quite common, because systems will internally relax upon some external strain. In thermodynamics one usually chooses the variables so that the relaxation of the system will attenuate the original modification, this is the common LeChatelier-Brown behavior [32]. Other behaviors of a property A are easily created :

$$\begin{array}{ll}
 \text{LeChatelier's damping behavior} & 0 < A^{\text{relaxed}} < A^{\text{frozen}} \\
 \text{reinforcement behavior} & 0 < A^{\text{frozen}} < A^{\text{relaxed}} \\
 \text{reversing behavior} & A^{\text{relaxed}} < 0 < A^{\text{frozen}}
 \end{array} \tag{2.6}$$

The situation is particularly simple, if the system is governed by the minimum of E , $dE/dR = 0$, with

$$E = A + B = a \cdot R + b/R. \tag{2.7}$$

If the physical parameters a , b are modified by the amounts $a \cdot \delta a$ and $b \cdot \delta b$, then one finds a situation as described in table 4. The counterintuitive reversing behavior is particularly common in chemistry and daily life as represented in table 1.

Table 4. LeChatelier's damping behavior, reinforcement behavior, and reversing behavior of properties A and B of model system described by eq. (7)

Modification of physical parameters a, b	$\delta b < -\delta a$	$-\delta a < \delta b < 0$	$0 < \delta b < \delta a$	$\delta a < \delta b$
Behavior of property A	reversing	damping	damping	reinforcement
Behavior of property B	damping	reversing	reinforcement	damping

References

- [1] G.Frenking, *Angew. Chem.*, **2003**, *115*, 152.
- [2] R.J.Gillespie, P.L.A.Popelier, *Chemical Bonding and Molecular Geometry : From Lewis to Electron Densities*, Oxford University Press, **2001**.
- [3] P.R.Schreiner, *Angew. Chem.*, **2002**, *114*, 3729; *Angew. Chem. Int. Edit.*, **2002**, *41*, 3579.
- [4] a) V.Pophristic, L.Goodman, *Nature*, **2001**, *411*, 568. b) L.Goodman, H.B.Gu, V.Pophristic, *J. Chem. Phys.*, **1999**, *110*, 4268. c) L.Goodman, H.B.Gu, *J. Chem. Phys.*, **1998**, *109*, 72. d) L.Goodman, V.Pophristic, in *The Encyclopedia of Computational Chemistry*, P.v.R.Schleyer, ed., Wiley, New York, **1998**, *4*, 2577. e) L.Goodman, V.Pophristic, F.Weinhold, *Acc. Chem. Res.*, **1999**, *32*, 983. f) V.Pophristic, L.Goodman, *J. Phys. Chem. A*, **2002**, *106*, 1642.
- [5] a) F.Weinhold, *Nature*, **2001**, *411*, 539. b) J.K.Badenhoop, F.Weinhold, *Int. J. Quantum Chem.*, **1999**, *72*, 269; c) *J. Chem. Phys.*, **1997**, *107*, 5406. d) A.E.Reed, F.Weinhold, *Isr. J. Chem.*, **1991**, *31*, 277.
- [6] R.F.W.Bader, J.R.Cheeseman, K.E.Laidig, K.B.Wiberg, C.Breneman, *J. Am. Chem. Soc.*, **1990**, *112*, 6530.
- [7] a) E.B.Wilson, *Adv. Chem. Phys.*, **1936**, *4*, 749. b) L.Radom, W.J.Hehre, J.A.Pople, *J. Am. Chem. Soc.*, **1972**, *94*, 2371. c) J.P.Lowe, *J. Am. Chem. Soc.*, **1970**, *92*, 3799; d) *Prog. Phys. Org. Chem.*, **1968**, *6*, 1; e) *Science*, **1973**, *179*, 527. f) W.J.Orville-Thomas, ed., *Internal Rotation in Molecules*, Wiley, New York, **1974**.
- [8] a) J.Urban, P.R.Schreiner, G.Vacek, P.V.Schleyer, J.Q.Huang, J.Leszczynski, *Chem. Phys. Lett.*, **1997**, *264*, 441. b) I.V.Alabugin, T.A.Zeidan, *J. Am. Chem. Soc.*, **2002**, *124*, 3175.
- [9] a) D.G.Lister, *Introduction to Large Amplitude Motions in Molecules*, Academic Press, New York, **1978**. b) H.Frei, *Large Amplitude Motion in Molecules*, Springer, Heidelberg, **1979**.
- [10] a) A.Eucken, K.Weigert, *Z. Phys. Chem. B*, **1933**, *23*, 265. b) E.Teller, K.Weigert, *Nachr. Ges. Wiss. Göttingen, Gesch. Mitt.*, **1933**, 218. c) J.D.Kemp, K.S.Pitzer, *J. Chem. Phys.*, **1936**, *4*, 749; d) *J. Am. Chem. Soc.*, **1937**, *59*, 276. e) K.S.Pitzer, *Disc. Faraday Soc.*, **1951**, *10*, 66. f) A.G.Császár, W.D.Allen, H.F.Schaefer, *J. Chem. Phys.*, **1998**, *108*, 9751.
- [11] see e.g. a) D.A.Brown, L.P.Cuffee, G.M.Fitzpatrick, N.J.Fitzpatrick, W.K.Glass, K.M.Herlihy, *Coll. Czech. Chem. Commun.*, **2001**, *66*, 99.
- [12] K.B.Wiberg, in *The Encyclopedia of Computational Chemistry*, P.v.R.Schleyer, ed., Wiley, New York, **1998**.
- [13] K.B.Wiberg, D.J.Rush, *J. Org. Chem.*, **2002**, *67*, 826.
- [14] C.K.Ingold, *Structure and Mechanism in Organic Chemistry*, Cornell University Press, Ithaca NY, **1953**.

- [15] E.L.Elidel, *Stereochemie der Kohlenstoffverbindungen*, Verlag Chemie, Weinheim, **1966**.
- [16] H.Beyer, W.Walter, *Lehrbuch der Organischen Chemie*, 19th ed., Hirzel, Stuttgart, **1987**.
- [17] R.T.Morrison, R.N.Boyd, *Lehrbuch der Organischen Chemie*, 2nd ed., Verlag Chemie, Weinheim, **1978**.
- [18] J.March, *Advanced organic chemistry, reactions, mechanisms, and structure*, 4th. ed., Wiley, New York, **1992**.
- [19] F.A.Corey, R.J.Sundberg, *Organische Chemie*, 3rd ed., VCH, Weinheim, **1995**.
- [20] K.P.C.Vollhardt, N.E.Schore, *Organische Chemie*, 3rd ed., Wiley-VCH, Weinheim, **2000**.
- [21] O.J.Sovers, C.W.Kern, R.M.Pitzer, M.Karplus, *J. Chem. Phys.*, **1968**, *49*, 2592.
- [22] P.A.Christiansen, W.E.Palke, *Chem. Phys. Lett.*, **1975**, *31*, 462.
- [23] K.Ruedenberg, *Rev. Modern Phys.*, **1962**, *34*, 326.
- [24] C.W.Wilson, W.A.Goddard, *Theoret. Chim. Acta*, **1972**, *26*, 195, 211.
- [25] H.Hellmann, *Z. Physik*, **1933**, *35*, 180.
- [26] J.P.Perdew, Y.Wang, *Phys. Rev. B*, **1992**, *45*, 13244.
- [27] E.J.Baerends et al., *ADF Program System*, Scientific Computing & Modeling, Vrije Universiteit Amsterdam, **2000**.
- [28] T.Ziegler, A.Rauk, *Theor. Chim. Acta*, **1977**, *49*, 143; *Inorg. Chem.*, **1979**, *18*, 1755.
- [29] J.C.Slater, *Phys. Rev.*, **1931**, *38*, 1109.
- [30] S.F.Boys, in *Quantum Science of Atoms, Molecules, and Solids*, p. 253, P. O. Löwdin, ed., Academic Press, New York, **1966**.
- [31] M.W.Schmidt et al., *J. Comput. Chem.*, **1993**, *14*, 1347; *GAMESS 6*, Dept. Chemistry, Iowa State University, Ames IA, **1999**.
- [32] a) H.L.Le Chatelier, *Compt. Rend.*, **1884**, *99*, 786; b) *Ann. Mines.* **1888**, *13*, 157. c) F.Braun, *Z. Phys. Chem.*, **1887**, *1*, 259.
- [33] a) K.Morokuma, *J. Chem. Phys.*, **1971**, *55*, 1236. b) K. Kitaura, K. Morokuma, *Int. J. Quantum Chem.* **1976**, *10*, 325.

Table 1. Physical origin and subsequent relaxation of quantum-chemical, physical and economic phenomena

Physical Phenomenon	Covalent bond formation	Ionic bond formation	Rotational barrier of σ -bonds (C_2H_6)	Singlet-Triplet splitting	Classical evolution of stars	Merging of two companies	Lowering of the orbit of a space shuttle
Physical Origin	Contragradient overlap of partially filled AOs	Atoms of different electronegativity	Pauli repulsion of occupied bond-orbitals	Electrons of same spin avoid each other (Pauli principle)	Stars emit radiation	Overlap of products palette	Firing the retrorocket
Physical mechanism	Quantum interference reduces E_{kin}	Charge transfer to more electro-negative atom	Different orbitals must not overlap (Pauli principle)	Coulomb repulsion of singlets/triplets contains \pm exchange terms	Energy loss cools plasma of star	Pooling of administrative efforts	Smaller centrifugal force of decelerated shuttle
Origin of relaxation	Reduced ‘kinetic pressure’ of inter-nuclear electron gas	Interelectronic repulsion; field of the cations	Overlapping CH-bond orbitals repel each other	Singlet electron pair has more Coulomb repulsion energy	Cooling reduces the pressure of star’s plasma	Reduced overhead costs	Decelerated shuttle “falls down” towards the earth
Relaxation Process	‘Thermal’ contraction of ‘cooled’ electron gas cloud	Anionic orbital expansion and polarization	C-C distance is expanded (and C-C-H angles adjust)	Orbitals of a singlet pair expand in comparison to a triplet pair	Plasma cloud contracts due to gravitation	Reduced piece costs	Speed of shuttle increases
Result of relaxation	Electron cloud nearer to nuclei, this improves nuclear-electron attraction, but increases E_{kin} due to ‘uncertainty principle’	Anionic radius is larger than atomic covalent radius, cationic radius is smaller, increase of E_{kin}	Longer C-C distance in eclipsed C_2H_6 reduces E_{Pauli} on the expense of the C-C bond energy	More diffuse singlet charge cloud has smaller Coulomb repulsion than the respective triplet cloud	Gravitational energy heats up the contracted star plasma, temperature goes up	More selling, expansion of production, finally slight increase of overhead	New orbit is nearer to earth, larger gravitational attraction, but the final speed is larger than before deceleration
Correct, but misleading interpretation	Origin of covalence is valence electron density increase in the vicinity of the attractive nuclei	According to virial theorem, any binding is due to electrostatic attraction	Staggered ethane has lager Pauli repulsion, but the C-C bond is stronger	Triplet energy is low because contracted orbitals have better nuclear attraction energy	In contrast to terrestrial bodies, stars become warmer when losing energy	Successful merging of companies sometimes even inceases the overhead	In order to come down to a lower orbit, the velocity must somehow be increased
Wrong interpretation	Classical Coulomb law does no longer work: covalence is due to density increase between nuclei	Ionic binding is a completely classical, electrostatic phenomenon	Hyperconjugation between the methyl groups determines the conformation of C_2H_6	Triples are higher in energy because they have higher Coulomb repulsion energy	Thermodynamic laws do not hold for stars	Company merging will always increase the overhead	For a freely moving body, Newton’s law does no longer work: acceleration by braking

3. Single bond length expansion

3.1. Introduction

It is well known that the bond lengths of F_2 , O_2R_2 and N_2R_4 are comparatively long, and correspondingly weak. For a long time this phenomenon was generally accepted as being due to the interatomic LP-LP (LP = Lone Pair) repulsions [1-5,39,40]. This explanation had intuitively been ‘derived’ from the empirical data, but till now there is no stringent quantum chemical and quantum computational verification. It had just been accepted as general wisdom that partly originated from the success of the VSEPR model (see Appendix I and [6-9], and seems to be more plausible than some other explanations [10-12]. The VSEPR model assumes that the steric repulsion between Lone Pairs (LP) and Bond Pairs (BP) shows the following order: $LP \leftrightarrow LP > LP \leftrightarrow BP > BP \leftrightarrow BP$. Thereby the VSEPR model successfully predicts the structure and conformation of many organic and inorganic compounds, for exceptions see [8,13].

In contrast, Sanderson [33] promoted the idea that “the lone pair bond weakening effect (LPBWE) does not depend on repulsions between lone pair electrons on adjacent atoms, but results from lone pair interference with bonding by its own atom”, that is “it is intra-atomic, not inter-atomic”, although “the exact mechanism is not yet understood”. We must here take into account that ordinary chemists attach a vague meaning to the phrase ‘interference’. They do not imply the physical and quantum chemical meaning of phase-dependent addition of amplitudes. The quantum chemical phrase of ‘orbital interference’ for one important contribution to two-center chemical bonding, however, has this latter physical meaning. So two questions remain, *how much one-centric and how much two-centric* is the LPBWE, and what is *the quantum mechanical mechanism*.

While the VSEPR model accounts for the *intra*-atomic steric interactions between the one center LPs and the respective two center BPs when explaining the *angular* aspects of molecular structures, there is no detailed analysis of the *inter*-atomic repulsions between LPs and BPs on two centers in order to explain the respective bond *lengths*.

To begin with, we compare and analyze bond lengths and energies of molecules from 2nd and 3rd row elements in section 2. Some surprises about the LP repulsion explanation arise from the traditionally oversimplified and unrealistic sketches of the *shape of the LPs* in classical textbooks, discussed in section 3. The consequences of the actual shape of LPs are investigated in section 4. We support the *two-centric* LP-LP repulsion explanation in section 5. Some difficulties with the LP repulsion explanation are described in section 6, and an additional *one-centric* LP-BP hybridization aspect is worked out in section 7.

The applied research tool is quantum chemical calculation. We used some common simple independent particle Molecular Orbital (MO) Self Consistent Field (SCF) approaches, namely *ab initio* Hartree-Fock (HF), second order Møller-Plesset (MP2) perturbation theory, Kohn-Sham (KS) Density Functional (DF) theory and Becke’s 3 parameter HF & Lee-Yang-Parr’s DF hybrid approach (B3LYP), as implemented in the commercial TURBOMOLE, ADF, and GAUSSIAN program packages. For details (basis sets etc.) and reliabilities of the applied procedures see Appendix II.

3.2. Bond length expansion of second and third row molecules

3.2.1. Definition and general magnitude of the bond length expansion

First we define the ‘bond length expansion’. It means that the bond is longer than bonds of the same atoms, where the partners that do not have (or have less) LPs. Concerning 2nd row atoms:

- The length of the C-C bond in C₂H₆ is assumed as normal, the respective C covalent radius is 76 pm.
- The bonds of C-N in CH₃NH₂, of C-O in CH₃OH, and of C-F in CH₃F have the least number of LPs among the X-NH₂, X-OH, and X-F compounds. They form the references for the covalent radii of N (70 pm), O (66 pm) and F (63 pm), see table 1 below.
- The ‘bond length expansion’ of a bond is then defined as its deviation from the sum of those covalent radii. For N₂H₄, NH₂OH, H₂O₂, NH₂F, HOF, F₂ the expansions vary from 3 to 16 pm.

For 3rd row molecules the same procedure uses Si₂H₆, SiH₃PH₂, SiH₃SH, SiH₃Cl, and obtains also bond length expansions, namely for P₂H₄, HSPH₂, H₂S₂, PH₂Cl, SHCl, Cl₂ from 5 to 22 pm (see below).

3.2.2. Bond length expansions of F₂, OHF, H₂O₂, NH₂F, NH₂OH, and N₂H₄

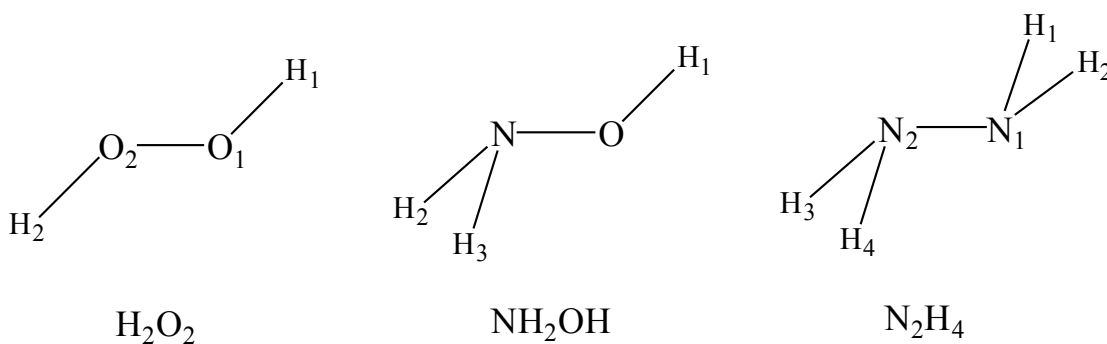
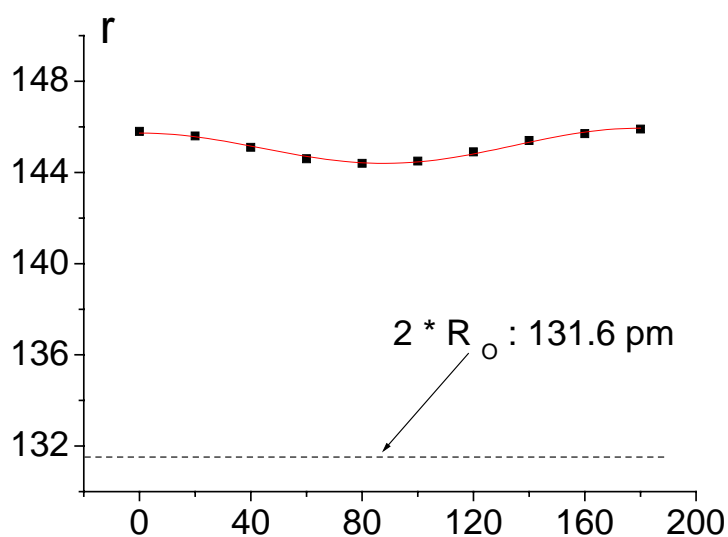
Calculations according to that definition were performed at the SCF-MP2 level with TURBOMOLE [14], using TZVPP basis sets and the RI approximation. The results are shown in tables 1 and 2. The bond length expansions increase in the order N₂H₄ < NH₂OH < NH₂F < H₂O₂ < OHF < F₂. The expansions of the latter molecules are quite significant from the chemical point of view, i.e. larger than 10 pm. Compared to the experimental values, the maximal deviation of the calculated bond lengths is 1.6 pm, the average deviation is less than 1 pm, the calculated ones being in general a little smaller. Accordingly the calculated structures are sufficiently reliable to discuss the bond length expansions.

Table 1. Experimental (1σ-accuracy of last digit in parentheses) and calculated (MP2) bond lengths, and covalent radii of C, N, O and F (in pm)

	C ₂ H ₆	CH ₃ NH ₂	CH ₃ OH	CH ₃ F
Exp. bond length	153.4(1) [15] 153.6 [16]	147.4(15) [15] 147.4 [16]	142.1(2) [15] 142.7 [17]	138.2 [15] 138.3 [18]
Calc. bond length	152.4	146.2	142.0	138.3
Covalent radius	R _C = 76.2	R _N = 70.0	R _O = 65.8	R _F = 62.1

Table 2. Experimental and calculated (MP2) bond lengths and expansions of F₂, OHF, H₂O₂, NH₂F, NH₂OH, N₂H₄ (in pm)

	N ₂ H ₄	NH ₂ OH	NH ₂ F	H ₂ O ₂	OHF	F ₂
Exp. bond length	144.9(4)[15] 144.6[19]	145.3(2)[15] 145.3[20]		145.2(4) [15]	144.2[21]	141.2[22]
Calc. bond length	143.2	144.1	142.0	145.1	142.6	139.9
Bond Expansion	3.2	8.3	9.9	13.5	14.7	15.7
% Expansion	2.2	5.7	7.0	9.3	10.2	11.1
Angular variation	5	2	0	1	0	0

Fig. 1 H₂O₂, NH₂OH, and N₂H₄ with dihedral rotation angle $\gamma = 180^\circ$ (present conformation is meant having a mirror plane)Fig. 2. r (O-O) in pm versus internal rotation angle of H₂O₂ in degree (atomic labels as in Fig. 1). The curve is a fit by $r = 145.1 - 0.107 \cos\gamma + 0.718 \cos 2\gamma$

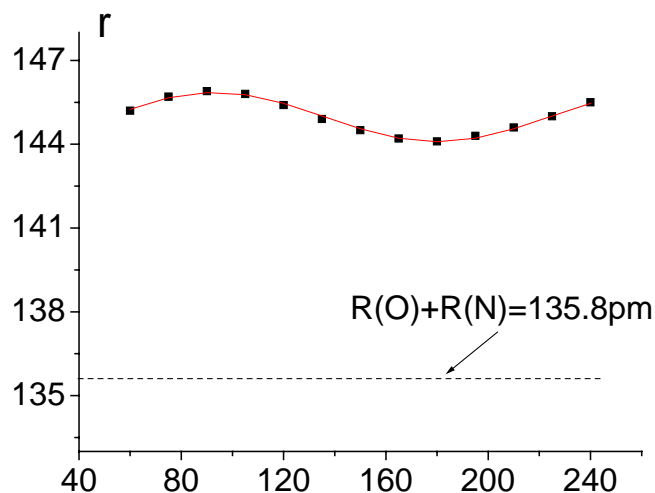


Fig. 3. r (O-N) in pm versus internal rotation angle of NH_2OH in degree (atomic labels as in Fig. 1). The curve is a fit by $r = 144.9 - 0.212 \cos\gamma - 0.986 \cos 2\gamma$

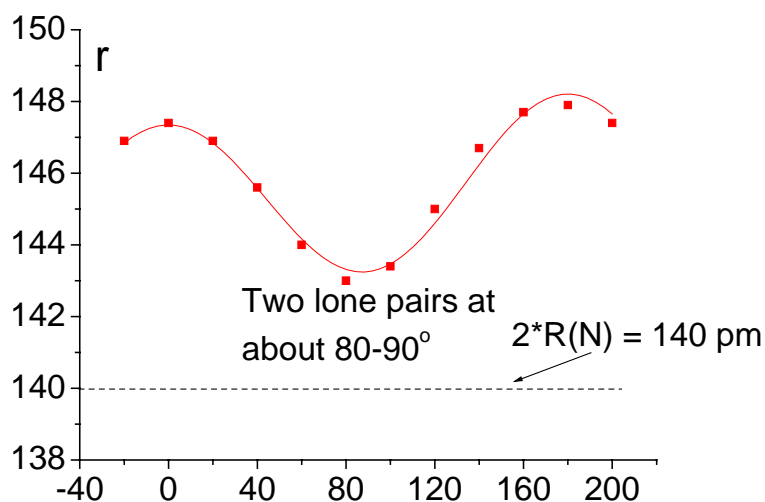


Fig. 4. r (N-N) in pm versus internal rotation angle of N_2H_4 in degree (atomic labels as in Fig. 1). The curve is a fit by $r = 145.5 - 0.431 \cos\gamma + 2.262 \cos 2\gamma$

The bond length variations of H_2O_2 , NH_2OH and N_2H_4 (Fig. 1) upon internal rotation, as obtained with B3LYP-SCF, are shown in Figs. 2, 3 and 4. We used GAUSSIAN [23] just because it is then particularly easy to prepare the input for partial structure optimizations and potential curve calculations. We note that the larger the number of lone pairs (sum or product of LPs on the two atoms, see below for analysis), the stronger the bond expansion. On the other hand we see that for single LPs on the atoms the angular variation of the bond length is large, for 2 LPs it is smaller, while for 3 LPs (the F atom) there is of course no

rotational dependence at all. For H₂O₂ and NH₂OH, the expansions are of significant magnitude, but the bond lengths change only a little during internal rotation. For H₂O₂ with 2+2 LPs the rotational variation is only about 10% of the total expansion, and for NH₂OH with 1+2 LPs it is about 15%. Therefore **the bond expansion must be caused by something that does not significantly change with internal rotation.** The influence of the 9 two-center pair-pair interactions (LP-LP, LP-BP, BP-BP) on the bond length or bond energy can be modeled by $r = a_0 + a_1 \cos\gamma + a_2 \cos 2\gamma$, with vanishing $\cos 3\gamma$ term (where we assume that all dihedral angles of two pairs are 0 or $\pm 120^\circ$). The fits of the bond length – rotational angle – correlation are shown in Figs. 2-6. The good fitting supports that it is reasonable to delete the $\cos 3\gamma$ term.

3.2.3. Bond length expansion of Cl₂, SHCl, H₂S₂, PH₂Cl, PH₂SH, and P₂H₄

The interatomic LP repulsions of 3rd row atoms are commonly assumed to be much smaller than those of the 2nd row atoms [1,33]. Their covalent radii are much larger, by about 0.4 Å, the bond energies decrease by 37 % [33]. The calculations were carried out as before. They are again sufficiently reliable, with an average error of 1.2 pm. The results are shown in tables 3 and 4. **3rd row molecules undergo similar or even larger bond expansions than 2nd row ones.** The order is P₂H₄ < PH₂SH < PH₂Cl < H₂S₂ < SHF < Cl₂. The trend is similar to the one in the 2nd row. The bond length variations of H₂S₂ and P₂H₄ during the internal rotation are shown in Figs. 5 and 6. The definition of rotation angles is analogous to Fig. 1. (Because of p instead of sp³ bonding in the 3rd row, the $\cos 3\gamma$ term does not vanish and must be included in the case of P₂H₄.) Our previous conclusions for the 2nd row also hold for the 3rd row.

Table 3. Covalent radii of Si, P, S and Cl (in pm)

	Si ₂ H ₆	SiH ₃ PH ₂	SiH ₃ SH	SiH ₃ Cl
Calc. bond length (exp. [24])	234.8 (232.0)	226.0	214.5	206.1
Covalent radius	R _{Si} = 117.4	R _P = 108.6	R _S = 97.1	R _{Cl} = 88.7

Table 4. Bond length expansion of Cl₂, SHCl, H₂S₂, PH₂Cl, PH₂SH, and P₂H₄ (in pm)

	P ₂ H ₄	PH ₂ SH	PH ₂ Cl	H ₂ S ₂	SHCl	Cl ₂
Exp. bond length	221.9[25]			205.6[26]		198.8[22]
Calc. bond length	221.8	212.8	207.0	206.4	203.7	199.8
Expansion	4.6	7.1	9.7	12.2	17.9	22.4
% Expansion	2.1	3.3	4.7	5.9	8.8	11.2
% Expansion of 2 nd row	2.2	5.7	7.0	9.3	10.2	11.1
Angular variation	4.0		0	6.0	0	0

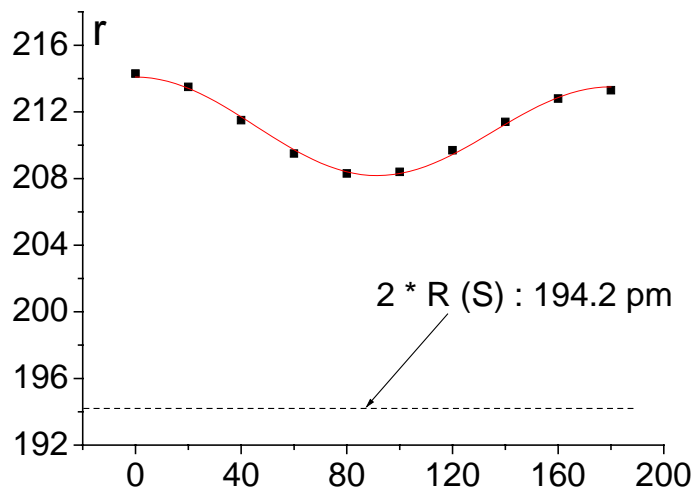


Fig. 5. r (S-S) in pm versus internal rotation angle of H_2S_2 in degree (atomic labels as in Fig. 1). The curve is a fit by $r = 211.0 + 0.294 \cos\gamma + 2.808 \cos 2\gamma$

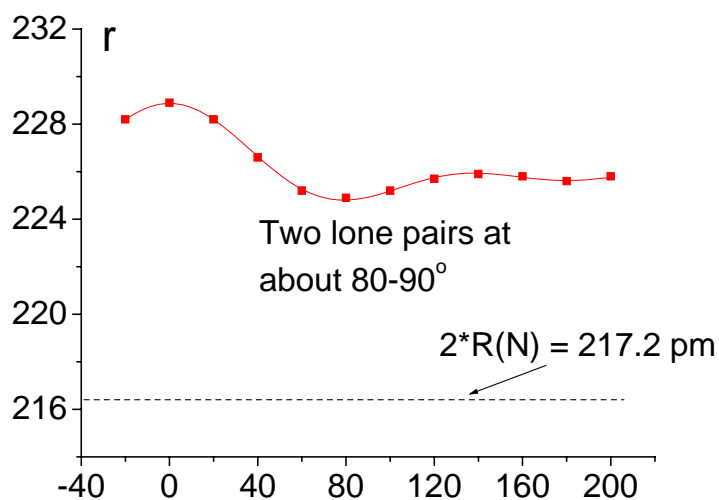


Fig. 6. r (P-P) in pm versus internal rotation angle of P_2H_4 in degree (atomic labels as in Fig. 1). The curve is a fit by $r = 226.1 + 0.920 \cos\gamma + 1.163 \cos 2\gamma + 0.703 \cos 3\gamma$. The HPH angle is 93°

3.3. The difference of LP and BP repulsions - Surprises due to the difference of images and graphic ciphers

In order to investigate the repulsions between different electron pairs, we choose several simple model systems: 1a) $\text{H}_2\text{O}\cdots\text{He}$, 1b) $\text{H}_2\text{O}\cdots\text{NH}_3$, 2) $\text{F}_2\cdots\text{F}_2$, 3) $\text{HO}-\text{OH}$. Below we first sketch the lone pairs in the symbolic manner as done in most textbooks [27-30]. In reality a

lone pair is much fatter and the interaction may be quite complicated, though the thin shape in Fig. 7a works quite well for the rationalization of many chemical structures and reactions. The actual shape of the lone pair has a broad main lobe and a smaller tail on the backside, and will be analyzed in a later section. In this section we will check this simplified shape concerning the relative strength of the lone pair – lone pair, bond pair – bond pair, and lone pair – bond pair interactions. We will also discuss the situation in some cases, when considering the LP tails explicitly.

3.3.1. Model Systems 1a and 1b: $H_2O \cdots He$ and $NH_3 \cdots He$.

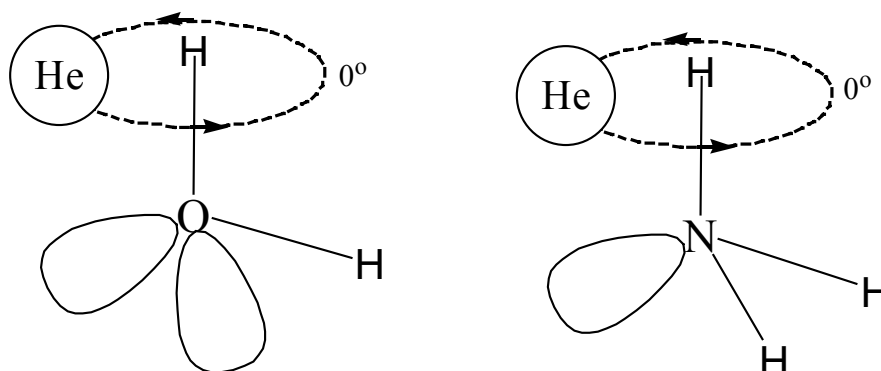


Fig. 7a. Symbolic molecular ciphers of chemists: **left side** He rotating around one O-H bond of H_2O and ‘through’ the other OH bond and the O lone pairs; **right side** H_2O replaced by NH_3 . 0° means He above the other O-H bond, or above middle of the two N-H bonds

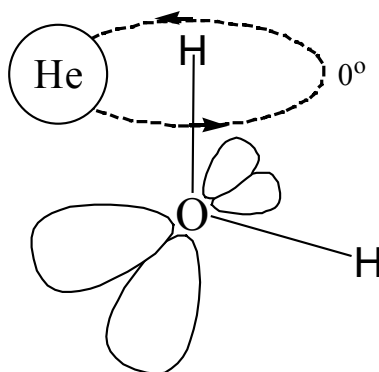


Fig. 7b. The lone pairs with tails, actually the main lobes and the tails are much bigger than that in the figure (see Fig. 14)

The He atom is used as a probe to detect the steric repulsion of H_2O in different directions. The molecular system is shown in Fig. 7a (left). The He is moved around one OH bond at different heights, thereby touching the other BP and the oxygen LPs. We determined and analyzed the steric interaction between He and H_2O along the rotational path. The energy partitioning technique described in [31] was used, as implemented in the ADF program [32]. The PW91 DF and basis sets TZ/2df for O, TZ/pd for He and H were used. The O-1s

core was frozen. The results are displayed in table 5a and Fig. 8a for arrangement $r_{\text{He}\dots\text{O}} = 170$ pm, $\text{HeOH} = 28^\circ$. We have tried several other distances and angles, and the trends were the same. At first sight it seems that there is a larger steric repulsion by the OH-BP than by the O-LPs. Correctly we should say, however, that two near-by LP-tails and a more distant BP gives a larger Pauli repulsion and a larger electrostatic overlap attraction than a near-by BP-tail and the more distant LP-main-lobes (see Fig. 7b).

Table 5a. Variation of Pauli repulsion E^{Pauli} , electrostatic attraction E^{elst} , and total steric interaction E^{steric} , between He and H_2O along the rotational path of Fig. 7a(left). Meaning of rotation angles He-H-O-H: 0° : He above OH; about $\pm 120^\circ$: He above one lone pair; 180° : He above the middle of the two lone pairs

rot. angle He-H-O-H	0°	20°	40°	60°	80°	100°	120°	140°	160°	180°
E^{Pauli} , kJ/mol	-0-	-1.3	-4.6	-9.0	-15.1	-24.1	-35.9	-48.3	-57.9	-61.4
E^{elst} , kJ/mol	-0-	0.3	1.3	2.7	4.7	7.6	11.1	14.8	17.6	18.7
E^{steric} , kJ/mol	-0-	-1.0	-3.3	-11.3	-19.7	-16.5	-24.8	-33.5	-40.2	-42.7

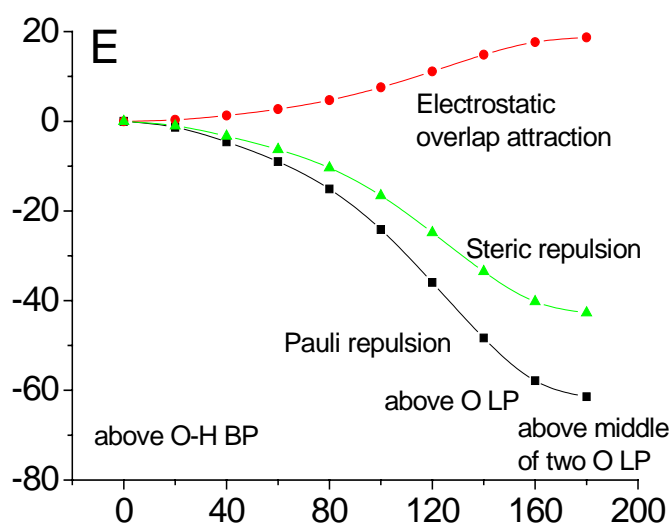


Fig. 8a H_2O -He interaction energy contributions (E in kJ/mol) versus angle (in degree) along the rotational path of Fig. 7a(left)

Table 5b. Same as table 5a, but H_2O replaced by NH_3 (0° : He above middle of two N-H bonds, 180° : He above the lone pair)

rot. angle He-H-N-H ₂	0°	20°	40°	60°	80°	100°	120°	140°	160°	180°
E^{Pauli} , kJ/mol	-0-	-3.8	-16.3	-37.6	-62.0	-79.8	-85.3	-89.7	-73.3	-69.9
E^{elst} , kJ/mol	-0-	1.1	4.5	10.2	16.8	21.7	23.6	22.7	21.1	20.3
E^{steric} , kJ/mol	-0-	-2.7	-11.8	-27.4	-45.2	-58.1	-61.7	-58.0	-52.2	-49.6

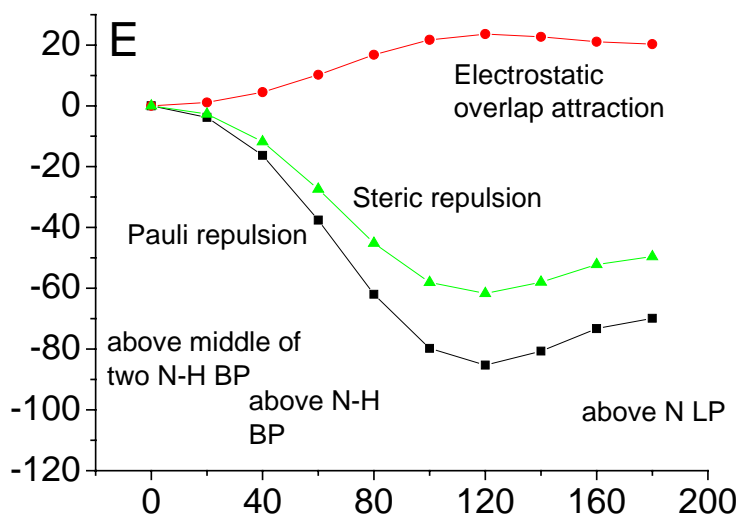


Fig. 8b. NH_3 -He interaction energy contributions (E in kJ/mol) versus angle (in degree) along the rotational path of Fig. 7a(right)

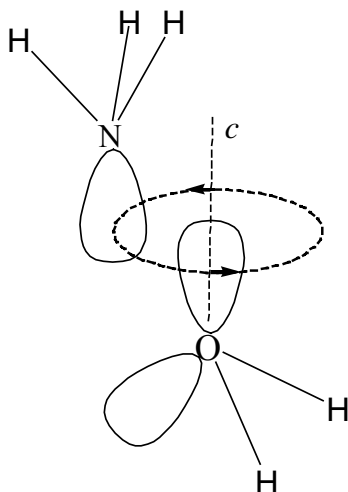
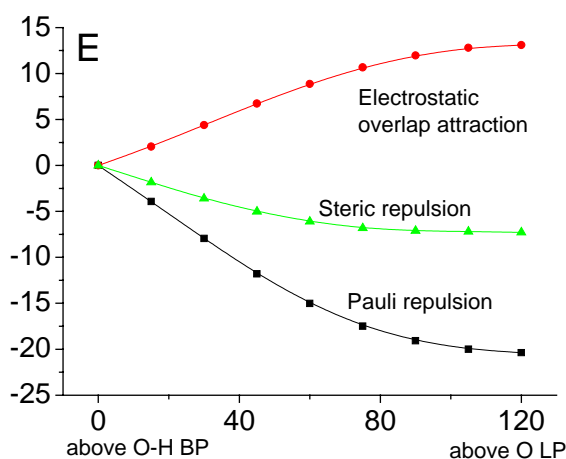
In Fig. 7a (right) the H_2O was replaced by NH_3 and the same calculation was carried out. The values were shown in table 5b and the result is quite similar: above the N-H bonds one gets larger Pauli repulsion and steric interaction than above the lone pairs, see Fig. 8b.

3.3.2. Model System 2: $\text{H}_2\text{O} \cdots \text{NH}_3$

In order to get more direct information about the LP-LP interaction, the He atom in the section above is now replaced by a 'more chemical' species, the backside of NH_3 . The model is sketched in Fig. 9. The NH_3 molecule rotates around the assumed axis c of one H_2O -LP. Thereby the NH_3 -LP touches the other LP, and also the two OH-BPs. (Rotation of NH_3 around an O-H-bond-axis was not investigated, because there would then be a near-coincidence between NH_3 and the other H atom for some dihedral angle.) The calculational procedure is as above.

We have supposed at first that the two OH-BPs and the two O-LPs form an ideal tetrahedron. According to the VSEPR model the LP-LP steric interaction should be the largest, therefore the actual LP-LP angle may be a little larger than 109.5° . We have also tried 120° as the other limit. The calculated steric interactions are quite similar, and the trends are completely the same.

Some typical results are displayed in table 6 and Fig. 10. This is for $r_{\text{N}\cdots\text{O}} = 200$ pm (van der Waals $\text{N}\cdots\text{O}$ distance is about 290 pm, N-O single bond distance is 145 pm) and the angle between N-O and c is 15° . The angle between the two LP is here assumed as 120° . We have also checked various N-O distances and NOH-angles, and again the trends were the same. The consistent result is: NH_3 above the BP gives larger Pauli and steric repulsion than above the LP, neglecting any backwards-tails of the pairs. That is, both the main-lobes and the tail-lobes are relevant. Also the direction of the pair densities is relevant. And the tail of a LP is more significant than the tail of a BP.

Fig. 9 Interaction between N-LP of NH_3 , and OH-BPs and/or O-LPs of H_2O Fig. 10. $\text{NH}_3 - \text{H}_2\text{O}$ interaction energy contributions (E in kcal/mol) versus angle (in degree) along the rotational path of Fig. 9Table 6. Variation of Pauli repulsion E^{Pauli} , electrostatic attraction E^{elst} , and total steric interaction E^{steric} , between NH_3 and H_2O along the rotational path of Fig.9. Meaning of rotation angles N-LP-O-H: 0° N-LP above OH-BP, about $\pm 120^\circ$ N-LP above O-LPs

rot. angle N-L-O-H	0°	15°	30°	45°	60°	75°	90°	105°	120°
E^{Pauli} , kcal/mol	-0-	-3.9	-7.9	-11.8	-15.0	-17.5	-19.1	-20.0	-20.4
E^{elst} , kcal/mol	-0-	2.0	4.4	6.7	8.9	10.7	12.0	12.8	13.1
E^{steric} , kcal/mol	-0-	-1.8	-3.6	-5.0	-6.1	-6.8	-7.1	-7.2	-7.3

3.3.3. Model System 3: Two F_2 molecules

The model is shown in Fig. 11. On the left side one molecule rotates around an axis vertical to the other molecule. The LPs of molecule F(3)-F(4) go through the LPs or the BP of molecule F(2)-F(1). The calculated results are displayed in table 7 and Fig. 12. Neglecting the LP tail, one concludes that the LP-BP steric repulsion is larger than the LP-LP one. However, if we do not decide to ignore the LP tail effect, we must conclude that one near-by LP-tail and one BP are more repulsive than one near-by LP main-lobe and one not-near small BP-tail.

For the model in Fig. 11(right), we get for the shown conformation $E^{\text{Pauli}} = 29.7$ kcal/mol, at 90° rotation 30.8 kcal/mol, and at 180° rotation 59.3 kcal/mol (these values are for $r(F_{(2)}-F_{(3)}) = 200$ pm). It means that (2LP+BP-tail)-(BP+2LP-tail) gives 60 kcal/mol more steric repulsion than (2LP+BP-tail)-(2LP+BP-tail). This means, neglecting the smaller BP-tail contributions, that LP-(BP+2LP-tail) is more repulsive than 2LP-LP.

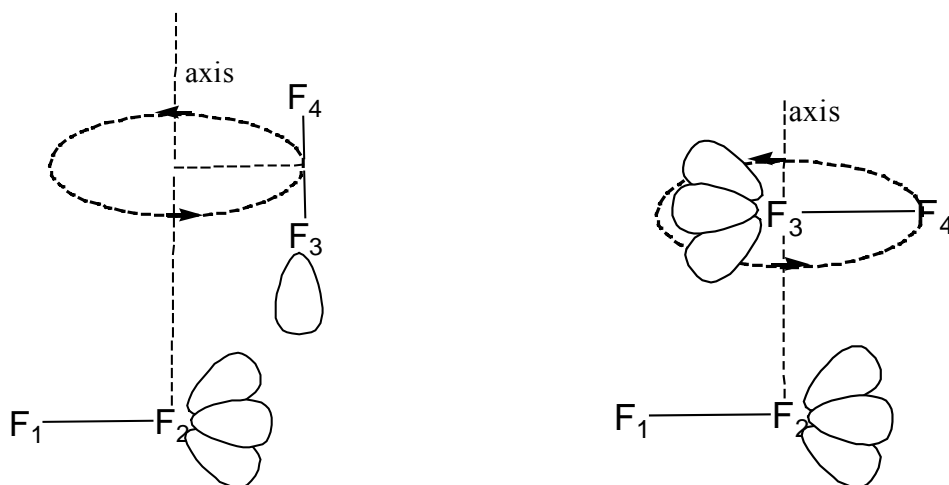


Fig. 11. Interaction of two F_2 molecules

Table 7. Interaction energy contributions in kcal/mol of two F_2 molecules. 0° denotes the conformation in Fig. 11(left), 180° denotes one F_2 above the F-F bond center of the other F_2 . $r(F_{(2)}-F_{(3)}) = 211$ pm, $F_{(2)}F_{(3)}F_{(4)} = 109^\circ$

Rotation	0°	30°	60°	90°	120°	150°	180°
E^{Pauli} in kcal/mol	-0-	-0.32	-1.10	-2.15	-3.61	-5.77	-8.59
E^{elst} in kcal/mol	-0-	0.08	0.31	0.65	1.13	1.81	2.66
E^{steric} in kcal/mol	-0-	-0.24	-0.79	-1.50	-2.48	-3.96	-5.93

3.3.4. Pauli repulsion energy changes and bond expansion during frozen structure internal rotation

The internal rotation of H_2O_2 gives the most direct and simplest example for changes of LP-LP, LP-BP and BP-BP interactions. The H-O and O-O bond lengths and H-O-O bond angles were kept frozen, otherwise we would obtain extremely large contaminations of the pair-interactions by bond-length/angle-energy changes.

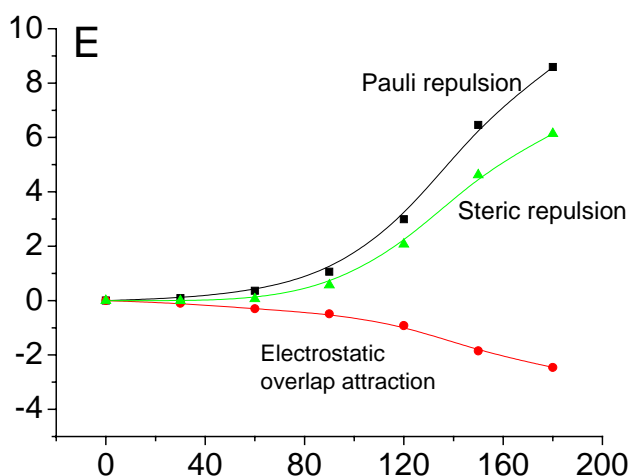


Fig. 12 $F_2 \cdots F_2$ interaction energy contributions E (in kcal/mol) along rotational path of Fig. 11(left)

The calculated Pauli repulsions are displayed in table 8 and Fig. 13. At dihedral angle $\alpha = 0^\circ$ the BP-BP and the two LP-LP contacts are shortest, the Pauli repulsion is highest. The Pauli repulsion decreases for increasing H-O-O-H angle, until it reaches the minimal 110° . From 110° to 180° it increases only very little. The minimum Pauli repulsion also appears near 110° .

Let BB, LL, BL be the repulsion energy between two BPs, between two LPs, and between a BP and a LP, respectively, and γ the rotation angle. The total energy for H_2O_2 is then $E = BB(\gamma) + 2LL(\gamma) + LL(120+\gamma) + LL(120-\gamma) + 2BL(120+\gamma) + 2BL(120-\gamma)$. For the case of trigonal pair arrangement, each interaction can be modeled by $a + b \cos \gamma + c \cos 2\gamma$, with vanishing $d \cos 3\gamma$ term. Then $E = 9 a_{\text{aver.}} + [BB(\gamma) - 2 BL(\gamma) + LL(\gamma)]$. The total repulsion gives an angle-independent sum, and a small angle-dependent difference.

Without considering the effect of the LP-tails, one would expect a large $b \cos \gamma$ term and a small $c \cos 2\gamma$ term. Then it is quite difficult to explain the curves in Figs. 2-6,8,10,13. There are extrema in the curves at 0° and 180° . Additional extrema depend on the relative values of b and c (and d) of the different interactions. The data in table 8 imply $b_{LL} + b_{BB} = 2 b_{BL} + 7.9$ kJ/mol and $c_{LL} + c_{BB} = 2 c_{BL} + 4.7$ kJ/mol. This does not directly determine the order of the coefficients, but is consistent with $B-B < B-L \ll L-L$.

As mentioned, the sum of the 9 pair interactions is not very sensitive to the angles, since some of the angular effects cancel each other. For H_2O_2 (Fig. 2) the absolute bond expansion is about 9 times the bond length changes upon internal rotation. Different systems show different rotational behavior, and systems with bigger expansion have smaller ratio of (variation of bond length expansion upon rotation) / (average total bond expansion), as already mentioned above.

Table 8. Variation of Pauli repulsion upon internal frozen structure rotation of H₂O₂

Angle H-O-O-H	0°	20°	40°	60°	80°	100°	120°	140°	160°	180°
E ^{Pauli} (kcal/mol)	-0-	-1.9	-7.66	-13.11	-16.52	-17.99	-18.21	-17.81	-17.31	-17.08

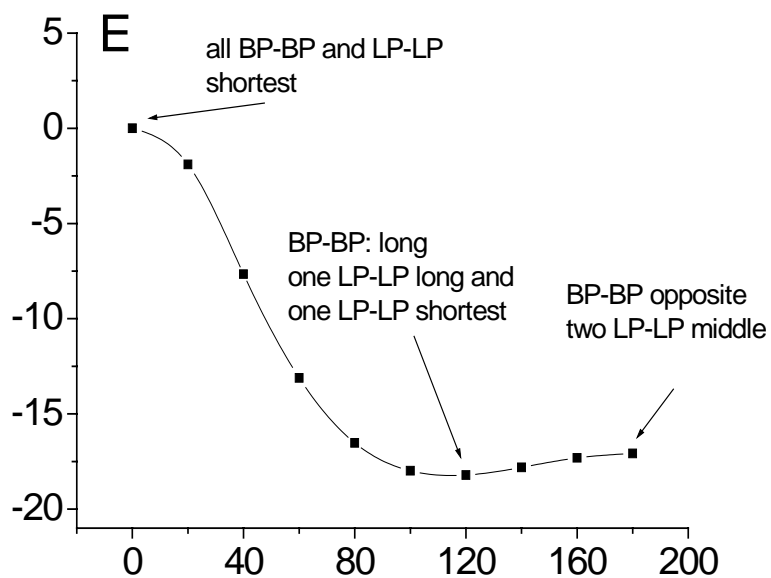


Fig. 13 Pauli repulsion energy E (in kcal/mol) for frozen structure internal rotation of H₂O₂.
 The fit is $E = -13.3 - 7.9 \cos \gamma - 4.7 \cos 2\gamma$; the minimum is at $\cos \gamma = -b/4c$; $\gamma = 115^\circ$

3.4. The actual shape of pair densities

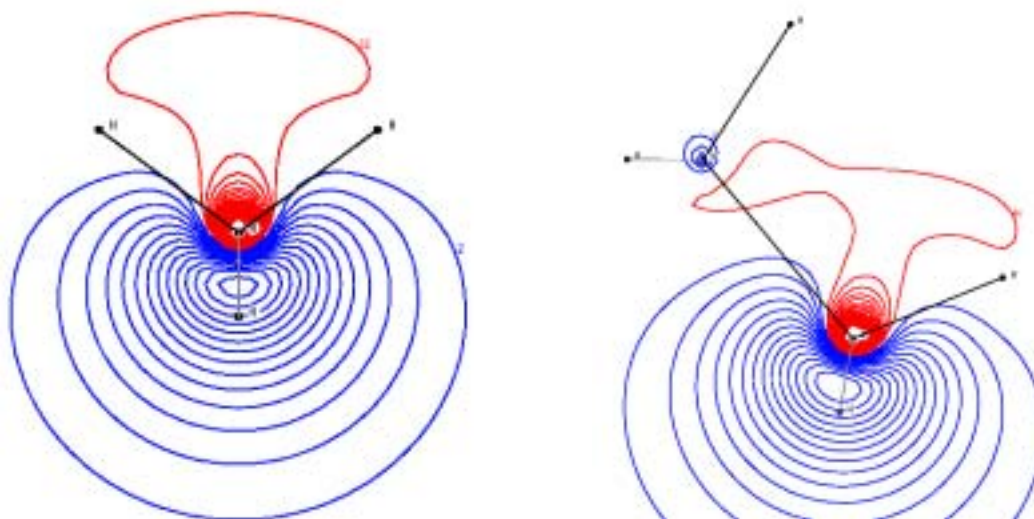


Fig. 14 The actual lone pair of NH₃ (left) and N₂H₄ (right) (much fatter, and has a not so small tail).

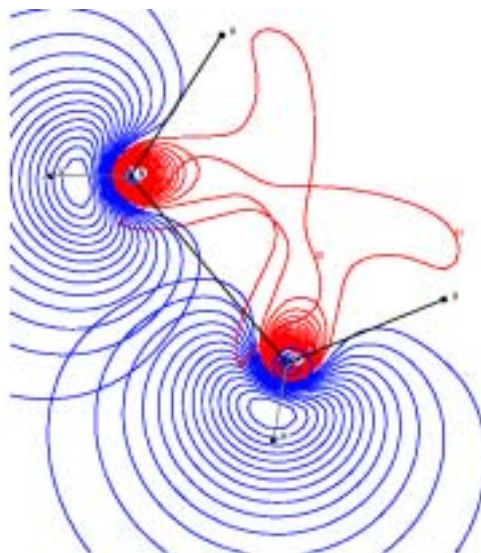


Fig. 15 The overlap of two lone pairs in N_2H_4 . The tails are not so well localized, however we can already see the obvious lobe-lobe overlap and tail-tail overlap.

In section 3 we have shown that both main lobes and tails of electron pair densities play a role. Obviously the sketches of pair densities as given in many common textbooks [27-30] are misleading, they are too slim, and the tails are too small. The actual pairs, in particular the LPs, are much fatter, see Fig. 14. **The tail of the LP plays a very important role if it points towards another pair.** See Fig. 15 concerning the overlap of the tails of two lone pairs in N_2H_4 .

Now the question is, can we find out the numerical magnitudes of the pair-pair effects, in particular its angular dependence, indicating the relative importance of the main pair lobe and its tail, by additional numerical data. It seems that the order of interaction is **main-main > main-tail > tail-tail, corresponding to the order to the above mentioned parameters.** This question will be investigated further in the next section.

3.5. Additional facts about the pair interactions

3.5.1. Calculation of pair overlaps

In this section we characterize the LP-LP, LP-BP, and BP-BP overlaps by the simple expression

$$D_{\mu\nu} = [\sum_{ij} (C_{i\nu} C_{j\mu} S_{ij})^2]^{1/2} \quad (3.5.1)$$

μ and ν are the indices of the localized pair orbitals, $C_{i\nu}$ are the LCAO-MO coefficients, and S_{ij} is the overlap matrix of the basis functions. It is a generalization of the Mulliken formula [36]. Because of the square under the sum, both the positive main lobe and the negative tail contribute positively to the D parameter. Boy's method [31] was selected for the determination of the localized pair orbitals from the delocalized occupied DF orbitals.

Here TZ/dp basis sets were applied for all atoms. In table 9 we list the D values of the H₂O – He model system (Fig. 7a-left) at various contact directions.

Table 9. Localized pair-pair overlap parameters D (eq. 1) of He···H₂O model, Fig. 7a-left

$\gamma(\text{He-H-O-H})$ in $^\circ$	0	30	60	90	120	150	180
He(1s) – O(2LP) D-value	0.254	0.252	0.279	0.282	0.262	0.233	0.219
He(1s) – OH(BP) D-value	0.138	0.130	0.116	0.112	0.123	0.138	0.144

We note that for 0° , i.e. for the middle of two LP tails pointing towards the He, the D-overlap parameter is larger than for 180° , i.e. for the middle of two LP main lobes pointing away from the He. Similarly the bond main lobe pointing away from the He (0°) has a smaller D than the BP tail pointing towards the He (180°). Furthermore, the He/O(LP) overlap parameter is nearly twice as big as the He/OH(BP) one. We note that the middle of two LPs with 120° dihedral angle has the same density as one LP in the middle. The a,b,c angular variation values are $a=0.258$, $b=0.015$, $c=-0.024$, and $a=0.127$, $b=-0.004$, $c=0.015$, respectively. The extremum, i.e. the place between main lobe and tail, is obtained for $\gamma = \arccos(-b/4c)$, i.e. for $\gamma_{\text{LP}} = 81^\circ$ and for $\gamma_{\text{BP}} = 86^\circ$. The respective energy function should have the shape $E = (a_{\text{BP}} + a_{\text{LP}}) + (b_{\text{BP}} - b_{\text{LP}}) \cos \gamma + (c_{\text{BP}} + c_{\text{LP}}) \cos 2\gamma$. We see that all these results are in accord with those of the previous section.

The pair overlap of H₂O₂ have also been calculated for frozen internal rotation. The average LP – LP, LP – BP, BP – BP parameters are listed in table 10. For the 3 upper 2-center terms the a-constants of the Taylor expansion are as above: LP-LP > LP-BP > BP-BP. The b cos γ terms are of the order LP-LP \approx LP-BP > BP-BP. Remarkably, the c-terms for the LPs are small: the LP tails overlap somewhat less than the LP main lobes, but there is no pronounced minimum in between. The LPs are so broad that the node region between the two lobes does not result in an overlap minimum at orthogonal arrangement.

Table 10. Pair- pair overlap parameters D (eq. 1) of H₂O₂

Dihedral angle γ	0°	60°	120°	180°	a	b	c
Average O(LP) – O(LP)	0.154	0.137	0.134	0.119	0.136	0.015	0.001
Average O(LP) – OH(BP) *	0.088	0.115	0.115	0.123	0.112	0.014	-0.006
OH(BP) – OH(BP)	0.114	0.081	0.075	0.088	0.086	0.012	0.015
Average OH(BP) – OO(BP)	0.151	0.149	0.148	0.150			
Average O(LP) – OO(BP)	0.234	0.235	0.235	0.236			

* angle = $180 - \gamma$

The pair overlaps of some other molecules are listed in table 11. In these molecules the situation of the pair interaction is quite complicated, and we will not analyze it in detail. However, the trend is quite clear: the interatomic LP – LP overlap is larger than the BP – BP one. The interatomic LP – BP interaction is usually in between, except for some special angles where one of the overlaps is small.

As shown in table 10, the overlap of the OH(BP) and O(LP) pairs with the OO(BP) is larger than the corresponding interatomic overlap, and the overlap between O(LP)–OO(BP) is larger than that of OH(BP)–OO(BP). However, this type of repulsion is of one center type. It makes the radius of O longer for O bonded to *any* atom. This effect was called ‘half bond weakening’ by Sanderson [33].

Table 11. Calculated pair overlaps of CH₃OH, CH₃F, NH₂OH, NH₂F and HOF

	CH ₃ OH	CH ₃ F	NH ₂ OH	NH ₂ F	HOF
Average LP – LP			0.151	0.153	0.121
Average LP – BP	0.137	0.136	0.133	0.112	0.096
Average BP – BP	0.116		0.091		

Here we have shown that the LP main-lobe is more repulsive than the BP main-lobe, and in §3.3.3 we found that the sum of a non-near BP main-lobe and a near-by LP-tail are more repulsive than the non-near LP main-lobe. All that indicates the importance of the LP-tails, in particular if pointing towards the partner.

3.5.2. *He*⋯*NH*₃ and *He*⋯*CH*₄ models

In §3.5.1 we have shown that the main lobe of a LP gives larger overlap than the BP, and the LP tail, pointing towards the partner, gives a larger overlap than the main LP lobe pointing away from it. The *He*⋯*NH*₃ and *He*⋯*CH*₄ models below will give further evidence about the relative effects of main and tail lobes.

As shown by the curves of Fig. 8b, a He above the middle of two NH bonds and near the tail of the LP gets more repulsion than a He above one NH bond and 60° besides the LP tail; the difference is about 37 kJ/mol. This difference is $\frac{1}{2} b^{\text{Pauli}}_{\text{He-LP}}$. On the other hand, in the case of CH₄ – He (Fig. 16), a He above the middle of two CH bonds gives a smaller repulsion than directly above one CH bond by 9 kJ/mol. This means that 1st, a bond tail is less repulsive than a LP tail, and 2nd, the angle variation of the repulsion of BPs needs higher cosine terms, in particular the $d \cos^3\gamma$ terms vanish for LP-LP and LP-BP but not for BP-BP of ‘trigonal atoms’. The situation has also been investigated for different bond lengths, for different bond angles, for different $r(\text{N-He})$, and for different $r(\text{C-He})$: in all cases **for He above the middle of two NH bonds of NH₃, and for He directly above the**

CH bond of CH₄, the repulsion energy is larger.

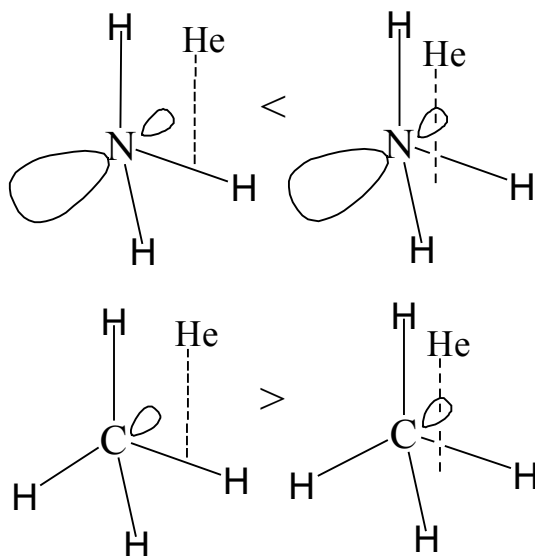


Fig. 16 Model to show the significance of the LP tail. Left: He above a NH bond of NH₃ gives smaller repulsion than between the two NH bonds above the LP tail. Right: He above a CH bond gives larger repulsion. The geometric parameters are the same as in §3.3.1.

Summarizing, a LP main lobe covers about a quarter sterad while a BP main lobe covers less space; and the LP tail is also comparatively spacy while a BP tail has a small repulsive effect. The LP tail seems to give about a few ten kJ/mol more repulsion than the bond main lobe.

3.5.3. Correlation between the number of LP – LP interactions and the bond length expansion

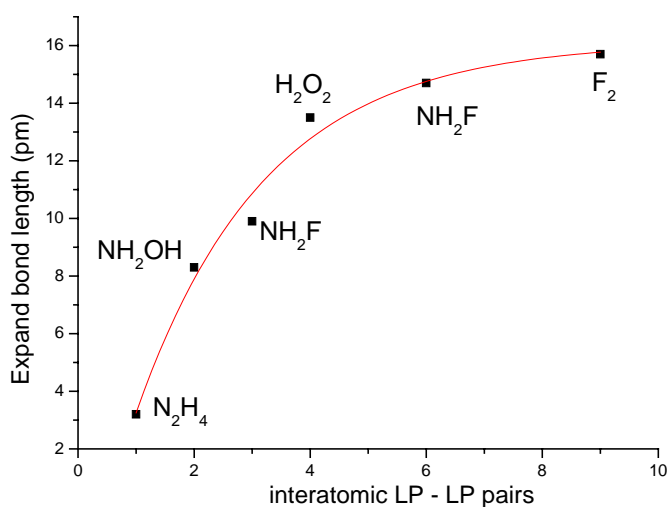


Fig. 17. Exponential fit of bond length expansion versus number of interatomic LP – LP pairs for 2nd row molecules

The number of the interatomic LP – LP pairs is a rough measure of the total LP repulsion. For C₂H₆ and the reference molecules in §3.2 the value is 0, and for N₂H₄, NH₂OH, NH₂F, H₂O₂, HOF, and F₂ the values are, respectively, 1*1=1, 1*2=2, 1*3=3, 2*2=4, 2*3=6, and 3*3=9. The correlation between the bond length expansion and the number of interatomic LP – LP pairs for 2nd and 3rd row molecules is shown in Figs. 17 and 18 with fitting curves. The difference in the curvature between the 2nd and 3rd row species is remarkable. Possibly, this is because 2nd row atoms are harder and therefore large deformations are somewhat weakened. The good correlation between interatomic LP – LP pairs and the bond length expansion shows that the LP repulsion must be an important reason for the bond length expansion.

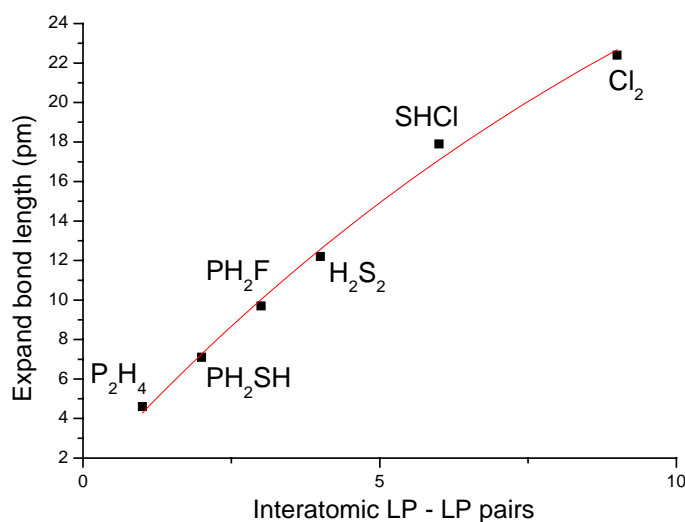
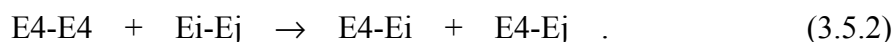


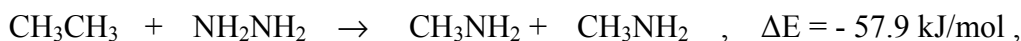
Fig. 18. Exponential fit of bond length expansion versus number of interatomic LP – LP pairs for 3rd row molecules

3.5.4. Correlation between the number of LP – LP interactions and the bond energy weakening

It is known that the bond length expansion goes along with a weakening of the bond energy. Therefore the analysis of bond strengths gives further insight into the origin of the bond length expansion. We define the bond weakening with the help of isodesmic reaction energies,



E_i means an atom from main group *i*, for instance E₄ is C or Si. E₄ atoms usually do not carry LPs and are a good reference for bond energy weakening. We have calculated the energies of reactions of type (2) at the MP2 level. As an example,



i.e. NH_2NH_2 is particularly destabilized. The respective bond weakenings are displayed in table 12. They correlate with the interatomic LP – LP pairs as the bond expansions do. These correlations are shown in Figs. 19 and 20 for the 2nd and 3rd rows. In both cases linear fitting works very well. The results imply that the lone pair repulsion are an important reason of the bond weakening.

Table 12. Bond weakening of 2nd and 3rd row molecules (in kJ/mol).

Molecules of 2 nd row	N_2H_4	NH_2OH	NH_2F	H_2O_2	HOF	F_2
Molecules of 3 rd row	P_2H_4	PH_2SH	PH_2Cl	H_2S_2	SHCl	Cl_2
Interatomic LP – LP pairs	1	2	3	4	6	9
Bond weakening, 2 nd row	58	100	157	194	282	407
Bond weakening, 3 rd row	39	75	118	163	255	376
% 2 nd row	15	18	33	44	56	70
% 3 rd row	13	21	26	37	49	62

3.5.5. Change of energy components upon bond expansion

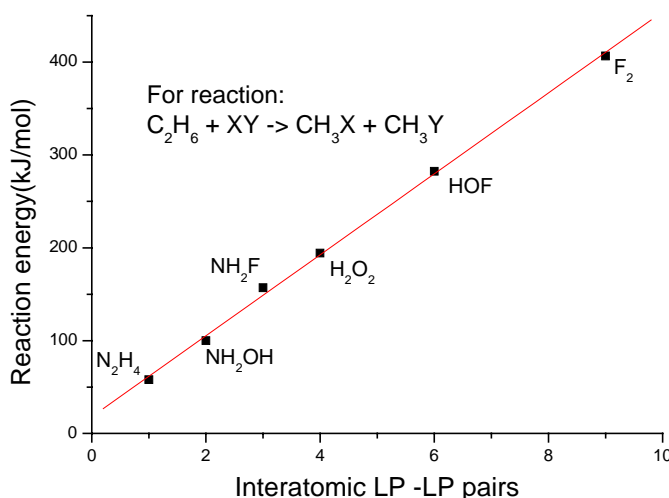


Fig. 19 Linear fit of bond weakening versus number of interatomic LP – LP pairs for 2nd row molecules

The bond length of O-O in H_2O_2 is significantly expanded with reference to CH_3OH and CH_3CH_3 . Its normal expanded, and hypothetically non-expanded bond lengths (at the DF-PW level) are 143 and 133 pm. The normal, non-expanded C-O bond length of CH_3OH is 143 pm. Concerning HOF, its normal, expanded and hypothetically non-expanded OF bond lengths are 142.6 and 129.5 pm, to be compared with CH_3F with ordinary CF bond length of 139.6 pm.

Energy partitioning calculations were carried out with the ADF program using the DF-PW91 approach. The energy derivatives with respect to bond lengths variations were calculated according to:

$$dE^X / dr = 2 (E^X(r_0+0.5\text{pm}) - E^X(r_0)) \text{ in kJ/mol per pm}$$

The results are listed in table 13. In comparison to the reference molecule, the LP-influenced bond shows an enhanced Pauli repulsion while the electrostatic overlap attraction is also a little higher. However the variation of Pauli repulsion with bond length is particularly large, and that means that the Pauli repulsion is the main driving force for the bond expansion.

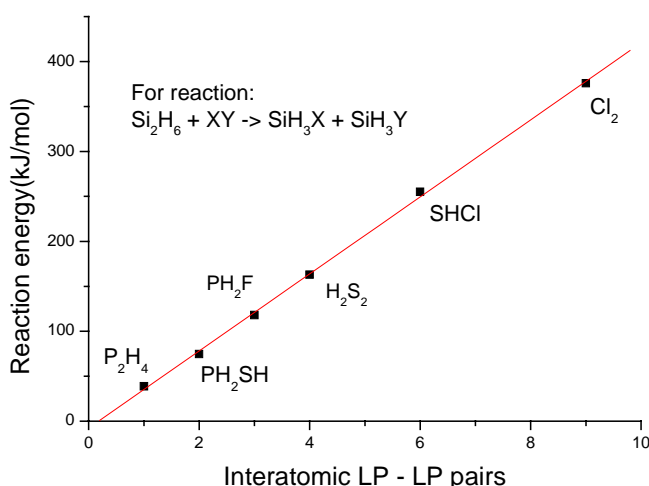


Fig. 20 Linear fit of bond weakening versus number of interatomic LP – LP pairs for 3rd row molecules

Table 13. Pauli, electrostatic, steric and orbital-interaction energy derivatives of several molecules for nonextended bond lengths (in kJ/mol/pm).

	dE^{Pauli}/dr	dE^{elst}/dr	dE^{steric}/dr	dE^{orbital}/dr
H ₂ O ₂ at 133pm (nonexpanded compressed)	89.6	-24.6	65.0	-60.0
CH ₃ OH at 143 pm (normal)	67.4	-17.4	50.0	-50.0
HOF at 129.5 pm (compressed)	94.8	-26.0	68.6	-62.0
CH ₃ F at 139.6 pm (normal)	68.1	-18.0	50.2	-50.2

3.6. Some problems of the LP explanation

In the previous sections the importance of the LP repulsion for the bond length expansion was supported by:

- a) The LPs give larger overlaps than the BPs, according to the overlap calculations.
- b) Near-by LP tails give larger repulsion than more distant LP or BP main-lobes
- c) There is a good correlation between bond length expansion and the number of interatomic LP – LP pairs.
- d) There is a good correlation between bond weakening and the number of interatomic LP – LP pairs.

However, there are still a few difficulties with this explanation:

a) The bond expansion due to LP repulsion of the third row molecules is of similar % as of second row ones. However, the inter-atomic LP repulsions of the third row molecules are expected to be much smaller than those of the second row molecules [1]. For bond lengths it may be because the third row molecules are more “soft”, but the bond energy weakening of the third row molecules is a little smaller than that of the second row molecules, while their bond length expansion is bigger (see table 12).

b) In tables 10 and 11 we have shown some pair overlap parameter values of second row molecules. Now we calculate the total interatomic pairs overlap for H₂O₂, CH₃OH, CH₃F and F₂. There are three pairs in each second row atom, and therefore there are a total of 9 interatomic pair overlaps. The total overlap parameters are listed in table 14, and we see: **CH₃OH has more total pair overlap than H₂O₂, and CH₃F has more than F₂.**

The LP repulsion explanation says that the LP repulsion is the reason for the bond expansion. According to this explanation the expansion occurs to reduce the interatomic pairs repulsion. We see: in F₂ and H₂O₂ the bond expands to reduce the overlap value to its current value, while CH₃OH and CH₃F have larger pair overlaps but do not expand any more. One explanation may be the paradoxical relaxation effect, known for the kinetic energy of covalent bond formation, or for the interelectronic repulsion of singlets and triplets, or for the BP-BP repulsion of staggered and eclipsed ethane (see §2). Another possibility was suggested by Sanderson [33], as mentioned in the introduction.

The overlaps of artificially non-expanded F₂ and H₂O₂ are bigger than for CH₃OH and CH₃F, and one must not say that the latter ones are not expanded: since they are used as reference, one can only say that they are less expanded than more expanded F₂ and H₂O₂. However, we cannot find any relaxation that can explain this problem. Possibly it just because we did not find it, or it may also because the bond expansion is still limited by some other effects.

Table 14. The total interatomic pairs overlap

Molecule	H ₂ O ₂ naturally expanded	H ₂ O ₂ artificially constrained	CH ₃ OH naturally 'halfexpanded'	F ₂ naturally expanded	F ₂ artificially constrained	CH ₃ F naturally 'halfexpanded'
Total overlap	1.071	1.349	1.170	1.069	1.527	1.224

What is the reason for these problems of logic? May be there indeed exists still another contribution to the bond expansion phenomenon? The additional factor makes the molecule expand further, and makes the pairs overlap of H_2O_2 and F_2 smaller than those of CH_3OH and CH_3F . The other one or more factors should have the following characters:

- a) It cannot change significantly during the internal rotation – in this sense it is similar to 3-pair/3-pair repulsion. One gets a quite small variation of bond expansion during the internal rotation.
- b) The additional effect should be similar for second and third row molecules, thereby it helps to explain the similar %age expansion of the second and third row molecules.
- c) The other factor(s) must also be of two-centric type, similar to the pair-pair repulsion effect.
- d) The other factor(s) should show good correlation with geometric bond expansion and energetic bond weakening, again as the pair-pair repulsion effect.

The mechanism unknown to Sanderson [33] might be the hybridization of the bonded atoms. We will discuss it in detail in the next section. This will be a somewhat difficult task, because at the moment we do not see an obvious criterion to distinguish between the two effects. During the numerical analysis we must try to find out whether hybridization and pair-repulsion are two independent effects, or only two sides of one complex phenomenon.

3.7. Hybridization effects

With hybridization effect we mean that the existence of a LP on an atom causes a change of the s-p mixture of the bond-forming AOs with respect to the case of no one-center LP and only two-center BPs on that atom.. We will investigate this point with the help of NBO analyses (using the pop=NBO keyword of Gaussian 98). We use the B3LYP-DF approach, with extended 6-311g(2df,pd) basis sets.

In tables 15 and 16 we list the calculated hybridizations of 2nd and 3rd row molecules. The correlations of the s-AO contributions with the bond expansions are shown in Figs. 21 and 22. In both cases linear fitting works well. This implies that the hybridization can also be taken as a reason of bond expansion. The AO hybridization highly depends on the other bonded atom(s), and therefore hybridization is a two-centric factor. Of course: s-p promotion costs energy, this can only be obtained by more efficient two-center bonding through better hybridized AOs. The hybridization effect gives rather similar results for second and third row molecules. So it shows that the LP-BP-rehybridization effect and the LP-LP' Pauli-repulsion effect are more likely two independent effects.

Table 15. s -AO participation in the $s^x p^{1-x}$ hybrids of N,O,F in the A-B bond orbitals of 2nd row molecules

N	x	O	x	F	x
N-C of CH ₃ NH ₂ :	0.322	O-C of CH ₃ OH:	0.296	F-C of CH ₃ F:	0.212
N-N of NH ₂ NH ₂ :	0.263	O-N of NH ₂ OH:	0.183	F-N of NH ₂ F:	0.146
N-O of NH ₂ OH:	0.178	O-O of H ₂ O ₂ :	0.120	F-O of HOF:	0.088
N-F of NH ₂ F:	0.136	O-F of HOF:	0.080	F-F of F ₂ :	0.055

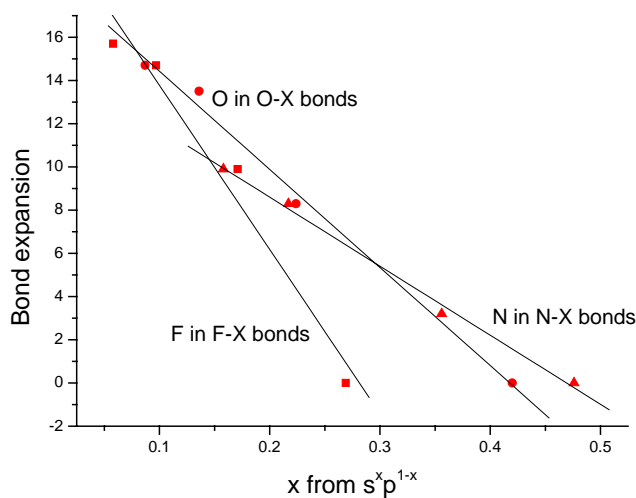
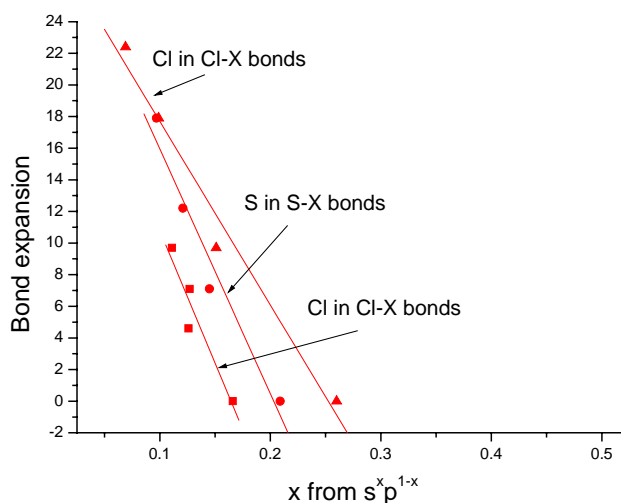
Fig. 21 Correlation between s contribution in the bond hybrid AO and bond expansion for 2nd row molecules. The bonding mate X is C, N, O, or F.Fig. 22 Correlation between s contribution in the bond hybrid AO and bond expansion for 2nd row molecules. The bonding mate X is Si, P, S, or Cl

Table 16. s-AO participation in the $s^x p^{1-x}$ hybrids of P,S,Cl in the A-B bond orbitals of 3rd row molecules

P	S	Cl
P-Si of SiH ₃ PH ₂ : 0.142	S-Si of SiH ₃ SH: 0.173	Cl-Si of SiH ₃ Cl: 0.206
P-P of PH ₂ PH ₂ : 0.112	S-P of PH ₂ SH: 0.127	Cl-P of PH ₂ Cl: 0.131
P-S of PH ₂ SH: 0.113	S-S of H ₂ S ₂ : 0.108	Cl-S of HSCl: 0.090
P-Cl of PH ₂ Cl: 0.100	S-Cl of HSCl: 0.088	Cl-Cl of Cl ₂ : 0.065

3.8. Summary

2nd and 3rd row molecules with single bonds between atoms, which both carry lone pairs, show the phenomenon of particularly long and weak bonding. With reference to an additive increment scheme, the bond lengths are expanded up to 20 pm or up to 10 %, and the bond energies are weakened up to 400 kJ/mol or 70 %. These effects correlate well with the product of the numbers of lone pairs on the two bonded atoms. The explanation through particularly large LP-LP repulsion has been supported here and it explains, why the effect is large, but varies only little with single bond rotation. An important point in this context is that any localized orbital in a polyatomic molecule has a main lobe and a backside tail. That tail is particularly large for lone pair orbitals. It is a pity that most introductory and advanced textbooks communicate a quite misleading impression of the shape of localized orbitals: the sketches of the pair lobes are not images of reality but only slim symbolic ciphers. The sketches of the tails (if not neglected at all) are too small in comparison to the main lobe; and the main lobe is too narrow. The importance of tail-tail interaction has here been proven numerically. An important aspect is also the direction of the pairs. In addition we have given hints that the nonlinear two-center dependence of bond length and strength on the hybridization of the bond-forming AOs contribute in the same direction as the LP-LP Pauli repulsion.

Summarizing, the bond expansion is caused by two factors with similar tendencies: a) the interatomic LP-LP repulsion, b) the interatomic bond weakening between two atoms with high-p bond-AO due to absorption of the s-population by the LPs at the same center. At the moment we have no idea of the %age contribution of the two mechanisms in the phenomenon of bond expansion.

References

- [1] L.Pauling, *The nature of the chemical bond*, 3rd Ed., Cornell University Press, Ithaca NY, **1960**.
- [2] W.L.Jolly, C.J.Eyermann, *Inorg. Chem.*, **1983**, 22, 1566.
- [3] C.E.Housecroft, A.G.Sharpe, *Inorganic Chemistry*, Prentice Hall, Harlow, **2001**.
- [4] D.F.Shriver, P.W.Atkins, *Inorganic Chemistry*, 3rd Ed., Oxford University Press, Oxford, **1999**.
- [5] L.E.Forslund, N.Kaltsoyannis, *New J. Chem.*, **2003**, 27, 1108.
- [6] R.J.Gillespie, R.S.Nyholm, *Quart. Rev.*, **1957**, 11, 339.
- [7] R.J.Gillespie, I. Hargittai, *The VSEPR Model of Molecular Geometry*, Allyn and Bacon, Boston, **1991**.
- [8] M.Kaupp, *Angew. Chem. Int. Ed.*, **2001**, 40, 3534.
- [9] D.E.Goldberg, *Fundamentals of Chemistry*, McGraw-Hill Science, New York, NY, **1996**.
- [10] K.S.Pitzer, *J. Chem. Phys.*, **1955**, 23, 1735.
- [11] G.L.Caldow and C.A.Coulson, *Trans. Faraday Soc.*, **1962**, 58, 633.
- [12] R.S.Mulliken, *J. Am. Chem. Soc.*, **1955**, 77, 884.
- [13] M. Kaupp, Ch.van Wüllen, R.Franke, F.Schmitz, W.Kutzelnigg, *J. Am. Chem. Soc.*, **1996**, 118, 11940.
- [14] R.Ahlrichs, et al., *TURBOMOLE 5.5*, University of Karlsruhe, Germany, **2002**.
- [15] L.V.Vilkov, V.S.Mastryukov, N.I.Sadova, *Determination of the Geometrical Structure of Free Molecules*, Khumuya, Moscow **1978**, engl. translation Mir, Moscow, **1983**.
- [16] G.Herzberg, *Electronic spectra and electronic structure of polyatomic molecules*, Van Nostrand, New York NY, **1966**.
- [17] E.Herbst, J.K.Messer, F.C.DeLucia, *J. Mol. Spect.*, **1984**, 108, 42.
- [18] J.Demaison, J.Breidung, W.Thiel, and D.Papousek, *Struct. Chem.*, **1999**, 10, 129.
- [19] M.Tsuboi, J.Overend, *J. Mol. Spec.*, **1975**, 52, 256.
- [20] L.V.Gurvich, I.V.Veyts, C.B.Alcock, *Thermodynamic Properties of Individual Substances, 4th Ed.*, Hemisphere, New York, NY, **1989**.
- [21] R.L.Redington, W.B.Olson, P.C.Cross, *J. Chem. Phys.*, **1962**, 36, 1311.
- [22] K.P.Huber, G.Herzberg, *Molecular Spectra and Molecular Structure. IV. Constants of Diatomic Molecules*, Van Nostrand Reinhold, New York, NY, **1979**.
- [23] M.J.Frisch et al., *Gaussian 98, Revision A.9*, Gaussian Inc., Pittsburgh PA, **1998**.
- [24] G.R.Gupte, R.Prasad, *Int. J. Mod. Phys. B*, **1998**, 12, 1607.
- [25] K.H.Hellwege, A.M.Hellwege Ed., *Landolt-Bornstein: Group II: Atomic and Molecular Physics Volume 7: Structure Data of Free Polyatomic Molecules*, Springer-Verlag, Berlin, **1976**.
- [26] J.Behrend, P.Mittler, G.Winnewisser, K.M.T.Yamada, *J. Mol. Spec.*, **1991**, 150, 99.
- [27] H.A.Staab, *Einführung in die Theoretische Organische Chemie*, Verlag Chemie, Weinheim, **1960**.
- [28] P.Atkins, J.Paula, *Physical Chemistry, 7th Ed.*, Oxford University Press, Oxford, **2001**.
- [29] J.D.Lee, *Concise Inorganic Chemistry, 4th edition*, Chapman & Hall, London, **1991**.

- [30] J.C.Bailar, T.Moeller, J.Kleinberg, C.O.Guss, M.E.Castellion, C.Metz, *Chemistry*, Academic Press, New York, NY, **1978**.
- [31] T.Ziegler, A.Rauk, *Theor. Chim. Acta.*, **1977**, 49, 143.
- [32] E.J.Baerends et al., *ADF Program System, Release 2002.02*, Scientific Computing & Modeling, Vrije Universiteit, Theoretical Chemistry, Amsterdam, **2002**.
- [33] R.T.Sanderson, *Polar Covalence*, Academic Press, New York, NY, **1983**.
- [34] R.J.Gillespie, P.L.A.Popelier, *Chemical Bonding and Molecular Geometry From Lewis to Electron Densities*, Oxford University Press, New York, NY, **2001**.
- [35] G.Frenking, *Angew. Chem. Int. Edit.*, **2003**, 42, 143; *Angew. Chem. Int. Edit.*, **2003**, 42, 3335.
- [36] S.G.Wang, W.H.E.Schwarz, *J. Am. Chem. Soc.*, **2004**, 126, 1266.

Appendix I.

Introduction to VSEPR (Valence Shell Electron Pair Repulsion) Model

General

One of the more obviously important properties of any molecule is its shape. Clearly it is very important to know the shape of a molecule if one wants to understand its reactions. It is also desirable to have a *simple* method to *predict* the structures of compounds. For main group compounds, the VSEPR method is such a predictive tool and is unsurpassed as a handy predictive method. It is a remarkably simple device that utilizes a simple set of electron accounting rules in order to predict the shapes. Organic molecules are treated just as successfully as inorganic ones. The assumptions and simplifications required by the method as outlined here should not encroach too far into descriptions of bonding: It is enough that the shapes of molecules are successfully predicted.

Application of the VSEPR method requires some strongly simplifying assumptions about the nature of bonding. Despite this, the correct structure is quite well approximated in many cases. In a complete analysis of the structure of a molecule it would be necessary to consider such factors as nuclear-nuclear interactions, nuclear-electron interactions, and electron-electron interactions, and the quantum-dynamical behavior of the electrons. In the VSEPR method outlined here it is *assumed* that the structure of a molecule depends *only* upon electron-electron interactions.

Some information is also needed before one can successfully apply the VSEPR rules. The connectivity of the atoms in the molecule must be known; in other words, one needs to know which atoms are bonded together. For instance, does the empirical formula C_2H_6O refer to MeOMe or to EtOH? It is also necessary to write down a Lewis electron dot structure for the molecule, but it will emerge that one can sometimes use a simplified Lewis structure.

Assumptions about the nature of the bonding

The underlying assumptions made by the VSEPR method are the following.

Atom pairs in a molecule are bound together by electron pairs. These are called *bonding pairs*. More than one set of bonding pairs of electrons may bind any two atoms together (multiple bonding). However, polycentric bonds such as in benzene, in the boranes, or in some metal halides are not considered.

Some atoms in a molecule may also possess pairs of electrons not involved in bonding. These are called *lone pairs* or *non-bonded pairs*.

The bonding pairs and lone pairs around any particular atom in a molecule adopt positions in which their mutual interactions are minimized. The logic here is simple. Electron pairs are negatively charged and will get *as far apart from each other as possible*. There are, however, two serious problems. It is well known from quantum mechanics that quantum

mechanical dynamics of the electrons is the all-dominating factor. Orthogonality of localized orbitals (LO) results in kinetic energy rise if the LOs overlap. So-called Pauli repulsion is more important than Coulomb repulsion, both factors play their roles. Second, Pauli repulsion is somewhat directional, depending of the shape and nodes of the LOs, while Coulomb repulsion is spherically symmetric.

The two basic rules of the VSEPR model are:

Lone pairs occupy more space than bonding electron pairs.

The 2 pairs of a double bond occupy much less space than to be expected, but still more than a single bond.

Structure predictions:

At first we should know the most favorable arrangement for any given number of electron pairs surrounding any particular atom. These arrangements are found using simple geometrical constructions. This involves placing the nucleus of the atom in question at the center of a sphere and then placing the electron pairs on the surface of the sphere so that they are as far apart as possible. The resulting arrangements are intuitively obvious.

VSEPR structures

<u>Electron pairs</u>	<u>Structure</u>
2	linear
3	trigonal planar
4	tetrahedral
5	trigonal bipyramidal
6	octahedral

For the case of just two electron pairs, the arrangement is simple and the minimum energy configuration is when the electron pairs form a linear arrangement with the nucleus. In this configuration the electron pair-nucleus-electron pair angle is 180° . The coordination structure of the central atom is described as *linear*.

Three electron pairs arrange themselves *trigonally*, that is with bond angles of 120° . For four electron pairs, one expects the *tetrahedral* structure with 109.5° bond angles. Nevertheless, there are cases (e.g. ML_4 from group 10) where a square-planar structure is preferred, although the smaller bond angles of 90° should yield more pair-pair repulsion in the square-planar than in the tetrahedral structure.

The case of five-coordination is a little trickier. Most molecules whose shape is determined by five electron pairs are *trigonal bipyramidal*. There are two chemically non-equivalent positions in a trigonal bipyramid, axial and equatorial. There is also another very reasonable candidate, and that is the square-based pyramid. In effect, this arrangement is

an octahedron in which one group is removed and in which the four adjacent groups move down slightly to partially occupy the resulting vacancy. In practice, this structure is only a little disfavored relative to the trigonal bipyramid. Therefore the occurrence of this structure is only a little serious defect of the VSEPE rule. The square-based pyramidal structure is very important in the interconversion of axial and equatorial positions in trigonal bipyramids (so-called pseudo-rotation).

For six-coordinate systems, the *octahedral* structure is by far the most important. An alternative structure, the trigonal prism, is less frequent, as are distorted octahedral structures. On the other hand, for systems with 7 valence pairs, the VSEPR model predicts distorted octahedral structures, while regular octahedral are also not uncommon.

One Example: NH₃

Ammonia has four electron pairs around the N and the *coordination structure* of nitrogen is derived from a *tetrahedral* arrangement. Since the lone pairs are 'invisible' (i.e. not easily detectable by x-ray methods, for instance), the *shape* of ammonia is *pyramidal*. (This holds, at least, for NH₃ frozen by environmental perturbations, e.g. in solution, while in the gas phase the structure is trigonal D_{3h} with the protons split by the inversion vibration).

Consider a bonding pair of electrons. The two electrons are located between two nuclei, and are attracted by both. A lone pair is different. It is only attracted to one nucleus and the consequence is that it adopts a position effectively *closer* to that one nucleus than the bonding pairs of electrons. Commonly the following classical argument is given, which gives the right answer for the wrong reason, an explanation strategy quite common in real chemistry. A classical electron cloud nearer to the nucleus gives an effective solid angle *greater* than that occupied by a bond pair. Lone pairs demand greater angular room, and are located closer to their atoms than bond pairs. A better explanation would discuss the s-p-d hybridization of the bond and lone pairs. In the present case the result is the same (in the case of 6 or 7 pairs, the classical argument works less well). The consequence of this for ammonia is that the lone pair makes room for itself by pushing the three hydrogen atoms a little together, and the H-N-H bond angles are slightly less (106.6°) than the ideal tetrahedral angles of 109.5°.

Appendix II. Calculation Details

II.1 Computational methods

Three different computational methods were used in this work. The method was selected based on their functionality and convenience for different studied objects. These three methods are:

- 1) Self-consistent field ab initio Hartree-Fock with 2nd order perturbation theoretical correction for electron correlation according to Møller and Plesset (SCF-MP2-RI)

- 2) Self-consistent field Kohn-Sham with density functional correction for electron correlation according to Perdew and Wang (PW91)
- 3) The intermediate hybrid method of Becke with 3 mixing parameters for Hartree-Fock exchange and Lee-Yang-Parr's density functional (B3LYP)

Three different types of one-particle basis sets were applied:

- 1) Gaussian triple-zeta type valence functions with double polarizing sets from Karlsruhe (TZVPP)
- 2) Slater triple-zeta type valence functions with double polarizing sets from Amsterdam (TZ& 2df/pd)
- 3) Gaussian triple-zeta type valence functions with double polarizing sets from Pittsburgh (6-311&2f/pd)

The respective commercial program codes, which allow the combination of the mentioned method with the mentioned basis set, are the following:

- 1) TURBOMOLE from Ahlrichs et al. (speeding up the two-electron part by the 'resolution of identity approximation' RI) for most structure optimizations and energy calculations
- 2) ADF from Baerends et al. for bond energy partition calculations
- 3) GAUSSIAN from Frisch, Pople et al. for the curves of internal rotation

AII.1.1. RI-MP2/TZVPP in TURBOMOLE

- [1] M.Feyereisen, G.Fitzgerald, A.Komornicki, *Chem. Phys. Letters*, **1993**, 208, 359.
 [2] F.Weigend, M.Häser, *Theor. Chem. Acc.*, **1997**, 97, 331.
 [3] F.Weigend, M.Häser, H.Patzelt, R.Ahlrichs, *Chem. Phys. Letters*, **1998**, 294, 143.

Resolution of the identity (RI) is a new method, which dramatically reduces the memory requirements for larger systems by approximating four-center integrals as products of three-center integrals. It is a highly efficient method, since it involves only a distributed matrix multiplication [1,2,3]. The TZVPP basis sets used are rather large. They are state of the art sets for reliable routine calculations. The typical input for such a calculation consists of four files: control, basis, coord, mos. "Control" steers the whole calculation. "Basis" specifies the basis sets. "Coord" specifies the starting structure coordinates of the molecule to be calculated, cartesian or so-called z-matrix. "Mos" give starting MOs for the SCF iterations. For simple problems, the guess made internally by the program is already sufficient. These files were prepared with the help of the "define" program.

The input files are designed with the help of routine "define". Then the DSCF is using for a SCF calculation or RIDFT for the RI-DFT calculation. For RI-MP2 calculation, after the DSCF calculation the "rimp2prep" routine is used to prepare the input for the RI-MP2

calculation. The default parameters were selected. For H₂O₂, the 1a and 1b core orbitals (energy: -20.63 a.u.) were kept frozen. Then with the routine “rimp2” one do the RI-MP2 calculation. The geometry optimization is carried out by the routine “jobex” with give parameters.

AII.1.2. B3LYP/6-311(2df,pd) in GAUSSIAN

This method is nowadays widely used by ordinary chemists in quantum chemical calculations, therefore we will here not give any further explanation. In this work we use this method to calculate the curves of internal rotation. The following is an example for the input of H₂O₂.

```
%mem=20000000
#p b3lyp/6-311g(2df,2pd) popt=z-matrix
```

```
H2O2
```

```
0 1
```

```
O
```

```
O 1 a1
```

```
H 1 a2 2 b1
```

```
H 2 a2 1 b1 3 0.0
```

```
a1=1.44
```

```
a2=0.97
```

```
b1=106.0
```

The dihedral angle 0.0° was then replaced by 20.0°, 40.0°, 60.0° ... 180.0° to get the curve. In principle the keyword SCAN can automatically generate the curve in one calculation. However, it requires that the symmetry of the molecules does not change for all angles studied.

AII.1.3. PW91/TZ(2f,pd) in ADF

This is also a widely used method and we will not explain it at here. We use our Model 1 of §2.1 (the interaction between H₂O and He) to show the procedure. First one must create the atoms using create keyword. Then the geometry H₂O molecules are optimized. The TAPE21 file is saved as t21.H2O. The following is the input to calculate the interaction between H₂O and He.

```

$ADF <<EOF
  title interaction between H2O and He
  xc
  gga PW91
  end
  symmetry Nosym

  ATOMS Z-Matrix
  1. O 0 0 0 f=f1
  2. H 1 0 0 0.9691 f=f1
  3. H 1 2 0 0.9691 104.54 f=f1
  4. XX 1 3 2 1.5 104.54 0.0
  5. He 4 1 3 0.8 90.0 c1
  END
  geovar
  c1=0.0
  end
  integration 5.0
  FRAGMENTS
  f1 t21.H2O
  He t21.He.V
  END
endinput
EOF
rm [A-Z]* logfile

```

By varying the c1-angle from 0 to 180, we get the results presented in §2.1.

AII.2. The reliability of these three methods

The QCISD configuration-interaction method with a Gaussian 6-311(2df,pd) basis was used as the reference to evaluate the reliability of other methods. The bond lengths, bond angles, dihedral angles and reaction energies were compared, and the results are shown in tables 1-3.

Concerning the bond lengths, both B3LYP and RI-MP2 give results very similar with QCISD. The average deviation for both cases is 0.4 pm, and the largest deviation for B3LYP is 1.1 pm, for RI-MP2 is 1.3 pm. For PW91, the average deviation is 1.2 pm, and the largest one is 2.9 pm. The calculated bond length expansions are in the range of 3.2 – 22.4 pm, and most of them are larger than 8 pm. That is, for all three methods the uncertainties are significantly smaller than the effect to be described, they are accurate

enough to evaluate the bond length expansion. In particular, B3LYP and RI-MP2 give the most reliable results. Therefore the values and the curves of bond length expansion have in this work all been determined by RI-MP2 and B3LYP.

For the bond angles and dihedral angles all three methods give good results. The only exception is the PW91 calculation of the delicate and soft dihedral angle of H-O-O-H in H₂O₂, where the deviation is 5.5°. All other deviations are less than 1°, and the average deviations are less than 0.5°.

Concerning the calculated reaction energies, the average deviation for all three methods are about 10 kJ/mol. The bond strength weakening studied in this work is about 40-400 kJ/mol, therefore all three methods are reliable, especially RI-MP2 and B3LYP. The PW91 method, used to evaluate the interaction energy components, is also accurate enough for the studied systems.

Table 1. Calculated bond lengths (in pm).

Molecules	QCISD	B3LYP	RI-MP2	PW91
H ₂ O r(O-H)	95.8	96.2	95.9	96.9
H ₂ O ₂ r(O-O)	143.8	144.9	145.1	146.7
r(O-H)	96.2	96.6	96.4	97.5
CH ₃ OH r(C-O)	141.3	141.7	142.0	143.1
r(C-H)	109.3	109.4*	108.9*	109.9*
r(O-H)	95.8	96.1	95.9	96.8
C ₂ H ₆ r(C-C)	152.5	152.6	152.4	153.1
r(C-H)	109.2	109.2	108.8	109.8
H ₂ S ₂ r(S-S)	207.4	208.1	206.4	
r(S-H)	133.9	134.9	133.8	
Average deviation	-0-	0.4	0.4	1.2

* Average value of the three C-H bonds.

Table 2. Calculated dihedral angles

Molecules	QCISD	B3LYP	RI-MP2	PW91
H ₂ O ₂ H-O-O-H	115.6°	116.6°	115.3°	110.1°
CH ₃ OH H-O-C-H	61.4°	61.5°	61.4°	61.5°
H ₂ S ₂ H-S-S-H	90.3°	90.6°	90.6°	
Average deviation	-0-	0.5°	0.2°	2.8°

Table 3. Calculated bond angles

Molecules	QCISD	B3LYP	RI-MP2	PW91
H ₂ O H-O-H	103.6°	104.0°	103.8°	104.5°
H ₂ O ₂ H-O-O	100.0°	100.2°	99.4°	100.0°
CH ₃ OH H-O-C	107.4°	108.1°	107.7°	107.5°
H-C-O	110.6°	110.6°*	110.3°*	110.4°*
C ₂ H ₆ H-C-C	111.3°	111.4°	111.2°	111.5°
H ₂ S ₂ H-S-S	98.1°	98.5°	97.8°	
Average deviation	-0-	0.3°	0.4°	0.3°

* Average value of the three H-C-O angles.

Table 4. Calculated reaction energy (in kJ/mol)

Reaction	QCISD	B3LYP	RI-MP2	PW91
H ₂ O ₂ +C ₂ H ₆ -> 2CH ₃ OH	-184.6	-176.7	-194.3	-171.8

4. Reduced nonbonded distances

4.1. Introduction

4.1.1. The empirical approach

A particularly important piece of information on a chemical substance is its structural specification. The interatomic distances indicate the interatomic interaction and the chemical reaction possibilities. Effective atomic radii R^{eff} are widely used with considerable success in the chemical sciences to estimate and to systematize the experimentally determined interatomic distances by an additive increment scheme [1]. Different types of radii sets are used for different assumed types of interactions between the atoms. Accordingly there are covalent, ionic, bonded and non-bonded radii etc. The latter ones are often called van der Waals radii. Furthermore different authors have suggested somewhat different numerical values for those radii [2,3,4]. This is naturally and necessarily so because chemical bonds are, for instance, not either purely covalent or purely ionic, but each bond is a specific example from a multidimensional continuum of bond types.

Generally speaking, the vibrationally and librationaly averaged distances r_{AB} between *two atoms* A,B in a *poly-atomic* system are multiparameter functions (see Fig. 1),

$$r_{AB} = f(A, B, \text{ligands of A and B, type of interaction between A and B}) . \quad (4.1.1)$$

However, they can, though only approximately, be represented by sums of *mono-atomic* increments,

$$r_{AB} \approx R_A^{\text{eff}} + R_B^{\text{eff}} . \quad (4.1.2)$$

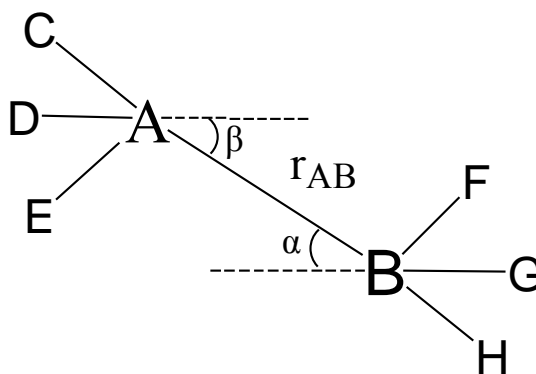


Fig. 1. The interatomic distance $r_{AB}(C,D,E; F,G,H; \alpha, \beta)$.

The first set of atomic radii was suggested by Bragg in 1920 [5] to reproduce the interatomic distances in several hundred crystals. In 1927, Pauling [6,7] proposed the first rather complete set of atomic radii which is still widely used [2]. The values of the effective radii depend sensitively on the atom's coordination number, and Pauling's radii were originally derived for coordination number 6. The atomic radii sets proposed by Biltz [8], and the ionic radii of Shannon et al. [9,10] are also widely used. In 1964 Bondi [3] refined the van der Waals radii using improved x-ray diffraction results.

$$R_{AB} \approx \sum_i^{A,B} R_i(\text{charge, valence state, coordination number}) \quad (4.1.3)$$

The assumption of spherical atomic shapes was studied by Zefirov and Porai-Koshits [11], by Row and Parnathy [12], and by Nyburg and Faerman [13]. It was found that the bond angles (α and β in Fig. 1) can significantly affect the effective atomic radii, and that the atomic shapes in molecular environment are better described as elliptical.

The partitioning of a diatomic parameter R_{AB} into a sum of monoatomic increments is not unique in principle. Accordingly the definition of an ‘ionic radius’ has been formulated by many different strategies, see for instance [2,13]. Gourary and Adrian’s work [14] shows a tendency of cations being smaller, and anions being larger, than the conventional radii, the deviations being up to 0.2 Å, what had already been recognized by Slater in 1964 [15]. In line with these results, Narayan’s [16] cation radii were smaller and anion radii were larger than those of Pauling. All these studies show that the effective radii are strongly dependent on the molecular environment, and on the recipe of construction of the radii parameters in eqs. (4.1.2).

4.1.2. Theoretical improvements

So far we have reviewed the numerical analysis of a broad amount of experimental data, dominantly of X-ray crystallographic type. They were used to construct a set of R_A values for equation (1.3). In order to improve on the quality and reliability of eq. (1.3) and on the results obtained therefrom, theoretical data should be included and the partitioning of observable R_{AB} data should be performed on the background of a deeper theoretical insight. Badenhoop and Reinhold [17] have employed their natural steric analysis to extract a set of effective radii for atoms H to Ar from ab-initio calculations using the approach of a helium probe to define the radii. In particular they investigated the dependence of the radii on the charge state and the directional anisotropy of the electron density.

4.1.3. The phenomenon of reduced distances

Particularly in the field of heavy element chemistry it is not unusual to find interatomic distances between atoms which are formally unbonded to each other according to the Lewis model with whole range of values more or less smaller than the sum of conventional van der Waals radii.

Recently, Zefirov [18] gave a detailed review about this topic and summarized the reduced ‘nonbonded’ contact distances between C, N, O, S, Se, Te, F, Cl, Br, I. This work was based on experimental results. Conventionally reduced intermolecular contacts are assumed to indicate some specific attractive interaction that is competitive to the steric repulsion of occupied atomic shells, but weaker than normal covalent bonds. The specific interactions may be of various origins, such as electrostatic interaction, weak covalent ‘secondary’ interaction, or London dispersion. So far it was common in chemistry to discuss such ‘secondary binding’ under the viewpoint of specific atoms, such as A...HD HYDROGEN bonding, Au...Au AUROPHILIC attraction or I...I IODINE interaction [18,19].

Here we want to analyse the phenomenon of secondary attractions from a more general theoretical viewpoint by partitioning the weak interaction energies of rather general molecular systems into their physical contributions.

4.1.4 Outline of the present study

We will here investigate a set of model systems, small enough to perform a larger number of sufficiently accurate calculations. These model systems will consist of light or heavy nonmetal atoms being in contact with nonmetal or metal atoms. We will apply the density functional (DF) approach, which works within the simple independent particle picture of one-electron molecular orbitals (MO). Ordinary chemists are familiar with this approximate MO picture. On the other hand, the DF approach corrects for the largest two-electron correlation effects, at least concerning the so-called exchange and dynamical correlation corrections. The closed shell molecules will exhibit no pronounced nondynamical correlations. And at shorter interatomic separations the DF approach still gives reasonable energy curves. This is found empirically [20] although the present DF approaches cannot yet reproduce the long-distance dispersion attractions; probably the reasonable performance of the DF approach near the equilibrium structure is due to fortuitous error cancellation. In addition, ab-initio post SCF calculations were performed as benchmarks, namely first, by the 2nd order Möller-Plesset perturbation approach MP2, and second by the high quality single-double-approximately triple substituted configuration mixing approach QCISD(T).

As our first strategy, following Weinhold [17], we use a He atom as a probe. He is a ‘hard’ and small system without pronounced electrostatic, inductive, dispersive or quantum interference interactions with ‘softer’ atoms. With He we can test the Pauli repulsion of the closed shells of the heavier atoms in different molecules in different directions. We obtain Pauli-repulsion energy curves. In the second step we investigate the attractive electric and orbital interactions. Finally we discuss, under which circumstances an overall attraction (secondary bond) or an overall ‘non-attraction’ (nonbonded interaction) will result.

4.2 Computational details

Quantumchemical methods: The density functional (DF) approximation as implemented in the Amsterdam Density Functional program package ADF [21] was used. The higher quality ab-initio post SCF calculations by MP2 and QCISD(T) as implemented in the GAUSSIAN package were used [22].

Atomic cores: In order to keep the computational expense manageable, the atomic cores of the heavier atoms were frozen (ADF) or replaced by pseudopotentials (GAUSSIAN). The so-called ‘small cores’ were chosen. That means, the optimized ‘valence shells’ comprise the ns,np valence shells for the lighter p-block atoms; for I the (n-1)d semicore and the ns,np chemical-valence shells, and for the metallic atoms from the left side and center of the periodic table the (n-1)s,(n-1)p semicore, the outer (n-1)d, and the ns,np chemical-valence shells.

Basis sets: The small core pseudopotentials from Stuttgart were used with valence triple-zeta double-polarized Gaussian-type (GTO) basis sets as provided by the GAUSSIAN program. For ADF calculations the orbitals were represented by triple-zeta Slater-type (STO) basis sets (but double zeta for the semicore (n-1)s and (n-1)p shells), extended by two d and one f polarization functions. These extended basis sets should lead to small basis set superposition errors (BSSE) which can be corrected by the so-called Counterpoise Correction (CC). At least concerning the DF approach, a single optimized f polarization function has proven sufficient. For H and He, the triple-zeta Slater-type basis set was

extended by one p and one d polarization function. The inner core wiggles of valence MOs were represented by single-zeta STO sets. These basis sets and polarization functions were used as provided by the ADF packages.

Correlation: Concerning the exchange-correlation density functional we have used and compared 3 different ones. Slater's basic local exchange term with adjustable parameter $\alpha = 0.7$ was improved by:

- 1) Vosko's [23] local correlation correction and by the gradient corrections of Becke [24] for exchange and of Perdew from 1986 [25] for correlation – BP.
- 2) Vosko's local correlation correction and Perdew and Wang's [26] gradient correction for exchange and correlation – PW.
- 3) Becke's [24] hybride of nonlocal Hartree-Fock exchange and Lee-Yang-Parr's [27] correlation potential – BLYP.

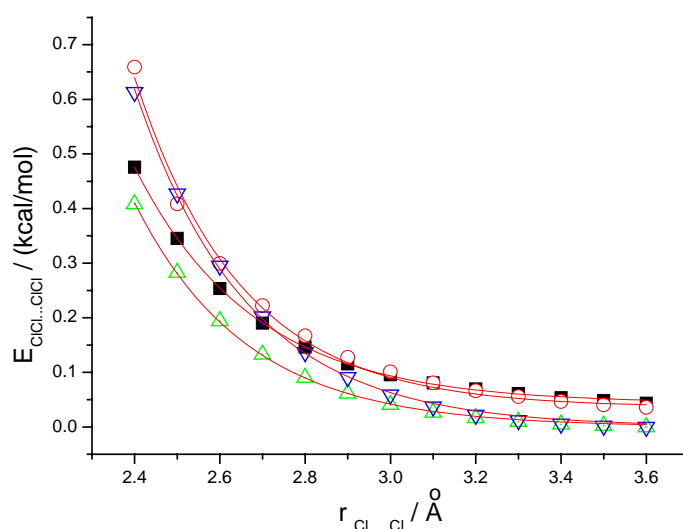


Fig. 2. Energy curves E_{tot} (exponential fits through the data points) of Cl-Cl \cdots Cl-Cl obtained with different DF and with QCISD(T). At the left side, from top to bottom: BL-DF (dot), QCISD(T) (up triangle), BP-DF (square), and PW-DF (down triangle). R is the distance between the two adjacent Cl atoms.

Numerical reliability: In Fig. 2 the potential energy curve for the Cl₂ \cdots Cl₂ interaction obtained by these three potentials and by the more sophisticated QCISD(T)/6-311g(2d) approximation are compared. At first we optimized the Cl₂ unit, then we let the two Cl₂ approach each other from long distance along the molecular axis. R is the distance of the adjacent two Cl atoms. Fig. 2 shows the significant closed shell interactions at shorter distances. The BLYP-DF gives the best agreement with QCISD(T) at short distances. For medium long distances R=3.0-3.6 only the PW91 DF yields good results. This distance region is the most important one to determine the effective radii. So in the current study, we have selected PW91 as the DF potential.

4.3. Detailed results

In this work, unless specified, all distances are in pm, and the energies are in kcal/mol.

4.3.1. The effective radii of F, Cl, Br, I, and O

In table 1 we list the most popular van der Waals radii of the atoms discussed in this section. These radii were obtained as averages from a large body of experimental structures and give us an impression of typical sizes of these atoms. However they do not suit to analyse the reduced distance problem very deeply because they lack any account of specific details. The atomic interaction surface in a molecular environment is better described as elliptical than by a spherical radius. Furthermore the atomic radii strongly depend on the effective charge of the respective atom, and also on the bond type to the adjacent atoms, and to the speciality of those atoms.

Table 1. Van der Waals radii (in pm) in the literature

O	F	Cl	Br	I	Reference
140	135	180	195	215	[2]
152	147	175	185	198	[3]
129		190	197	214	[4]

4.3.2. Radii and atomic charges

At first we discuss the charge dependence of the van der Waals radii of I, Cl, F and O. The radii given by Pauling and other authors were obtained as averages of a large sample of quite different compounds. However, it is to be expected that negatively charged atoms are bigger than positively charged ones. Now, atoms like F, O or N are usually somewhat negative in most of their compounds, so their average radii will show a bias towards being enlarged.

Weinhold and coworker [17] defined the radii using the ambient thermal energy, kT , at room temperature as the reference value of the repulsive Pauli energy:

$$E_{\text{Pau}}(\text{reference distance}) = k \cdot T_{\text{reference}} \quad (4.3.1)$$

with $T_{\text{reference}} = 298\text{K}$, yielding an E_{Pau} reference value of 0.592 kcal/mol. This criterion turns out to yield somewhat large radii. For the radii determined here we have therefore chosen a somewhat higher reference value:

$$E_{\text{Pau}}(\text{reference distance}) = 1.0 \text{ kcal/mol} . \quad (4.3.2)$$

The respective radii are also numerically better defined, because the critical energy is not that small. Our radii are about 5 pm smaller than Weinhold's.

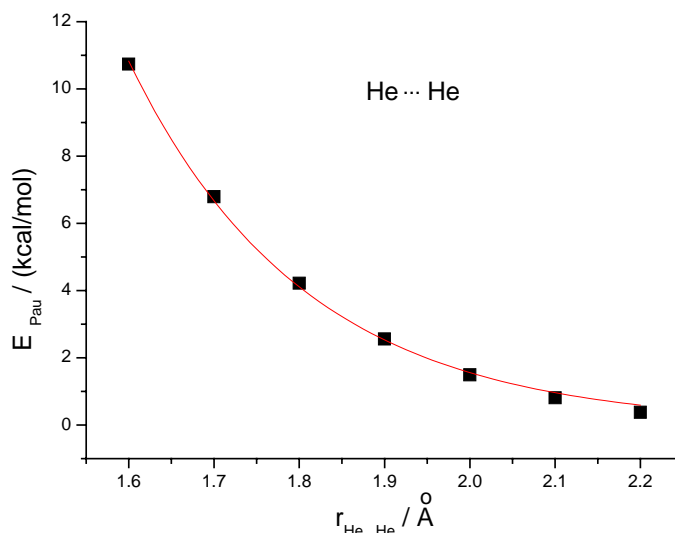


Fig. 3. He...He Pauli repulsion energy curve E_{Pau} (exponential fit through the data points)

Fig. 3 shows the Pauli energy curve of He...He. At $E_{\text{Pau}} = 1.0$ kcal/mol, $R_{\text{HeHe}} = 2.06 \text{ \AA}$. This implies $R_{\text{He}} = 1.03 \text{ \AA}$, while Weinhold's definition yielded $R_{\text{He}} = 1.07 \text{ \AA}$. According to this definition, we have calculated the effective radii of a larger number of halogen and oxygen containing molecules. At first we discuss the radii in the direction parallel to the bond axis (R_{\parallel}). The Pauli repulsion energy curves between the respective molecules and the He atom, $\text{XF}\cdots\text{He}$, $\text{XCl}\cdots\text{He}$, $\text{XBr}\cdots\text{He}$, $\text{XI}\cdots\text{He}$, $\text{XO}\cdots\text{He}$, are displayed in Figs. 4, 6, 8, 10 and 12, respectively. The resulting effective radii and the corresponding Mulliken charges and Hirshfeld charges are listed in tables 2-6. The relations between effective radii and Hirshfeld charges are shown in Figs. 5, 7, 9, 11 and 13.

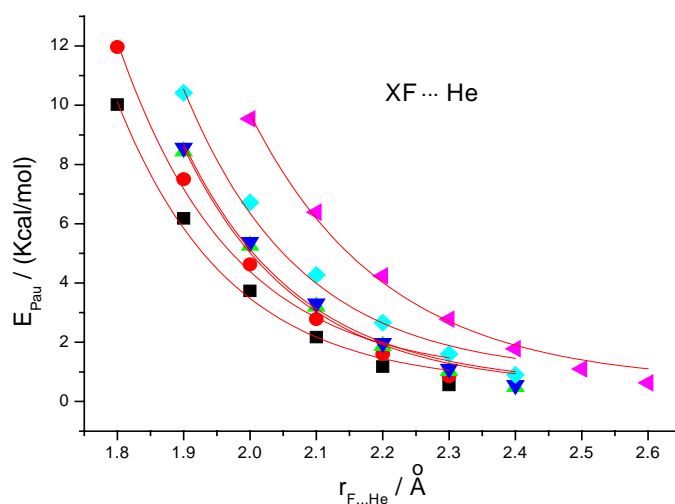
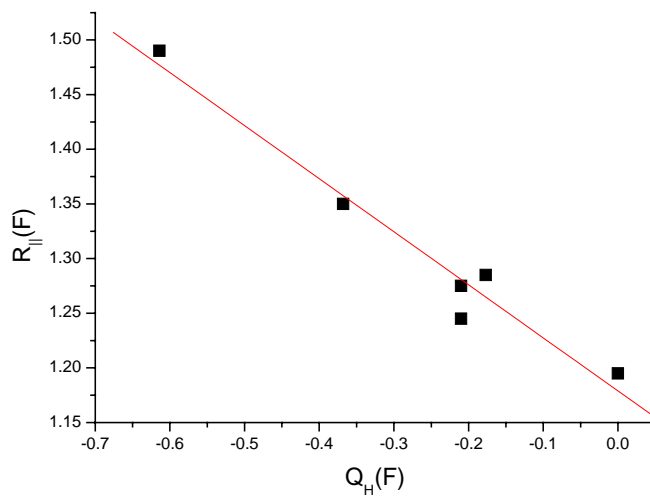
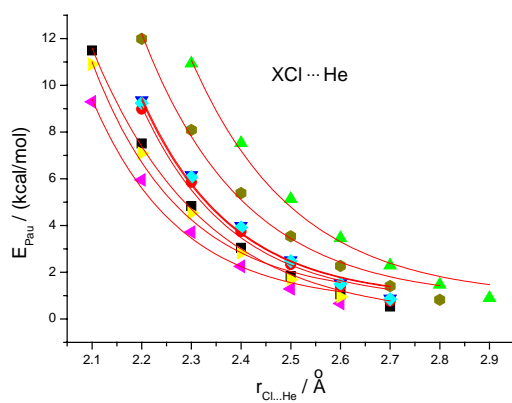
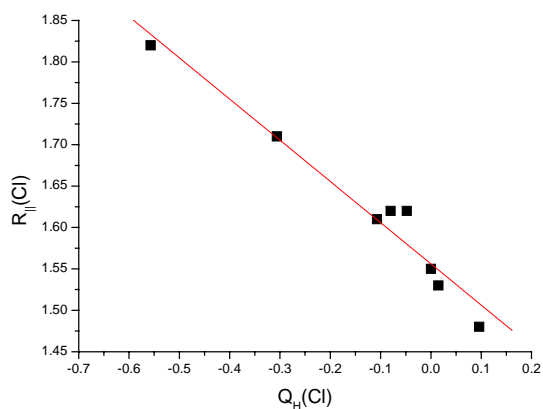


Fig. 4. E_{Pau} curves of $\text{XF}\cdots\text{He}$. At the top, from left to right: X = Na, Cu, I and H, Cl, F

Fig. 5. Dependence of $R_{||}(F)$ on the Hirshfeld charge $Q_H(F)$ Fig. 6. E_{Pau} curves of $XCl \cdots He$. At the top, from left to right: $X = F, HO, Cl, H, CH_2Cl$ and CH_3, Cu, Na Fig. 7. Dependence of $R_{||}(Cl)$ on the Hirshfeld charge $Q_H(Cl)$

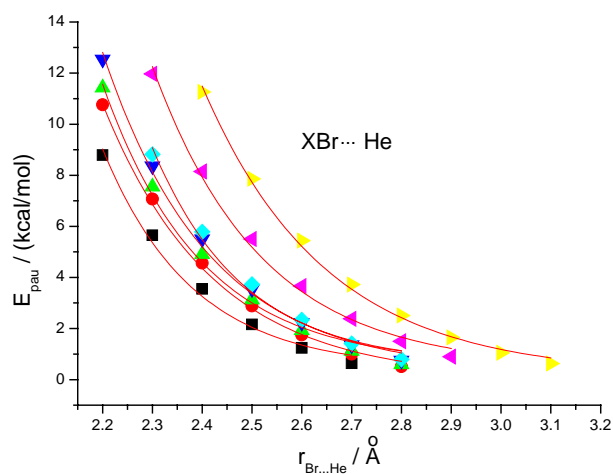


Fig. 8. E_{pau} curves of $\text{XBr}\cdots\text{He}$. At the top, from left to right: $\text{X} = \text{Na}, \text{Cu}, \text{H}, \text{I}, \text{Br}, \text{Cl}, \text{F}$.

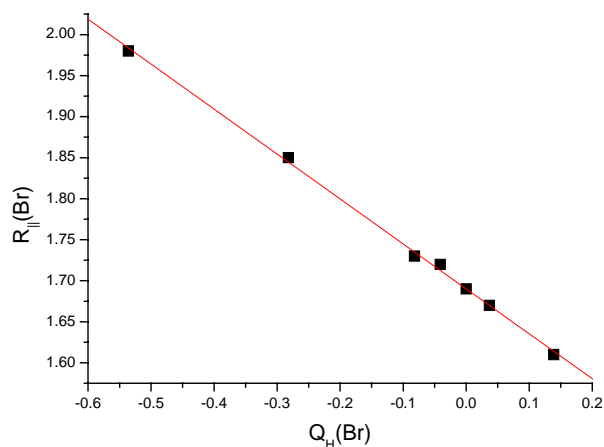


Fig. 9. Dependence of $R_{\parallel}(\text{Br})$ on the Hirshfeld charge $Q_{\text{H}}(\text{Br})$

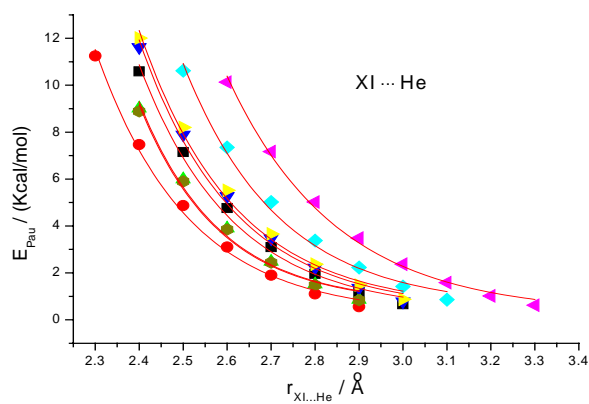
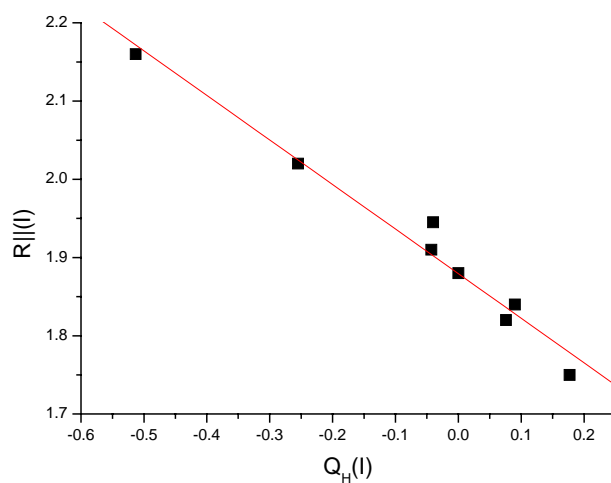
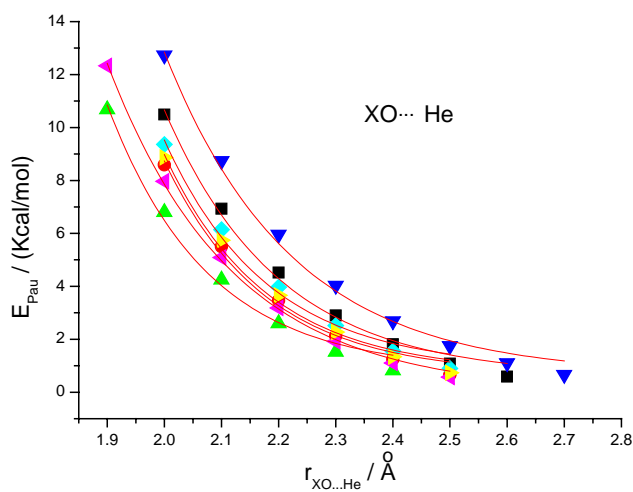
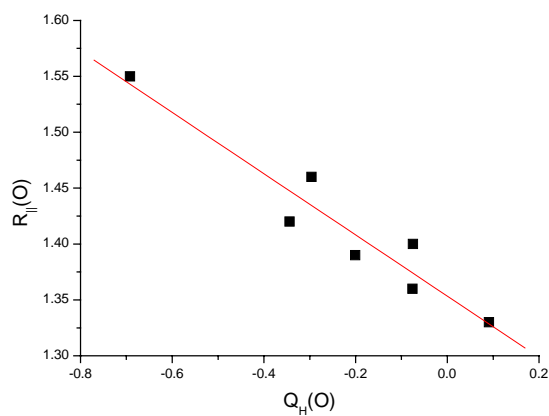


Fig. 10. E_{pau} curves of $\text{XI}\cdots\text{He}$. At the top, from left to right: $\text{X} = \text{Na}, \text{Cu}$ and $\text{CH}_3, \text{H}, \text{I}, \text{HO}, \text{Cl}, \text{F}$.

Fig. 11. Dependence of $R_{||}(I)$ on the Hirshfeld charge $Q_H(I)$ Fig. 12. E_{Pau} curves of $\text{XO}\cdots\text{He}$. At the top, from left to right: $X = \text{Ca}, \text{Cu}, 2\text{H}, 2\text{I}, \text{C}, 2\text{Cl}, 2\text{F}$.Fig. 13. Dependence of $R_{||}(O)$ on the Hirshfeld charge $Q_H(O)$

We want to get a rather general relationship between E_{Pau} , atomic partial charge q_A and radius R_{\parallel} , which is not biased through an arbitrarily chosen energy criterion. For each atom, we select a number of compounds with various effective charges on that atom, and we determine the energy curve $E_{\text{Pau}}(r)$ in the direction parallel to the bond axis. The Pauli energies are fitted by

$$E_{\text{Pau}} / \text{kcal mol}^{-1} = e^{-\alpha(r-R_{\parallel})} . \quad (3.3/4)$$

We study the dependence of α and R_{\parallel} on the atomic effective charge q . Both Mulliken and Hirshfeld charges were used. We found that Hirshfeld charges in general give more systematic trends than Mulliken charges. Therefore we will discuss the Hirshfeld charges only in the following.

The fitted parameter values α and R_{\parallel} are somewhat affected by the r range used for the fit. We have here chosen the range of $E_{\text{Pau}} = 1$ to 10 kcal/mol. This is the important range of repulsive and attractive energies determining the equilibrium distance. Furthermore this energy range can already be calculated with sufficient statistical reliability, which is the order of 10^{-1} kcal/mol. The energy range is sufficiently wide for covering the different molecular cases, and is sufficiently small to be represented by the simple 2-parameter formula (3.3), see the Figs..

In Fig. 6, for instance, curves for the Pauli repulsion between He and Cl in F-Cl, HO-Cl and so on to Na-Cl are shown. In this order the effective charge of Cl goes from slightly positive to more and more negative, while the energy curves move up to the right. It means that the Cl atom becomes larger and larger. The figure also shows that the Pauli repulsion of Cl in NaCl decays more slowly than that in FCl, i.e. a more negative and bigger Cl is also softer.

When we correlate the Pauli repulsion curves with the Cl effective charges, we must consider the exponential type of eq. (3.3). The weighing of data points becomes more balanced when eq. (3.3) is introduced into the Gaussian error minimization procedure in logarithmic form:

$$\ln (E_{\text{Pau}}(r) / \text{kcal mol}^{-1}) = \alpha (R_{\parallel} - r) \quad (4.3.4)$$

We find a pronounced dependence of the parameters α and R on the atomic effective charge q_A . It turned out that because of strong interrelations only one additional parameter is sensefully to be introduced. We have chosen for $E_{\text{Pauli}}(\text{He...A})$, and R_{\parallel} , respectively:

$$\ln (E_{\text{Pau}}(r) / \text{kcal mol}^{-1}) = p_0 + p_1 \cdot q_A - \alpha \cdot r , \quad (4.3.5)$$

$$R_{\parallel} = (p_0 / \alpha) + (p_1 / \alpha) \cdot q_A = R_0 + \Delta R \cdot q_A . \quad (4.3.6)$$

This linear dependence of effective radii with the effective charge was suggested by Figs. 5, 7, 9, 11 and 13. The fit parameters are listed in table 7, yielding the following results for the radii in pm (with $\pm 2\sigma$ in parenthesis):

$$\begin{aligned} \text{For F: } R_{\parallel(\text{F})} &= 121 (\pm 9) \text{ pm} - 40 (\pm 3) \text{ pm/e} \cdot q_{\text{F}} \\ \text{For Cl: } R_{\parallel(\text{Cl})} &= 160 (\pm 9) \text{ pm} - 43 (\pm 3) \text{ pm/e} \cdot q_{\text{Cl}} \\ \text{For Br: } R_{\parallel(\text{Br})} &= 170 (\pm 9) \text{ pm} - 47 (\pm 3) \text{ pm/e} \cdot q_{\text{Br}} \\ \text{For I: } R_{\parallel(\text{I})} &= 191 (\pm 9) \text{ pm} - 48 (\pm 2) \text{ pm/e} \cdot q_{\text{I}} \\ \text{For O: } R_{\parallel(\text{O})} &= 139 (\pm 8) \text{ pm} - 25 (\pm 2) \text{ pm/e} \cdot q_{\text{O}} . \end{aligned} \quad (4.3.7)$$

Table 2. X-F...He: effective charges (in |e|, q_m = Mulliken charge, q_h = Hirshfeld charge) and $R_{\parallel(F)}$ values (in pm)

X-F	F ₂	ClF	HF	IF	CuF	NaF
q_m	0.0	-0.445	-0.724	-0.534	-0.764	-0.954
q_h	0.0	-0.096	-0.210	-0.177	-0.368	-0.614
R_{\parallel}	119	125	127	129	135	149

Table 3. X-Cl...He: effective charges (in |e|, q_m = Mulliken charge, q_h = Hirshfeld charge) and $R_{\parallel(F)}$ values (in pm)

X-Cl	Cl	HOCl	Cl ₂	HCl	CH ₂ Cl ₂	CH ₃ Cl	CuCl	NaCl
q_m	0.445	0.133	0.0	-0.008	-0.094	0.169	-0.474	-0.636
q_h	0.096	0.015	0.0	-0.107	-0.048	-0.080	-0.306	-0.557
R_{\parallel}	151	156	158	163	164	165	173	185

Table 4. X-Br...He: effective charges (in |e|, q_m = Mulliken charge, q_h = Hirshfeld charge) and $R_{\parallel(F)}$ values (in pm)

X-Br	FBr	ClBr	Br ₂	Ibr	HBr	CuBr	NaBr
q_m	0.456	0.042	0.0	-0.141	-0.033	-0.439	-0.635
q_h	0.139	0.037	0.0	-0.041	-0.082	-0.282	-0.536
R_{\parallel}	161	167	169	172	173	185	198

Table 5. X-I...He: effective charges (in |e|, q_m = Mulliken charge, q_h = Hirshfeld charge) and $R_{\parallel(F)}$ values (in pm)

X-I	FI	ClI	HOI	I ₂	HI	CH ₃ I	CuI	NaI
q_m	0.534	0.169	0.280	0.0	0.001	-0.046	-0.331	-0.569
q_h	0.177	0.076	0.090	0.0	-0.043	-0.040	-0.255	-0.513
R_{\parallel}	179	185	184	190	193	195	204	217

Table 6. X-O...He: effective charges (in |e|, q_m = Mulliken charge, q_h = Hirshfeld charge) and $R_{\parallel(F)}$ values (in pm)

X-O	OF ₂	OCl ₂	CO	OI ₂	H ₂ O	CuO	CaO
q_m	0.548	-0.352	-0.347	-0.655	-0.358	-0.663	-1.336
q_h	0.091	-0.076	-0.075	-0.201	-0.296	-0.344	-0.692
R_{\parallel}	134	139	141	142	149	145	159

Table 7. Fit parameters of eq. (3.6) (standard deviation σ in parentheses, for Hirshfeld charge)

	F	Cl	Br	I	O
p_0	11.5(2)	12.3(2)	12.6(2)	13.0(2)	11.4(2)
p_1 in e ⁻¹	-2.05(10)	-1.99(9)	-2.19(8)	-2.13(7)	-1.17(7)
α in pm ⁻¹	0.0515(1)	0.0468(9)	0.0462(8)	0.0442(7)	0.0471(8)

The radii of Cl in the compounds of table 3 vary between 1.5 and 1.85 Å, with 1.6 Å for neutral Cl. In most compounds the radius is bigger, because Cl usually carries a negative effective charge. In Weinhold's work [17] a formula (3.6) is given: $R_{\parallel(\text{Cl})} = 189 \text{ pm} - 16 \text{ pm}/e \cdot q_{\text{Cl}}$, where however q_{Cl} means Weinhold's so-called natural instead of Hirshfeld charge. According to Meister and Schwarz [40], the ratio of natural to Hirshfeld charges is about 2.0, so the coefficient 16 corresponds to 32 for Hirshfeld charge. Weinhold's radius for neutral chlorine of 1.89 seems too large. For instance Pauling's average radius for Cl of 1.8 Å refers to more or less negatively charged chlorine atoms. Finally we note the unsatisfactory correlation of Weinhold's results (see [17], page 5427, Fig. 3) as compared to our Fig. 4.

Eqs. (3.7) show that from F to Cl to Br to I, the atoms become bigger and softer with respect to the change of partial charge. A given negative charge blows I more up than F. In contrast the radius of O is much less flexible upon charge change. In general the radii increase significantly when going down in the periodic table. However, because of the pronounced charge dependence of the radii it may happen that oxygen from the second row (if strongly negative charged) is larger than chlorine from the third row (if positively charged).

4.3.3. Angular dependence of the radii

The effective contact radii of atoms are sensitive to the direction of the contact. The atoms are elliptic (see Fig. 14). It is found that R_{\perp} (vertical to the adjacent bond axis) is always larger than R_{\parallel} for all the systems studied here. The difference of R_{\perp} and R_{\parallel} can be up to 30 pm. We have studied the angular dependence of the Cl radius in XCl molecules in detail. These molecules can be divided in two types. The first type is when the bond to Cl is strongly ionic. In this case the angular dependence is not so significant, $R_{\perp} - R_{\parallel}$ is about 10 pm. The angular dependence of the Pauli repulsion can be described by $\cos(\alpha)$, where α is the angle between $\text{He} \cdots \text{Cl}$ and Cl-X . The other type is when the Cl bond is dominantly covalent. In this case the angular dependence is very strong, $R_{\perp} - R_{\parallel}$ is about 15 to 30 pm. The functional dependence of the Pauli repulsion on the angle can be approximated by $\cos(2\alpha)$. These two cases are depicted in Fig. 15. If the molecule lies between the completely covalent and ionic cases, then the angular dependence also lies between the two types mentioned.

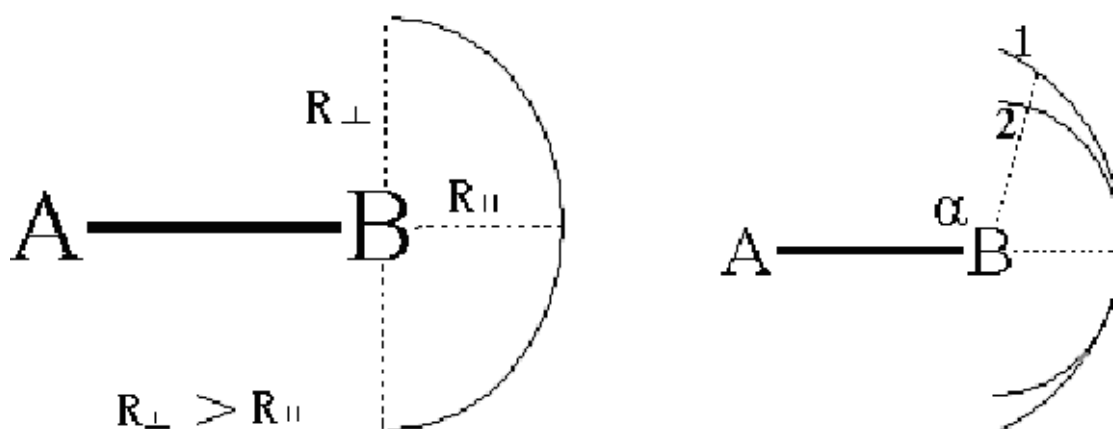


Fig. 14. Angular dependence of atomic effective radii

4.3.3.1. $\text{Cl}_2 \cdots \text{He}$

We have calculated E_{Pau} curves of $\text{Cl}_2 \cdots \text{He}$ for $\alpha = 180.0^\circ$ to 100.0° , in steps of 10° (see Fig. 16). Lower angles are not treated because then the He overlaps significantly with the other Cl atom. It is found for $E_{\text{Pau}} = 1 \text{ kcal/mol}$ that R_{\perp} is about 180 pm, 20 pm larger than R_{\parallel} , in Cl_2 . E_{Pau} changes with angle as $\cos(2\alpha)$. This means, near 90° and 180° it changes slowly, and near 135° it changes quickly. The simple expression

$$\ln(E_{\text{Pau}} / \text{kcal mol}^{-1}) = 11.840 - 0.447 \cdot \cos(2\alpha) - 4.251 \text{ \AA}^{-1} \cdot r \quad (4.3.8)$$

gives a rather good fit. For the smaller α angles, both Cl atoms interact with He, then one should use

$$\ln(E_{\text{Pau}} / \text{kcal mol}^{-1}) = P_0 - (P_1 \cdot \cos(2\alpha) + P_2 \cdot r) - (P_1' \cdot \cos(2\alpha') + P_2' \cdot r'), \quad (4.3.9)$$

where α' and r' refer to the other Cl atom. P_1' and P_2' are not equal to P_1 and P_2 . This is because the bond region of the atom is quite different to its opposite region. The bond region is in general not important to discuss the interatomic interactions. Here the P_2 and P_2' correspond to the α in eq. (3.5/4).

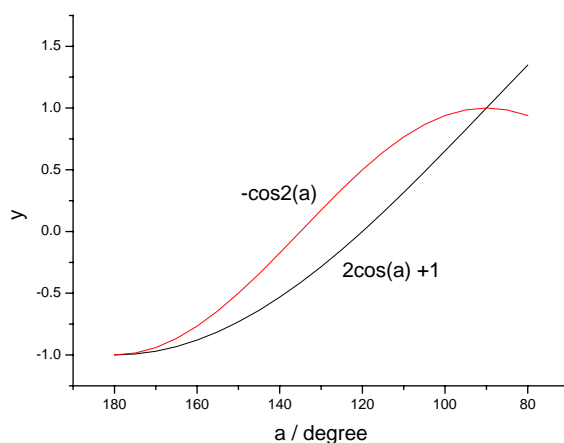


Fig. 15. The graphs of $y = 2\cos\alpha + 1$ and $-\cos 2\alpha$

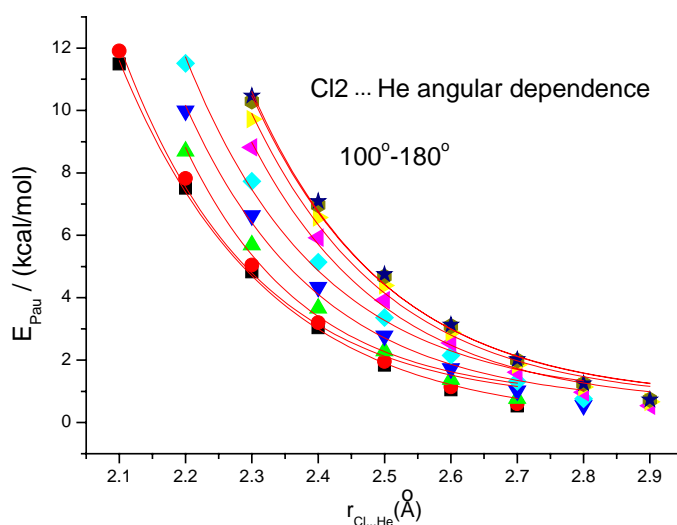


Fig. 16 Pauli energy curves of $\text{Cl}_2 \cdots \text{He}$ at various angles

4.3.3.2. *FCl··He and HCl··He*

The situations are very similar to the $\text{Cl}_2\cdots\text{He}$ case. The angular dependence of E_{Pau} is also of $\cos(2\alpha)$ type, but HCl has a larger $dE_{\text{Pau}}/d\alpha$ value near 90° than FCl and Cl_2 for which $dE_{\text{Pau}}/d\alpha$ is nearly vanishing near 90° . HCl has more ionic character than FCl and ClCl . At $E_{\text{Pau}} = 1\text{ kcal/mol}$, R_\perp is about 182 pm for FCl and 185 pm for HCl, which are larger than their respective $R_{||}$ values by 31 and 22 pm, respectively.

4.3.3.3. *NaCl··He*

NaCl is a typical ionic molecule, and its E_{Pau} is of $\cos(\alpha)$ type. R_\perp is about 1.98 Å, which is larger than $R_{||}$ by 13 pm. The fit function is:

$$\ln(E_{\text{Pau}} / \text{kcal mol}^{-1}) = 11.393 - 0.264 \cdot \cos(\alpha) - 3.803 \text{ \AA}^{-1} \cdot r \quad (4.3.10)$$

The charge dependence of R_\perp is much smaller than that of $R_{||}$. For ionic molecules $R_{||}$ is only slightly smaller than R_\perp .

4.3.3.4. *Angular dependence of F, Br, I and O*

The situations are similar as for Cl. There are two types of angular dependences, for the covalent and for the ionic molecules. The angular dependences decrease in the order: $\text{I} > \text{Br} > \text{Cl} > \text{F} > \text{O}$, and this sequence is the same as the sequence of the charge dependences. In covalent molecules, the typical difference between $R_{||}$ and R_\perp is about 30 to 40 pm for I, 25 to 35 pm for Br, 20 to 30 pm for Cl, 10 to 20 pm for F, and 5 to 15 pm for O. The I atom has the largest angular dependence and charge dependence, and the effective radii can change a lot in different environments. In our study, the maximum radius is as large as 229 pm (R_\perp for NaI), and the minimum radius is 179 pm ($R_{||}$ for FI). The different directions and the different charge states are one group of reasons that a nearly continuous series of radii was found experimentally for iodine compounds.

Table 8 displays the angular dependences of the molecules studied here. In the $\text{A-B}\cdots\text{He}$ complexes, if A is much larger than B, or if the bond length of A-B is small, the Pauli repulsion energies may obtain a significant contribution from A, especially for angles around 90° . Therefore near 90° , the angular dependence deviates from the simple $\cos(2\alpha)$ behavior, and then we get a $\cos(2\alpha) + \cos(\alpha)$ variation. This is the case for $\text{OC-O}\cdots\text{He}$, $\text{I-F}\cdots\text{He}$, $\text{HO}_2\text{I-O}\cdots\text{He}$ and $\text{HO}_2\text{Cl-O}\cdots\text{He}$ etc. Therefore we also give the radii for 135° (R_{135}). If $R_\perp - R_{45}$ is much larger than $R_{45} - R_{||}$, it means R_\perp is significantly affected by the adjacent atoms and not well defined.

Except in O_3 , O has small angular dependences. In most cases it is less than 10 pm. CO is a special case. Although CO is a covalent molecule, it exhibits an angular dependence of $\cos(\alpha)$ type. The Pauli repulsion between 180° - 140° is rather constant, and then increases dramatically. This exception may be rationalized as follows: (a) the C-O bond length is very small, therefore E_{Pau} of $\text{C-O}\cdots\text{He}$ is significantly affected by the C atom. (b) ADF in principle exhibits some numerical integration errors, in particular if the default parameters are applied. For instance at very large atomic separation E_{Pau} is zero, but at medium large distances ADF may give a small negative Pauli repulsion of a few 0.1 kcal/mol, which is of course impossible. If this numerical inaccuracy happens with negative sign for some angles of intermediate $\text{C}\cdots\text{He}$ separations, the total Pauli repulsion might be slightly underestimated. We here mention this point although we have never found any other indication. For instance we found always the same angle trends for different $\text{O}\cdots\text{He}$ distances. (c) The CO triple bond is special. Other results already showed that the angular

dependence of double bonded molecules deviated somewhat from the $\cos(2\alpha)$ type and exhibits a $\cos(2\alpha)+\cos(\alpha)$ type behavior.

Table 8. Angular dependence of effective radius of atom B in molecules A-B

A-B...He	$R_{ }$ (Å)	R_{135° (Å)	R_{\perp} (Å)	Relation	Dependence
I-F	1.29	1.33	1.50	$\cos(2\alpha)$	Small
H-F	1.27	1.34	1.41	$\cos(2\alpha)$	Small
Na-Cl	1.85	1.88	1.99	$\cos(\alpha)$	Small
Cu-Cl	1.73	1.81	1.90	$\cos(\alpha)+\cos(2\alpha)$	Small
I-Cl	1.63	1.76	1.82	$\cos(2\alpha)$	Middle
Cl-Cl	1.58	1.74	1.80	$\cos(2\alpha)$	Middle
F-Cl	1.51	1.73	1.81	$\cos(2\alpha)$	Large
H-Cl	1.63	1.76	1.85	$\cos(2\alpha)$	Middle
F-I	1.79	2.09	2.19	$\cos(2\alpha)$	Very large
Na-I	2.17	2.23	2.31	$\cos(\alpha)$	Small
HO ₂ Cl-O	1.37	1.42	1.56	$\cos(2\alpha)+\cos(\alpha)$	Small
HO ₂ I-O	1.40	1.46	1.67	$\cos(\alpha)+\cos(2\alpha)$	Middle
H ₂ C-O	1.41	1.49	1.50	$\cos(2\alpha)$	Very Small
OC-O	1.38	1.42	1.49	$\cos(2\alpha)+\cos(\alpha)$	Very Small
C-O	1.41	1.41	1.52	$\cos(\alpha)$	Very small
OO-O	1.32	1.43	1.53	$\cos(2\alpha)$	Middle

In general R_{\square} is smaller than R_{\perp} , therefore molecules will contact each other in bond-parallel arrangement in order to generate a compact cluster, provided there are no other geometric constraints or specific interactions which induce smaller interaction angles. Then larger contact radii result.

4.3.3.5. Differences between our radii and the empirical ones from the literature

When comparing our radii with the empirical ones for an average of many compounds (table 1), there is agreement if we consider the average atomic partial charges. For the halogens we obtain agreement for an average effective charge of about $-1/2$ e. Since atoms cannot always contact in the parallel direction, the respective angular blow-up must also be considered. This means that theoretical-empirical agreement is achieved for an average halogen partial charge of about -0.4 e. This looks reasonable.

Concerning O, our radius for the neutral atom agrees with the literature value, which is unexpected. We must admit that the fitting of our O data is poorer than for F, Cl Br, and I. One may speculate about the following reasons: 1) The bond type of oxygen may be more complicated and more variable, it can be a single or a double bond. 2) O can bond to one (as in CO or CO₂) or to two atoms (as in H₂O); in the latter case there is no well defined parallel direction. 3) The He probe atom is rather close to the other atoms connected to the small O atom. 4) We note that the angular dependence of O obtained from our fitting is much smaller than for halogen atoms.

4.4 Reduced nonbonded distances

Which distances belong to a reduced nonbonded kind mentioned in the introduction? On the empirical side, the popular method is to sum up the fixed van der Waals radii of the

contact atoms, and compare this to the experimentally determined distance. If the experimental distance is shorter by, say, more than 15 pm, then a reduced distance is assigned by the experimentalists. Here we would like to propose another criterion, which will turn out to cause less fruitless discussions.

The first important point is, as mentioned above, that the radius of an atom is charge dependent. Let us suppose that an atom X approaches an I-A molecule with gross partial charge of +0.5 on I. From eq. (3.7) we know that $I^{0.5+}$ is smaller than a neutral I by 24 pm. If X is neutral the X-I will be shorter than the sum of their classic radius by 24 pm. Nevertheless the X-I separation should not be called reduced, if it is just short because the atoms in the free molecules are already comparatively small. If we talk about a reduced distance interaction, we mean that there should exist some special attraction, and that because of this special attraction the atoms come particularly close to each other (see Fig. 17). The special interaction could be electrostatic attraction between polar molecules, or inductive polarization attraction, or covalent orbital interference interaction or all of them. If two atoms come close to each other at a distance where the Pauli repulsion energy is already rather large, there must be some specific attraction to balance it. If this physical criterion is used to define a reduced distance, it is coupled with some insight into the interactions and is more than an arbitrary statistical one. In the following we will discuss several typical systems in detail.

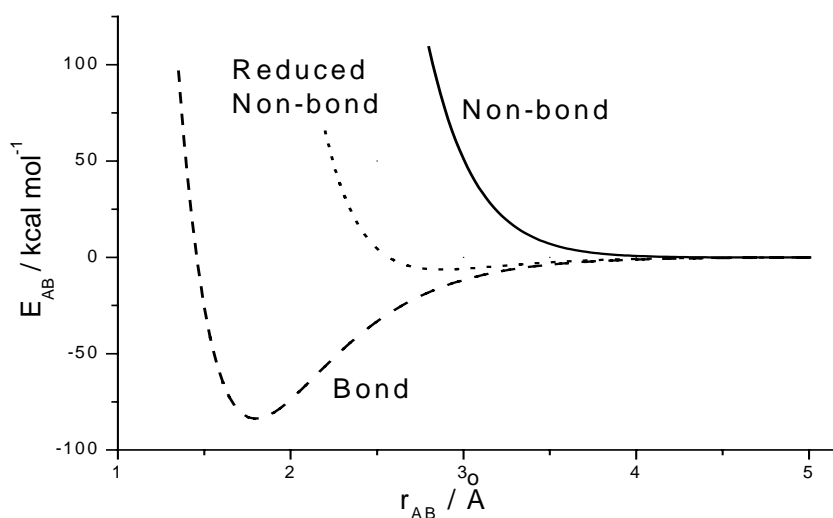


Fig. 17. Energy curves for „bonding“, „non-bonded“ and „reduced nonbonded distance“ interactions

4.4.1. The $F \cdots F$ interaction

Because F has the largest electronegativity of all neutral atoms, it is always negatively charged in compounds, except of course in F_2 . Accordingly, the F atom is smallest in F_2 (about 1.2 Å), and largest in completely ionic fluorides (about 1.5 Å). However, bonded and open-shell nonbonded atoms are nonspherical in general, i.e. they are multipolar. This was stressed in Bader's 'Atoms in Molecules' theory [28] and by Schwarz et al. [29]. For instance, bonded F atoms carry an atomic dipole, which has its positive end in the lone pair region and its negative end in the bond overlap region. Accordingly, the smallest

electrostatic repulsion between F atoms is expected, when they are weakly negative charged. The experimental data support our speculation. The smallest intermolecular distances have been found in solid $(MF_5)_4$ ($M = Mo, Ru, Os, Nb, Ta$) and $(WOF_4)_4$, here the $F \cdots F$ contacts are about 2.59-2.65 Å [30], i.e. $R(F) \approx 1.3$ Å. In these molecules, each of the five (or four, respectively) F atoms connected to M, carries a small negative charge. Our calculated Hirshfeld charge of F in MoF_5 is -0.17e for the equatorial triangle atoms and -0.23e for the apex atoms. The charges of F are about the same as those in ClF . Several experimental chemists felt surprised about the rather short $F \cdots F$ distances mentioned above. Two explanations were offered. 1) The experimental data are not reliable because of the low accuracy achieved for these heavy metal atom fluorides. It is remarkable that the experimentalists did not trust their own results. 2) The repulsive negative charges on the fluorine atoms are compensated by a five times larger (but more distant!) positive charge on M, and then the electrostatic component of the intermolecular interaction energy introduces the mutual attraction of the molecules [31]. To pose such an antirational argument is no privilege of experimentalists, as was demonstrated, for instance, by the famous theoretical matter physicists Slater [32]. From eq. (3.7) we know that the charge dependent radius of $F^{0.2-}$ is about 1.3 Å. Accordingly the above found contact radii are quite consistent. As we said already, the F is here much smaller than the average value found in compounds, because on the average F has a much larger negative charge. There is no special intermolecular contracting interaction in these molecules.

4.4.2. The $Cl \cdots Cl$ reduced distances



Fig. 18. $Cl_2 \cdots Cl_2$

Widely used effective radii of Cl are 1.8 Å or 1.9 Å. Above we had obtained 1.6 Å for the neutral Cl atom. The difference is again attributed to Cl being negative in most compounds. 1.6 Å for neutral Cl seems quite reasonable in the light of the $Cl \cdots Cl$ contact distance in Cl_2 (see Fig. 18) of 328 pm [33 - 35]. Our value of $2 \cdot 1.60$ Å = 3.20 Å is only 8 pm shorter than the experimental separation. The difference probably comes from the repulsion of small positive charges in the contact region, as in the case of F_2 (see § 2.4.1.). According to our charge dependent radii, there is no distance reducing effect at all in $[Cl_2]$. Since Cl is a middle hard atom with ordinary closed Lewis shell in nearly all of its compounds, there are no pronounced electrostatic or orbital interactions between the Cl atoms of two A-Cl molecules. There seems no need to postulate and to search for a distance reducing specific interaction, which will be hard to find.

The “reduced intermolecular $Cl_2 \cdots Cl_2$ contact” of the experimentalists belongs to the most well studied [36 - 38] type of intermolecular halogen-halogen contacts. Most so-called “reduced distances” in the literature belong to the category of separations between neutral and positively charged atoms. The problem is that the standard average radii of metalloids electronegative atoms refer to negatively charged and blown-up atoms. The $Cl_2^0 \cdots Cl_2^0$ and $-Cl^{\delta+} \cdots Cl^{\delta-}$ distances of the order of 3.2 to 3.3 Å are obviously non-reduced ordinary nonbonded separations, trivially!

According to our criterion, we have only found one reduced distance among the present collection of molecules, namely in $\text{CCl}_2(\text{CONH}_2)_2$ [36] (see Fig. 19 left and the calculated model Fig. 19 right versus Fig. 20). The experimental intermolecular $\text{Cl}\cdots\text{Cl}$ distance is only 310.4 pm. This is the shortest $\text{Cl}\cdots\text{Cl}$ distance found till now. Here the Cl is approximately neutral, and this $\text{Cl}\cdots\text{Cl}$ distance is 0.1 Å shorter than the 320 pm expected for *neutral* Cl, while textbook radius for Cl, i.e. for $\text{Cl}\delta^-$, would yield the expanded value of 360 pm. The $\text{Cl}\cdots\text{Cl}$ distance of $\text{CCl}_2(\text{CONH}_2)_2$ can be successfully reproduced by the theoretical calculations. Already a dimer with only two hydrogen bonds, without packing constraints and without cooperative effects already yields 315 pm for the nonbonded $\text{Cl}\cdots\text{Cl}$ separation (Fig. 19 (right), PW91-DF calculation). However, for the model in Fig. 20 we obtain a much larger $\text{Cl}\cdots\text{Cl}$ distance (360 pm). Thus the reduced distance in the molecular solid does not come from the special interaction between two contacting Cl atoms, but from the two strong $\text{NH}\cdots\text{O}$ hydrogen bonds that press the Cl atoms close together.

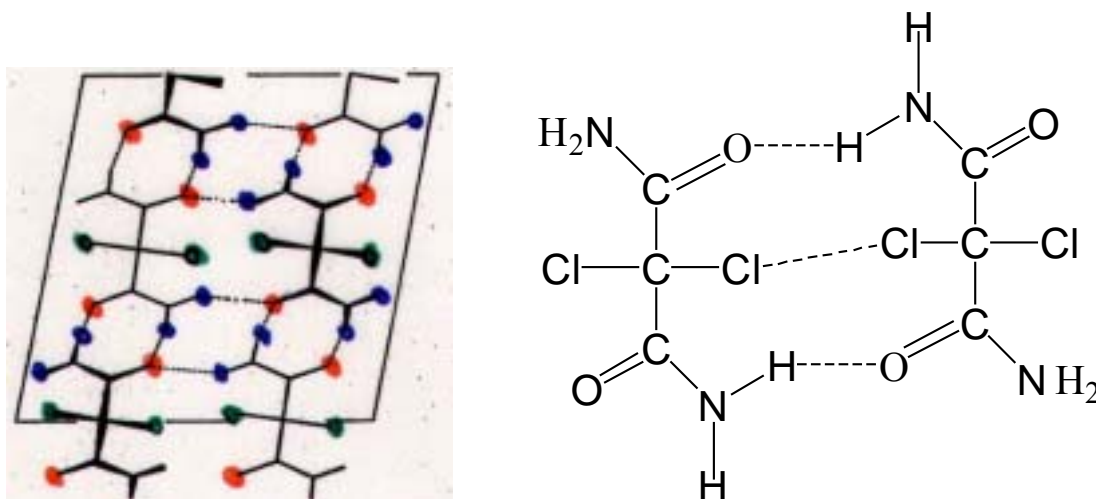


Fig. 19. $\text{CCl}_2(\text{CONH}_2)_2$. Left: the experimental structure of the solid. Right: the calculated model

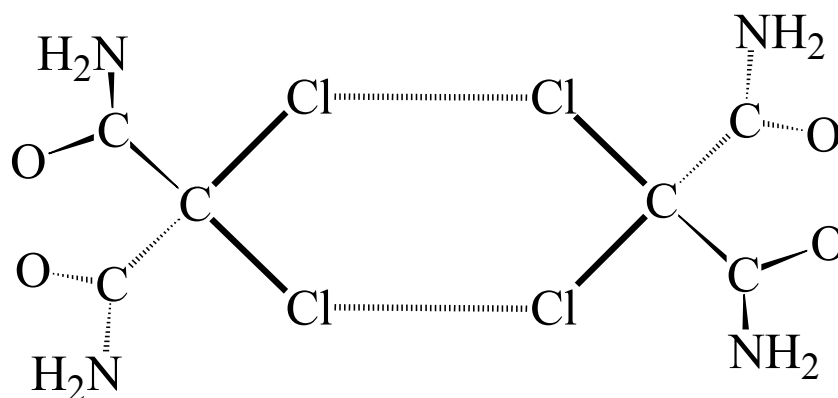


Fig. 20. A different structure of $\text{CCl}_2(\text{CONH}_2)_2$ without intermolecular compressing hydrogen bonds

4.4.3. Contacts between XY_3 ($X = I, Cl$, $Y = F, Cl$)

We have investigated the dimers $(IF_3)_2$, $(ICl_3)_2$, and $(ClF_3)_2$ (for structures see Fig. 21). The results are listed in Table 9. Two XY_3 molecules approach each other and form a C_{2h} dimer. The total interaction energy curves are shown in Fig. 22. The curves are a little different from the fully optimized data because the structures of the monomers were frozen. The charges listed in table 9 refer to the contact atoms. The Y apex atom of XY_3 has a slightly different charge than the other two Y atoms. Using eq. (3.7), we can calculate the effective radii of the charged X and Y atoms. For simplicity we simply take $R_{||}$. According to table 9, we can find that the reduced or no reduced distance interaction in these complexes are obvious, and include the angular dependence are not expected to affect the conclusion.

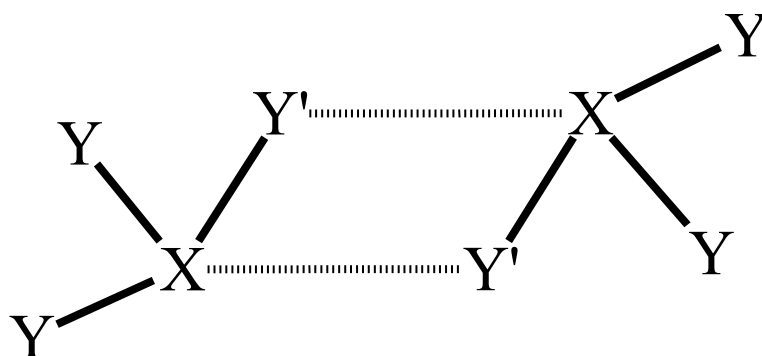


Fig. 21 The structure of a $(XY_3)_2$ model system

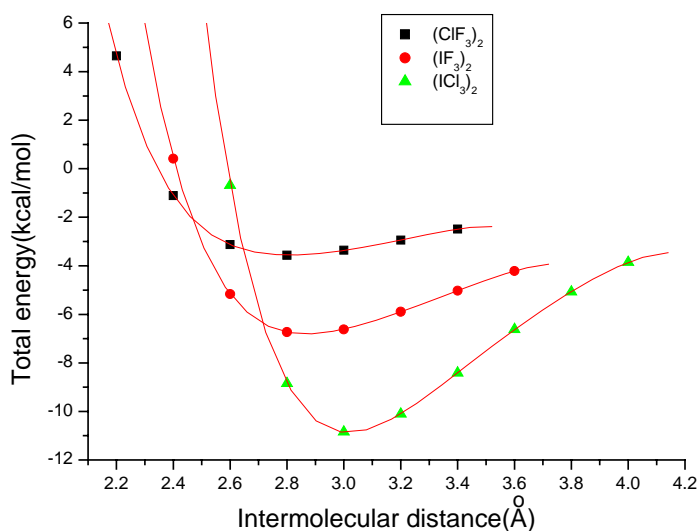


Fig.22 Energy curves of $(ClF_3)_2$, $(IF_3)_2$, $(ICl_3)_2$

Table 9. Dimers of frozen of XY_3 monomers. Distances in Å, energies in kcal/mol.

	$(IF_3)_2$	$(ICl_3)_2$	$(ClF_3)_2$
Optimized intermolecular distance	$R(F\cdots I') = 2.57$	$R(Cl\cdots I') = 2.88$	$R(F\cdots Cl') = 3.09$
Charge on contact atoms	I: 0.62, F: -0.23	I: 0.44, Cl: -0.20	Cl: 0.45, F: -0.20
Sum of effective "charged" radii	2.91 ($\Delta R=0.34$)	3.39 ($\Delta R=0.57$)	2.70
$E[(XY_3)_2] - 2 \cdot E[XY_3]$	-5.1	-10.4	-3.2
Angle of X-Y \cdots X'	112.5°	91°	106.3°

Among the three $(XY_3)_2$ complexes, $(ClF_3)_2$ does not exhibit a reduced distance. The two iodine halides, however, do, in particular $(ICl_3)_2$. To understand this sequence, we have calculated the electrostatic and orbital interaction energies at a distance where the Pauli repulsion energy is 10 kcal/mol (to avoid a complication by angular dependences, we fixed the X-Y \cdots X' angle at an average value of 105°). This distance is near the sum of effective radii in the present cases. The results are listed on table 10.

Table 10. Comparison of Pauli repulsion, electrostatic and orbital interaction energies (in kcal/mol) of dimers $[XY_3]_2$ (monomers with frozen structure) at fixed angle X-Y \cdots X' = 105° and distances (in Å) so that E_{pau} is 10 kcal/mol.

	$(IF_3)_2$	$(ICl_3)_2$	$(ClF_3)_2$
$R_{(Y\cdots X')}$	3.00	3.48	2.72
Pauli repulsion (reference value)	10.0	10.0	10.0
Electrostatic interaction	-9.61	-8.11	-7.64
Orbital interaction	-6.47	-9.03	-5.99

Table 10 shows that the absolute values of electrostatic attraction of overlapping shells varies in the order $(IF_3)_2 > (ICl_3)_2 > (ClF_3)_2$. This is in parallel with the sequence of partial charges: $(IF_3)_2 > (ClF_3)_2 \approx (ICl_3)_2$ (see table 9). In general, the electrostatic attraction is smaller than the Pauli repulsion for overlapping neutral closed shell systems. For IF_3 there is no large difference: E_{elstat} is comparatively large because of the high electron density of F and the high nuclear charge of I., and because of the strongly polar I-F bonds which result in rather large partial charges.

The orbital interaction is another attractive component. It acts together with electrostatic interaction to form the total attractive force. Orbital interaction comes from three sources. If a, a^* and b, b^* are the occupied and virtual orbitals of the interacting monomers, *induction polarization* is due to $a-a^*$ and $b-b^*$ mixing induced by the partner molecule, while symmetric and asymmetric $a-b^*$ and $b-a^*$ mixing contribute to secondary *covalent interference*, and respectively, to polar *charge transfer*. The order of polarizabilities is $I > Cl > F$, therefore the order of polarization energies should have the order $(ICl_3)_2 > (IF_3)_2 > (ClF_3)_2$. This has been confirmed by polarizabilities. The calculated polarizabilities are 78.3 a.u. for ICl_3 , 36.8 a.u. for IF_3 , and 25.2 a.u. for ClF_3 .

The inter-monomer orbital interactions are more complicated. Large effects are obtained for small HOMO-LUMO gaps and for large densities on the contact atoms. Here the order of the gaps is $ICl_3 < IF_3 \approx ClF_3$, see table 11.

Table 11. The HOMO and LUMO of IF₃, ICl₃, and ClF₃ from the DF approach

	IF ₃	ICl ₃	ClF ₃
HOMO	-7.443 eV 67% on I, 11% on each F	-7.021eV 34% on I, 22% on each Cl	-8.441eV 44% on Cl, 19 on each %F
LUMO	-4.758eV 71% on I, 10% on each F	-5.459eV 53% on I, 16% on each Cl	-5.725eV 62% on Cl, 13% on each F
Energy gap	2.68 eV	1.56 eV	2.72 eV

Pauli repulsion, electrostatic overlap and orbital interference energies show exponential decay with interatomic distance r , while the electrostatic multipole interaction goes as $1/r^3$ at long distances, and exponentially at overlap distances. Therefore at larger distances the electrostatic multipole attraction dominates, at medium distances electrostatic overlap and orbital interference attractions dominate, until at shorter separations the Pauli repulsion of interfering occupied shells begins to dominate.

In summary, (ICl₃)₂ has the largest orbital interactions, (IF₃)₂ has the largest electrostatic attraction, while (ClF₃)₂ has the smallest electrostatic and orbital interactions. The order of dimerization energies is (ICl₃)₂ > (IF₃)₂ ≈ (ClF₃)₂. ClF₃ forms a dimer at ordinary charge-dependent nonbonded separations.

Another topic in these complexes is the geometric structure of the dimer. From table 11 we know that the angles are different. This may be because the effective radii are different. Based on eq. (3.7) we estimate the effective radii ($R_{||}$ for simplicity) of the charged atoms as follows. In IF₃, $R_{(I)} = 1.60 \text{ \AA}$, $R_{(F)} = 1.30 \text{ \AA}$, in ClF₃, $R_{(Cl)} = 1.41 \text{ \AA}$, $R_{(F)} = 1.29 \text{ \AA}$, in ICl₃, $R_{(I)} = 1.70 \text{ \AA}$, $R_{(Cl)} = 1.69 \text{ \AA}$. In order to minimize the repulsions and to maximize the attractions, IF₃ and ClF₃ take X-Y'...X angles near 110° for $R(X) > D(Y)$. In ICl₃, the sizes of the two contact atoms are similar, and then X-Y'...X is about 90°.

4.4.4. Contacts between HClO₃ and HIO₃

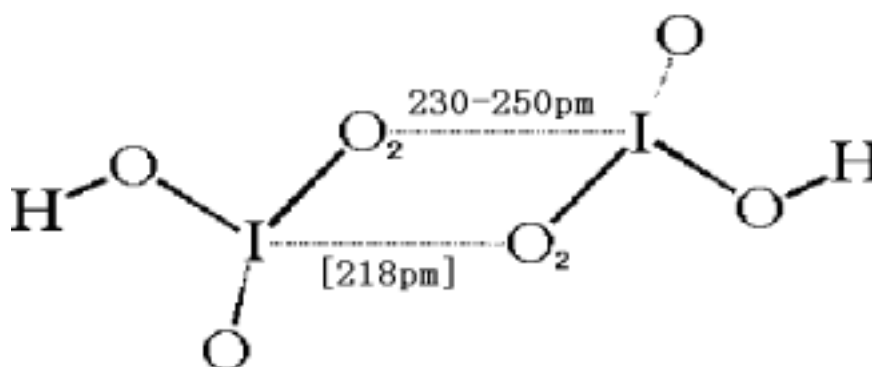


Fig. 23. Structure of (HIO₃)₂ with short I...O distances (number in [] is the calculated value. In the solid it is polymeric, and the I...O distances are from 230 to 250pm).

Recently it has been found that HIO₃ in its different crystalline phases forms stable adducts [39]. The dimer building blocks exhibit significantly reduced distances between I and O, and between I and I (see Fig. 23), while similar structures of HClO₃ have not been reported.

Three questions arise, i) is it really a real reduced distance, ii) why does a reduced distance occur in HIO_3 , and iii) is a short distance HClO_3 also possible but has just not been found so far by the experimentalists.

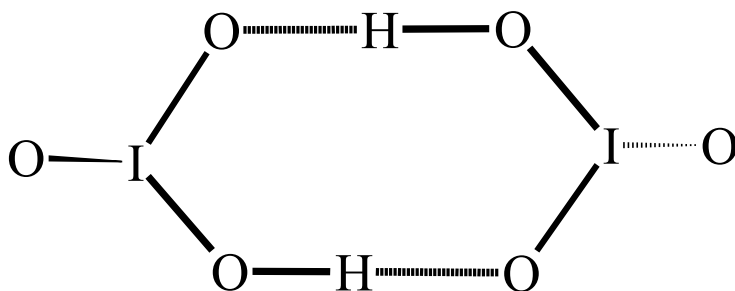
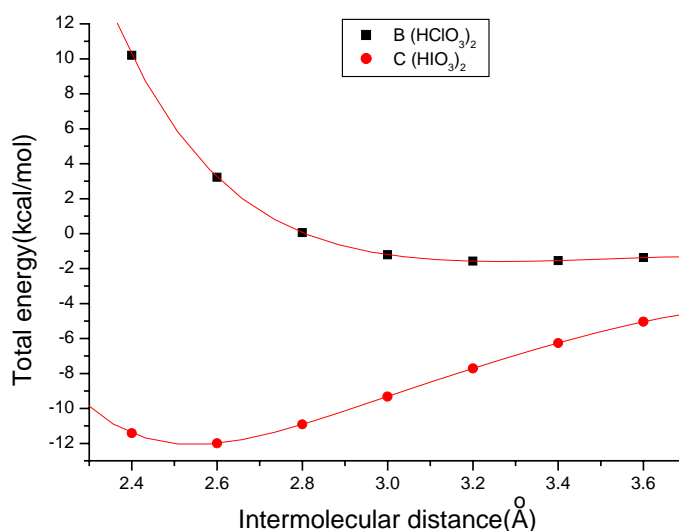
We have optimized $(\text{HIO}_3)_2$ and the imaginary $(\text{HClO}_3)_2$ (for the structure, see Fig. 23). For $(\text{HIO}_3)_2$ we have found $\text{I}\cdots\text{O}' = 2.18 \text{ \AA}$, and the dissociation energy (of a dimeric molecule in vacuum) is 16.6 kcal/mol. For $(\text{HClO}_3)_2$, the separation is much larger although Cl is smaller than I, $\text{Cl}\cdots\text{O}' = 3.48 \text{ \AA}$, and the dissociation energy is only 1.6 kcal/mol. The optimized geometry of the molecular dimer $(\text{HIO}_3)_2$ is in reasonable agreement with the experimental structure in the respective solids. Dimeric total energy curves are shown in Fig. 25. The curves are a little different from the full optimization results because the structure of dimer was derived from frozen single molecules.

The interaction energies between two HClO_3 and HIO_3 are analyzed in table 12. In general closed shell systems do not develop special attractive forces. There are long range van der Waals and electrostatic multipole attractions; when the overlap begins at shorter separations electrostatic overlap attractions and weak orbital interactions set in, which are soon outbalanced by the Pauli overlap repulsion. The minimum separation then occurs near the sum of charge dependent radii. However if one closed shell is flexible, i.e. can be deformed through orbital interactions, the Pauli repulsion can increase at a slower rate, and/or the closed shell can be energetically stabilized, the total energy minimum will occur at a shorter separation: the reduced nonbonded distance. In the condensed phase the situation can be more complicated by cooperative effects.

Table 12. Interaction energy contributions (in kcal/mol) of $(\text{HClO}_3)_2$ and $(\text{HIO}_3)_2$ at various intermolecular distances.

R/ \AA	$(\text{HClO}_3)_2$				R/ \AA	$(\text{HIO}_3)_2$			
	E_{Pau}	E_{elstat}	E_{orb}	E_{total}		E_{Pau}	E_{elstat}	E_{orb}	E_{total}
2.6	25.14	-13.87	-8.04	3.23	2.4	124.2	-74.6	-61.03	-11.4
2.8	12.02	-7.72	-4.24	+0.06	2.8	33.94	-25.81	-19.06	-10.93
3.0	5.55	-4.43	-2.34	-1.22	3.0	17.36	-15.84	-10.86	-9.33
3.2	2.38	-2.61	-1.34	-1.57	3.4	4.15	-6.65	-3.77	-6.27
3.4	0.84	-1.60	-0.79	-1.55	3.8	0.65	-3.23	-1.47	-4.05

In the crystalline solids of HIO_3 and HClO_3 , one possibility is that the molecules connect each other by intermolecular hydrogen bonds (for a possible structure, see Fig. 24). In the dimer systems there is a competition of $\text{X}\cdots\text{O}'$ attraction ($\text{X} = \text{Cl}, \text{I}$) and $\text{OH}\cdots\text{O}'$ hydrogen bond formation. The common hydrogen bond energy is about 5-10 kcal/mol. The stabilization energy of $(\text{HIO}_3)_2$ with $\text{I}\cdots\text{O}$ interaction is a little larger than that, thus $(\text{HIO}_3)_2$ with $\text{I}\cdots\text{O}$ interaction is preferred and can be found in HIO_3 solid. However the stabilization of $(\text{HClO}_3)_2$ by $\text{O}\cdots\text{Cl}$ interaction is much smaller than the hydrogen bond, therefore in solid HClO_3 one can only find conventional hydrogen bond chains, but not $(\text{HClO}_3)_2$ unit with $\text{Cl}\cdots\text{O}$ interaction.

Fig. 24. Structure of a hydrogen bonded $(\text{HIO}_3)_2$ dimerFig. 25. Energy curves of $(\text{HClO}_3)_2$ and $(\text{HIO}_3)_2$, frozen monomer structures assumed

Now we discuss the reduced distance attraction between the contacting atoms $\text{I}\cdots\text{O}$ and $\text{Cl}\cdots\text{O}$. In HClO_3 , $q(\text{O}_2) = -0.23$, $q(\text{Cl}) = +0.50$. According to eq. (3.7), $R_{(\text{O}_2)} = 1.45 \text{ \AA}$, $R_{(\text{Cl})} = 1.39 \text{ \AA}$. The distance sum is 2.84 \AA . This is the $R_{\parallel(\text{Cl}\cdots\text{O})}$, the R at the bent contact angle should be a little larger. In accordance with that, the energy curve of $(\text{HClO}_3)_2$ has a zero value near 2.8 \AA and a very flat minimum above 3 \AA . On this basis one would expect no $\text{Cl}\cdots\text{O}$ reduced distance in $(\text{HClO}_3)_2$.

In HIO_3 , $q(\text{I}) = 0.76$, $q(\text{O}) = -0.33$, thus $R_{(\text{I})} = 1.55 \text{ \AA}$, $R_{(\text{O}_2)} = 1.47 \text{ \AA}$. The respective sum is 3.02 \AA , so the above mentioned calculated and experimental $\text{I}\cdots\text{O}$ distance values indicate a very strong reduced distance. The polarizabilities of HClO_3 and HIO_3 were calculated using ADF program, and the results are 28.4 a.u. and 44.5 a.u. , respectively. The polarizability of HIO_3 is much larger than that of HClO_3 , also the charge of I in HIO_3 is larger than that of Cl in HClO_3 , and the HOMO-LUMO gap of HIO_3 (3.81 eV) is smaller than that of HClO_3 (4.28 eV). All these properties show that $(\text{HIO}_3)_2$ can form a nonbonded reduced distance interaction much easier than $(\text{HClO}_3)_2$. In summary, $(\text{HClO}_3)_2$ does not show a specific $\text{Cl}\cdots\text{O}$ interaction but only hydrogen bonding, while the softer I in HIO_3 develops in addition an even stronger $\text{I}\cdots\text{O}$ interaction.

4.5. Summary

We have defined nonbonded atomic radii following a suggestion of Badenhoop and Weinhold [17]. The atom is probed by a He atom. We have applied a slightly larger critical Pauli repulsion energy of 1 kcal/mol and accounted for the direction of the interaction and the effective atomic charge. Hirshfeld charges have proven particularly useful for this purpose. Based on these concepts we have studied the charge and angular dependence of the atomic radii of halogen and oxygen atoms in three dozen of molecular systems. We have reevaluated some of the reduced nonbonded distances proclaimed in the literature. The results are:

(1) Atomic radii depend not only on the bond type, the formal charge, the coordination number, but also on the effective atomic charge, and on the direction of the 'nonbonded' interaction with respect to the ordinary bond directions. The charge dependence in particular is quite significant and must not be overlooked.

(2) Most reduced distances proclaimed in the literature on the basis of a naïve interpretation of experimental data occur just because of the universal charge dependence of the effective radii, which is often simply neglected in the discussions. The atomic blow-up with increasing negative charge (or decreasing positive charge) leads to a simple explanation of the empirical findings, and no fruitless search for nonexistent specific interactions is necessary any longer. However, in some molecular complexes there indeed exist really reduced nonbonded distances. This happens typically in molecules that contain heavy atoms with significant effective charges.

(3) The multipole interaction of two neutral molecules is always attractive at large separations for the optimized arrangement. The minimum of the potential energy curve obtains when the attraction is balanced by the shortrange Pauli repulsion. An unusually short equilibrium distance obtains if due to specific mechanisms the Pauli repulsion increases slowly (due to deformation of the closed shells through easy polarization by single-fragment orbital interaction of a soft monomer) and/or some double-fragment covalent orbital interference stabilizes the nonbonding orbitals slightly. Heavy polar systems accord these requirements, therefore common comparatively large intermolecular forces & comparatively soft closed shell repulsions result in "reduced nonbonded distances" for those heavy polar systems.

References

- [1] L.Pauling, *The Nature of the Chemical Bond, 1st Ed.*, Cornell Univ. Press, Ithaca, NY, **1939**.
- [2] L.Pauling, *The Nature of Chemical Bond and the Structure of Molecules and Crystals*, 3rd Ed., Cornell Univ. Press, Ithaca, NY, **1960**.
- [3] A.Bondi, *J. Phys. Chem.*, **1964**, 68, 441.
- [4] Y.V.Zefirov, P.M.Zorky, *Zh. Strukt. Khim.*, **1974**, 15, 118; **1976**, 17, 745; **1980**, 21, 150; **1986**, 27, 74.
- [5] W.L.Bragg, *Philos. Mag.*, **1920**, 40, 169.
- [6] L.Pauling, *J. Am. Chem. Soc.*, **1927**, 49, 765.
- [7] L.Pauling, *Z. Kristallogr.*, **1928**, 67, 377.
- [8] W.Biltz, *Raumchemie der festen Stoffe*, Voss, Leipzig, 1934.
- [9] R.D.Shannon, C.T.Prewitt, *Acta Crystallogr. B*, **1969**, 25, 925.
- [10] R.D.Shannon, *Acta Crystallogr. A*, **1976**, 32, 751.
- [11] Y.V.Zefirov, M.A.Porai-Koshits, *J. Struct. Chem.*, **1980**, 21, 526; **1986**, 27, 239.
- [12] T.G.Row, R.Parthasarathy, *J. Am. Chem. Soc.*, **1981**, 103, 477.
- [13] C.Nyburg, C.H.Faerman, *Acta Crystallogr. B*, **1985**, 41, 274; **1987**, 43, 106.
- [14] B.S.Gourary, F.J.Adrian, *Solid State Phys.*, **1960**, 10, 127.
- [15] J.C.Slater, *J. Chem. Phys.*, **1964**, 41, 3199.
- [16] R.Narayan, *Pramana*, **1979**, 13, 559.
- [17] J.K.Badenhop and F.Weinhold, *J. Chem. Phys.*, **1997**, 107, 5422.
- [18] Y.V.Zefirov, *Crystallography Reports*, **1997**, 42, 865
- [19] S.G.Wang, W.H.E.Schwarz, *J. Am. Chem. Soc.*, **2004**, 126, 1266.
- [20] Y.X.Qiu, S.G.Wang, W.H.E.Schwarz, *Chem. Phys. Letters*, **2004**, in press.
- [21] E.J.Baerends et al., *ADF Program System, Release 2002.02*, Scientific Computing & Modeling, Vrije Universiteit, Amsterdam, Netherlands, **2002**.
- [22] M.J.Frisch et al., *Gaussian 98, Revision A.9*, Gaussian, Inc., Pittsburgh PA, **1998**.
- [23] S.H.Vosko, L.Wilk, M.Nusair, *Can. J. of Phys.*, **1980**, 58, 1200.
- [24] A.D.Becke, *Phys. Rev. A*, **1988**, 38, 3098.
- [25] J.P.Perdew, *Physical Review B*, **1986**, 33, 8822.
- [26] J.P.Perdew, J.A.Chaevary, S.H.Vosko, K.A.Jackson, M.R.Pederson, D.J.Singh, and C.Fiolhais, *Physical Review B*, **1992**, 46, 6671.
- [27] C.Lee, W.Yang, R.G.Parr, *Phys. Rev. B*, **1988**, 37, 785.
- [28] R.F.W.Bader, *Atoms in Molecules - A Quantum Theory*, Oxford University Press, Oxford, **1990**.
- [29] L.Mensching, W.v.Niessen, P.Valtazanos, K.Ruedenberg, W.H.E.Schwarz, *J. Am. Chem. Soc.*, **1989**, 111, 6926,6933; W.H.E.Schwarz, H.L.Lin, S.Irle, J.E.Niu, *J. Mol. Struct.*, THEOCHEM, **1992**, 225/87, 435.
- [30] A.J.Edwards, R.D.Peacock, W.H.Small, *J. Chem. Soc.*, **1962**, 4486.
- [31] Y.V.Zefirov, M.A.Porai-Koshits, *Koord. Khim.*, **1983**, 9, 454.
- [32] J.C.Slater, *J. Chem. Phys.*, **1933**, 1, 687.
- [33] E.D.Stevens, *Molec. Phys.*, **1979**, 37, 27.
- [34] R.L.Collin, *Acta crystallogr.*, **1952**, 5, 431.
- [35] J.Dinohue, S.H.Goodman, *Acta crystallogr.*, **1965**, 18, 568.
- [36] J.A.Lerbscher, K.V.K.Rao, J.Trotter, *J. Chem. Soc. A*, **1971**, 1505.
- [37] E.D.Stevens, *Mole. Phys.*, **1979**, 37, 27.
- [38] E.Garnier, *Acta Crystallogr. C*, **1993**, 49, 578.
- [39] M.Panthöfer, *Ph.D dissertation*, University of Siegen, **2001**.
- [40] J.Meister, W.H.E.Schwarz, *J. Phys. Chem.*, **1994**, 98, 8245.

5. Dye Molecules in Zeolite Channels

5.1. Introduction

Zeolite microcrystals are currently a hot topic in host-guest chemistry. They can act as hosts for the supramolecular organization of molecules, complexes, clusters and quantum-size particles. Thus they provide opportunities to prepare materials with new properties such as nonlinear optical properties, quantum-size properties, micro laser action, or artificial antenna characteristics [1-11]. Unfortunately, a controlled precise preparation of materials with well-defined properties is still quite difficult because of the lack of knowledge about the detailed host-guest interactions. Information about the orientation of the dye molecules inside the nano channels of the zeolite crystals is highly desirable [2,7,9]. However, traditional methods such as X-ray analysis or NMR spectroscopy are only applicable to a restricted number of favorable cases because of the limited sensitivity in single molecule cases. Recently, polarized IR spectroscopy [2], coupled thermogravimetry / FTIR [7], and fluorescence microscopy techniques [1] have been applied in the field. Among them fluorescence microscopy is the most sensitive method.

Zeolite microcrystals are a difficult topic for theoretical studies: Zeolites have a complex structure. Therefore a model in the form of a small cut of the crystal structure cannot in general exactly reproduce the zeolite environment of the embedded molecules and clusters, while a larger model is constrained by computing resources.

Focusing on supramolecular organized dye molecules in channels of hexagonal zeolite L crystals, the first question would be the orientation of the dye molecules inside the channels. Using fluorescence microscopy, Calzaferri, Meixner and their coworkers [1] have investigated the orientations of the $S_1 \leftrightarrow S_0$ π, π^* transition dipole moment of oxonine (Ox^+), pyronine (Py^+), and 5,5'-diphenyl-2,2'-*p*-phenylene-bisoxazole (POPOP) in the channels of zeolite L crystals (the size and structures of these molecules are shown in Fig. 1). The detailed investigations on Ox^+ indicated a cone-shaped distribution of the transition moments with a half-cone angle of $72 \pm 2^\circ$ (the structure of zeolite L and the orientation of Ox^+ in the channel are shown in Fig. 2). The orientation of the transition moment of Ox^+ is parallel to the molecule's long axis. In [1] it was also said that the zeolite L structure gives room only for a cone-angle up to 40° . The discrepancy between geometrical considerations and spectroscopic results was rationalized by assuming that the Ox^+ molecules are exposed to strong electric fields in the zeolite channels, which should rotate the transition dipole by 30° . If this explanation is true, it means that fluorescence microscopy can hardly give direct information about the molecular orientation in zeolites.

In the following investigation we at first describe our calculational method in section 2. Then we reevaluate the geometrical model of oxonine in zeolite channels [1] in section 3, determining the molecular orientation. In section 4 we perform quantum chemical calculations. Our aim is to find realistic positions and angles of oxonine in zeolite. We use the simple AM1 method and fully optimize the Ox^+ position inside an appropriately designed cut of the zeolite. Then we calculate the energy curve as a function of the position of the molecular center, and of the angles between the molecular axes and the zeolite channel. Using improved density functional methods, we recalculate the energies at the AM1 local minima and transition states. Finally in section 5 we calculate the π, π^* transition dipole moment of the free oxonine mo-

lecular cation, of oxonine in a small and in a larger cut of the zeolite channel, and of oxonine surrounded by some model molecules. The aim is to study the environmental dependence of the transition dipole moment.

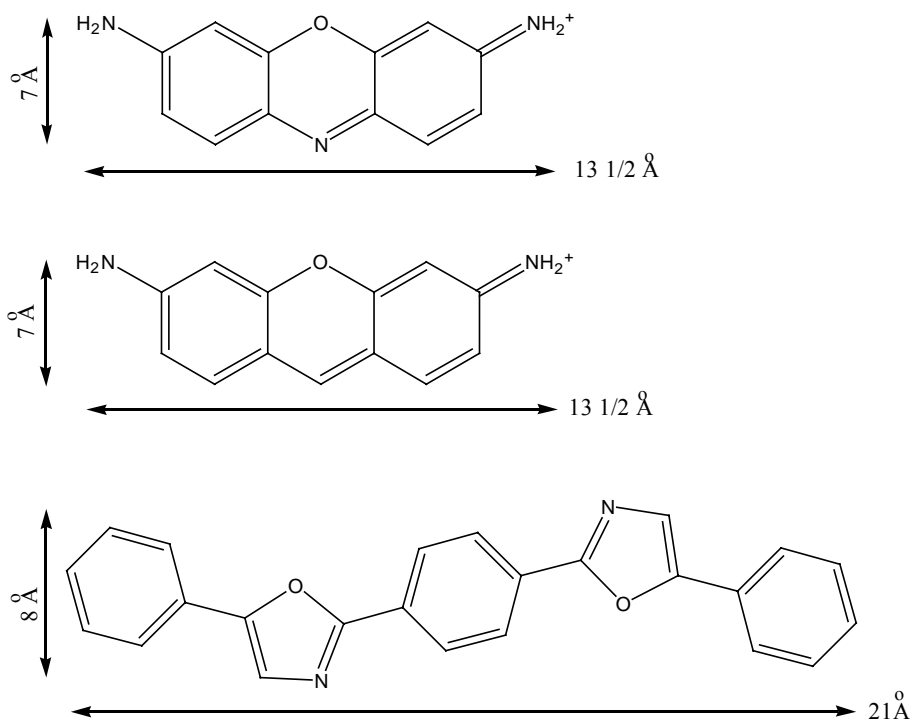


Fig. 1. Formula and outer size of a) oxonine (Ox⁺), b) pyronine (Py⁺), and c) 5,5'-diphenyl-2,2'-p-phenylene-bisoxazole (POPOP)

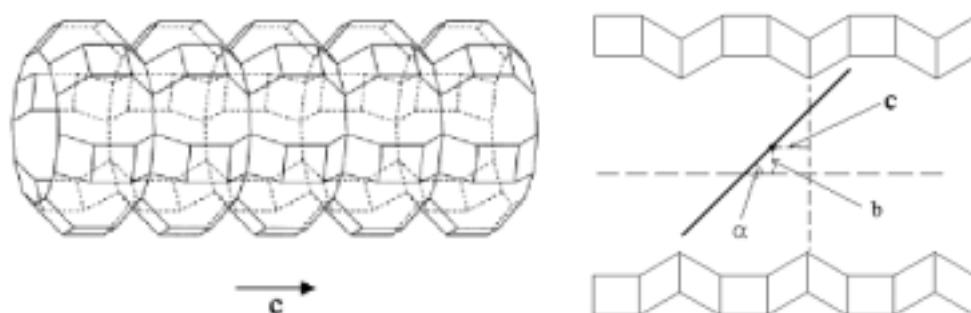


Fig. 2. Structure of zeolite L channel (left) and orientation and position of Ox⁺ inside (right)

5.2. Applied methods

For survey investigations we apply simple semi-empirical AM1 [12] and PM3 [13] MO-SCF approaches. For more reliable energy calculations the density functionals (CF) of BP86 [14,15] and B3LYP [16]. For benchmark calculations of small model systems MO-MP2 [17].

For the calculation of excited states and transition moments we use time dependent density functional theory, using the ESCF keyword in Turbomole [18-20].

The following program packages were applied, available either in Siegen or in Shanghai: Gaussian 98 [21], TURBOMOLE 5.5 [22]

The inner atomic core shells were either treated explicitly (B3LYP, MP2 and BP86) or replaced by effective core potentials (ECP: cep and ecp-n-sdf for B3LYP calculation) or by using effective empirical integrals (AM1, PM3).

Minimal basis sets for MNDO and PM3. Split valence shell bases (SV) such as 31G are Stevens/Basch/Krauss [23] and ecp-n-sdf (unpublished but included in TURBOMOLE package) for BP86 and B3LYP. For any reasonable ab-initio calculation a minimum of valence polarization must be included. This is done with SV(P) [24,25]: [2s1p] for H, [3s2p1d] for C, N, O, [4s3p1d] for Si, but in some calculations we simply used [2s] for H (DZ [24,25]). The best basis used here were of triple valence polarized type (TZP) [24,25], (6-311g(d,p) [26,27] Finally for some BP86 calculations four-center integrals were approximated with the help of three-center integrals, this is the well-known resolution of the identity approach (RI) [28-30])

As the most important interaction between the dye molecule and the zeolite is the $O^{\delta-}\cdots H^{\delta+}N^{\delta-}$ hydrogen bond, the reliability of the applied methods was examined by the simply hydrogen bonded system $H_2NH\cdots OH_2$. The results from the ab initio MO-MP2-TZP approach were taken as reference. The validity of this approach for the weak intermolecular interaction was underpinned by its good reproduction of the F \cdots F distance in the (HF)₂ cluster (here calculated: 272 pm; experimental value from the molecular beam spectrum: 272±3 pm [31]).

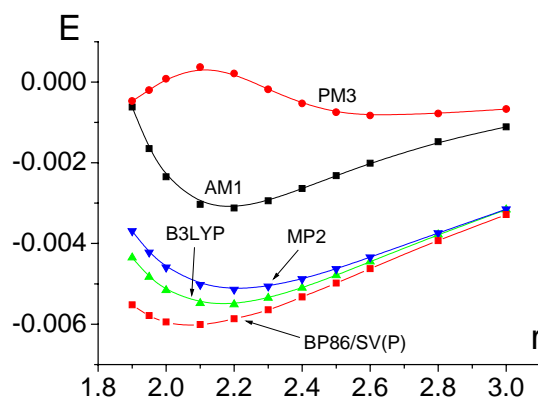


Fig. 3. Energy curves for the $NH_3\cdots OH_2$ hydrogen bonded complex. E = interaction energy in a.u. with respect to separated $NH_3 + H_2O$; r = $NH\cdots O$ distance in Å

Two semi-empirical and two density functional methods, namely AM1, PM3 [13], BP86/SV(P)/RI and B3LYP/6-311g(d,p), with MP2 are used to calculate the energy curves of $H_2NH\cdots OH_2$. The results are shown in Fig. 3. The minima are 2.17 Å for AM1, 2.20 Å for

MP2, 2.18 Å for B3LYP, and 2.11 Å for BP86. Reasonable minimum structures are obtained for B3LYP, BP86 and AM1, reasonable repulsion energies with B3LYP and BP86, and still acceptable repulsion energies (needed for the transition energies of the molecular motion in the zeolite channel) with PM3.

5.3. Geometrical Reasoning

The zeolite channels (Fig. 2) look like a pile of tires. The open diameter of the $\text{Si}_{12}\text{O}_{12}$ waists is 9 Å, the larger diameter between them is $13\frac{1}{2}$ Å, and the periodic distance is 7.5 Å. Molecules of lengths below 9 Å such as biphenyl can move rather freely through the channels, very long molecules such as POPOP (Fig. 1c) can only shift parallel through the channels. Medium sized molecules such as Ox or Py (Figs. 1 a,b) can also lie in skew direction at some tilt angles α .

5.3.1. From where comes the $\alpha \leq 40^\circ$ limitation?

Our impression is that the oxonine can lie much more skew in the channel, for two reasons.

-1-) The 40° limit [1] had been deduced from the condition that 290 pm for C-H \cdots O, 270 pm for N-H \cdots O, and 310 pm for N \cdots O are the lowest limits for the corresponding nonbonded distances (Fig. 4). We suspect that the AH \cdots O distance was confused with the (by X-ray diffraction) much more easily measurable A \cdots O separation (for examples, see [32]). Table 1 lists some van der Waals radii, table 2 lists the experimentally observed NH \cdots O and CH \cdots O hydrogen bond distances, and table 3 lists N(H) \cdots O separations. Tables 2 and 3 were taken from older books [32,33], where some newer experimental results are not included. For CH \cdots O distances, the shortest value found so far is 187 pm [34]. For NH \cdots O the very short H \cdots O distance of 155 pm was found recently [35]. So we must conclude that the NH \cdots O distances are in the region of 155 – 240 pm, and the CH \cdots O ones in the region of 187-265 pm, but not many 10 pm larger.

Table 1. Van der Waals radii of H and O in Å

	Pauling [36]	Bondi[37]	Fluck [38]	Zefirov [39]
H	1.2	1.20	1.0	
O	1.4	1.52	1.4	1.29
N	1.5	1.55	1.5	1.50
C	1.7	1.70	1.7	1.71
Si	2.1	2.10	2.1	

Table 2. Experimentally observed (X)H \cdots A(Y) hydrogen bond distance-ranges in Å.

H...A :	(O-)H...O	(N-)H...O(=C)	(N-)H...O	(C-)H...O	(C-)H...N
[32]	1.44-2.10	1.58-2.05	1.60-2.40	2.04-2.65	2.50-2.75
Used by [1]			>2.7	>2.9	
This work			1.9-2.7	>2.15	

Table 3. X(H)...A hydrogen bonded X...A separations in pm from ref. [33]

X(H)...A(Y)	Range	Average	Used as H...A in [1]	Here suggested (s.b.)
N(H)...N	2.88-3.38	3.10		
Ammonia N(H)...O	2.68-3.24	2.88	3.1	
Amine N(H)...O	2.57-3.22	3.04		3Å(linear) - 2 Å (bent)
Amide N(H)...O	2.55-3.04	2.93		
O(H)...N	262-2.93	280		

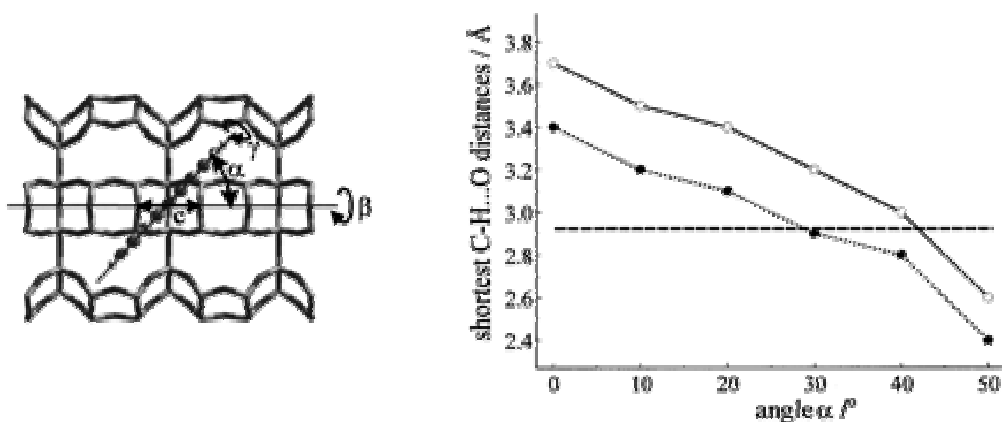


Fig. 4. From [1]: *Left* - Position *c* and orientation angles α, γ of dye molecule in main channel of zeolite *L*. *Right* - Shortest $C_{\text{dye}}\text{-H}\cdots\text{O}_{\text{zeolite}}$ distances of Py^+ (dotted) and Ox^+ (solid) when the molecule is centered in the waist of the zeolite channel, and $\gamma = 0^\circ$. The horizontal line at 2.93 Å corresponds, however, to experimental C-(H)...O separations

-2-) The relative position of two 3-dimensional objects is defined by 6 parameters. However, in the geometrical model of [1] only 4 parameters were varied. It was assumed that the oxonine is centered in the middle of the 12 ring-waist of the zeolite channels (Figs. 2 left and 4 left), but this position was not proven to be the optimal one. At least for small tilt angles α , the

oxonine molecule prefers to sit near the edge of the ring, but not centered in the middle. This means, the position of Fig. 2 (right) is more favorable because in this case oxonine has stronger hydrogen bond interactions with the O-atoms of the zeolite on the inner channel surface.

5.3.2. Reasonable $CH\cdots O$, $NH\cdots O$, $N\cdots O$ and $Si\cdots H$ distances

In order to estimate the relevance of the different shortest $NH\cdots O$ and $CH\cdots O$ distances mentioned above, and since there are no experimental distances available for the current system, we have determined them quantum theoretically. Weak interaction distances vary a lot for different environments. In order to model the individual dye-zeolite weak atom-atom interactions, we construct small model systems for the oxonine (Fig. 5 left) and for the zeolite environment (Fig. 5 right): $C_6H_5NH_2$ replaces the oxonine NCH ($C_6H_3NH_2$)₂, and the small cut $O(Si(OH)_3)_2$ replaces the inner surface of the zeolite channel. The respective calculated energy curves of $NH\cdots O$ and $CH\cdots O$ are shown in Fig. 6. The calculation method was B3LYP/6-311g(d,p).

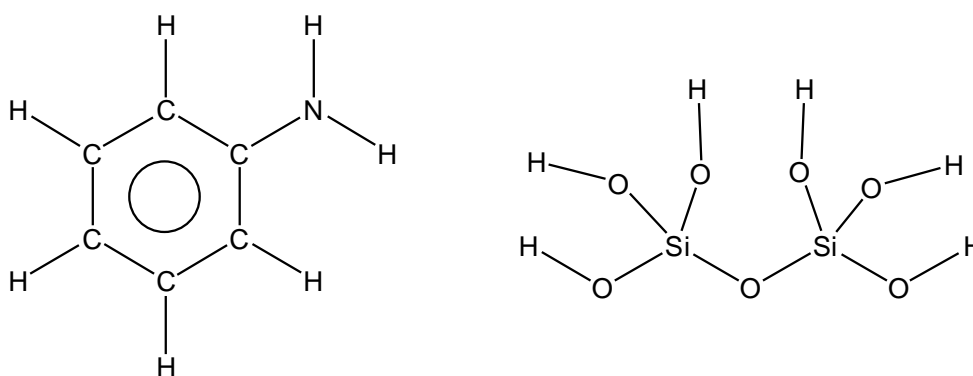


Fig. 5. Model molecules to study the $H\cdots O$, $H\cdots Si$ and $N\cdots O$ interactions simulating the individual oxonine-zeolite interactions

From Fig. 6 we see both $CH\cdots O$ and the $NH\cdots O$ curves are quite flat, meaning that the distances can change quite a bit within the thermal energy range. If we choose only the average thermal energy, i.e. $3/2 kT$ with $T = 333$ K, i.e. 1 kcal/mol, then the accessible distance ranges are already rather large. For $NH\cdots O$ the energy minimum is 2.2 Å, easily reducible thermally to 1.90 Å, and for $CH\cdots O$, respectively, 2.6 and 2.15 Å. Using the same compound model (Fig. 5) with different orientations, we also get the $N\cdots O$ and $H\cdots Si$ distances. The curves are shown in Fig. 7. Again the curves are quite flat, and we get for both cases ranges above 2.8 Å. The attraction holding the compound system together in this case is mainly hydrogen bonding of the neighbor groups.

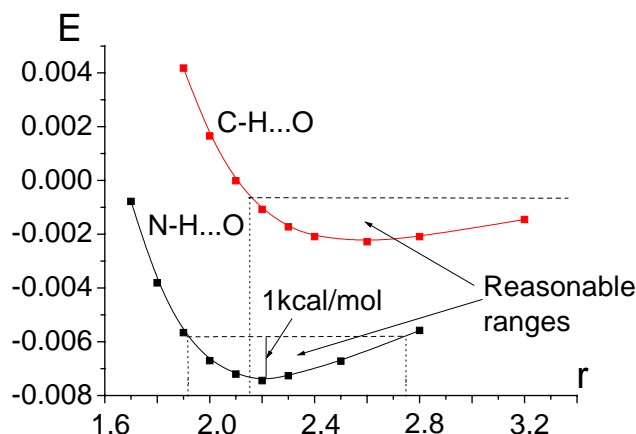


Fig. 6. Calculated (B3LYP/6-311g(d,p)) interaction energy E (in a.u.) of a $C_6H_5NH_2 - O(Si(OH)_3)_2$ compound system versus $O \cdots H$ contact distances r (in Å) for (N-)H \cdots O and (C-)H \cdots O contacts.

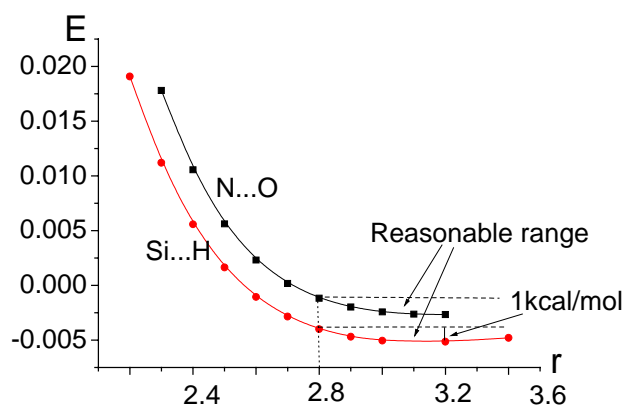


Fig.7. Calculated (B3LYP/6-311g(d,p)) interaction energy E (in a.u.) of a $C_6H_5NH_2 - O(Si(OH)_3)_2$ compound system versus $N \cdots O$ and $Si \cdots H$ contact distances r (in Å)

5.4. Oxonine in zeolite L: structures and energies

5.4.1. Structure model

Our system is the practically infinite periodic zeolite structure containing mobile K^+ and H_2O , and some oxonine cations, separated by small inorganic anions. The latter, together with the K^+ cations, however, may have more or less diffused out into the dye solution.

We cut out a part as the studied object. The cut should include a piece of the channel, somewhat longer than the oxonine molecule so that the molecule can be moved inside. Our cut is

shown in Fig. 8. The channel model is composed of two A levels and four B levels (A_2B_4). The length of the A_2B_4 unit is about $17 \frac{1}{2}$ Å, which is long enough compared to oxonine with a length of about $13 \frac{1}{2}$ Å. The rules to construct this model were: a) every Si atom keeps its four O neighbor atoms, b) replace the Si atoms connected to the outer O atoms by H, which are moved on the O-Si bond line to an O-H distance of 0.95 Å. The model has 324 atoms, and the formula is $Si_{72}O_{180}H_{72}$.

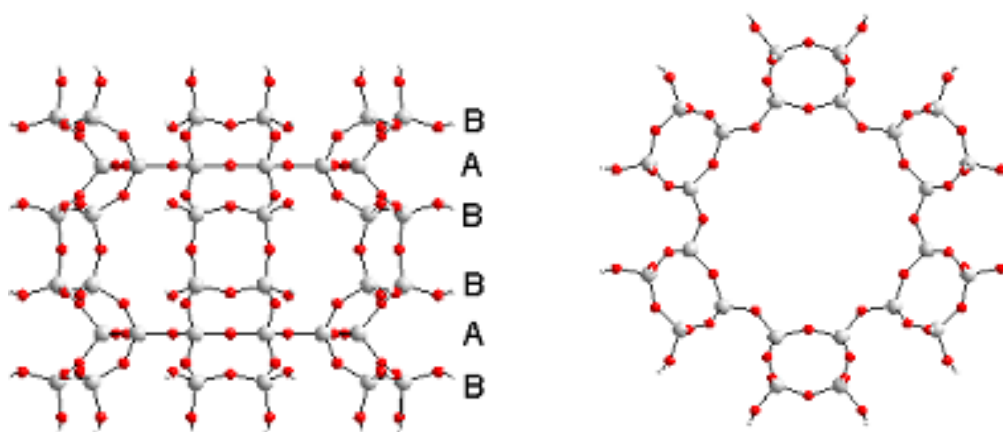


Fig. 8. Two views of the zeolite model ($Si_{72}O_{180}$) that was used to optimize the oxonine position in zeolite. A and B indicate the projections of different x-y planes

The structure of the oxonine molecule was shown in Fig. 1. Figs. 2 and 4 show how the molecule sits in the zeolite channel. There are six parameters concerning to the relative position of the molecule in the zeolite: the 3 position coordinates of the molecule (e.g. atom O as reference), and the 3 Euler angles. All these six parameters were optimized. The most important parameter is α , the angle between the long molecular axis and the channel axis. This parameter had been determined experimentally by fluorescence microscopy.

5.4.2. Thermodynamics: Which molecular angles are stable?

Using the AM1 method, we have optimized the relative position of oxonine in zeolite. The internal structures of zeolite and oxonine were fixed. From various starting points we got three different minima (table 4): $\alpha = 25.1^\circ$, 56.3° , and 90.0° . $\alpha = 90.0^\circ$ is weakly preferred. The minima correspond to Figs. 10 b,d,g. The energy differences are quite small, compared to calculational reliability and to thermal energy. Among the three minima, only for the last one the oxonine sits in the center of the zeolite channel. The results are listed in table 4.

As mentioned above, the AM1 optimized structures are reasonable, but the energies should be verified by more accurate methods. We have tried B3LYP with GAUSSIAN and BP86 with TURBOMOLE (using the RI integral approximation). Single point calculations were carried out at the three AM1 optimized minima. Checking the structure of the three minima, we found that already a smaller A_2B_2 zeolite cut is enough. All atom pairs with distances below 350 pm

are retained. Therefore an A_2B_2 model was used. The results are listed in table 4, too. The third minimum is now definitely the lowest, and the first minimum is weakly higher than the second one. Table 4 also displays the shortest $CH\cdots O$, $NH\cdots O$, $N\cdots O$ and $Si\cdots H$ distances. The calculated ones are all in the expected range. The particular stability of the $\alpha = 90^\circ$ structure is possibly caused by the absence of any $N\cdots O$ and $Si\cdots H$ repulsive near-contacts.

Table 4. AM1 results for structure minimization of oxonine in zeolite and DFT energies (energies in kcal/mol, distances in Å)

Minimum no.	AM1 α ($^\circ$)	AM1 energy	AM1 shortest $NH\cdots O$	AM1 shortest $CH\cdots O$	AM1 shortest $N\cdots O$	AM1 shortest $Si\cdots H$	B3LYP energy	P86 energy
1	25.0	-1.8	2.28	2.74	2.98	2.90	Failed	+0.8
2	56.2	- 0 -	2.01	2.22	2.99	2.72	- 0 -	- 0 -
3	89.6	-3.5	2.23	2.89	>3.00	>3.00	-14.3	-13.2
expected			>1.9	>2.15	>2.8	>2.8		

5.4.3. Kinetics: Why is no oxonine found at 90°

In ref. [1] there were no experimental indications of orientations as small as $\alpha = 25^\circ$ or as large as $\alpha = 90^\circ$. When the oxonine enters the zeolite, the molecular axis must be parallel to the zeolite channel, $\alpha = 0^\circ$. We know, there are 3 energetic minima. Now the question is: can the oxonine molecule find its way to these minima, overriding the energy barriers. We must study the transition paths. Therefore we calculated the path with the AM1 approach, for $\alpha = 0^\circ$ to 30° at steps of 5° , for $\alpha = 30^\circ$ to 60° at steps of 3° , and for $\alpha = 60^\circ$ to 90° at steps of 2.5° to 1.25° (Fig. 9). This yielded smooth variations of all variables. The other 5 parameters of oxonine were optimized at each step. We now discuss the energies and the structures.

5.4.3.1 Energies

The energy curve of the ‘oxonine rotation’ is shown in Fig. 9. The energy decreases a very little from $\alpha = 0^\circ$ to the first minimum at $\alpha = 25^\circ$, then it goes up and reaches the first barrier at $\alpha = 39^\circ$. This barrier is only about 6.4 kcal/mol high. According to the transition state theory [40] the key equation for calculating rates is:

$$k(T) = k_B T/h \cdot c_0 \cdot \exp(-\Delta G^\circ/RT) \quad (5.1)$$

At room temperature, $k_B T/h$ is $6.25 \cdot 10^{12} \text{ s}^{-1}$. Taking for the concentration for simplicity $c_0 = 1 \text{ mol/l}$, the reaction rate for a 6.4 kcal/mol barrier is of the order of $10^8 \text{ mol l}^{-1} \text{ s}^{-1}$. So, such a barrier is quite easy to be overcome, and the oxonine molecule can nearly freely rotate from minimum 1 to minimum 2 (56°). A second barrier exist around 70° , the barrier height is 26.7

kcal/mol. According to eq. (1), the reaction rate is of the order of $10^{-7} \text{ mol l}^{-1} \text{ s}^{-1}$. So this barrier is quite difficult to be overridden.

Since this barrier blocks the motion of the oxonine into the inner cavity, Fig. 9, we want to substantiate the barrier height. Single point calculations were carried out with the B3LYP and BP86 approaches for the AM1 transition state structure at $\alpha = 71.25^\circ$. The results were listed in table 5. The AM1 result is corroborated by the B3LYP and BP86 ones. So we are sure that oxonine cannot arrive at position $\alpha = 90^\circ$. Therefore we conclude that oxonine can move rather freely between 0° to 65° , the most preferred position being around 56° .

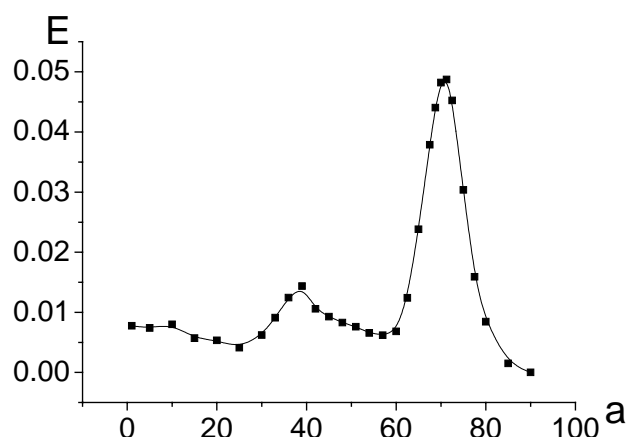


Fig. 9. Rotating oxonine in zeolite: energy E (in a.u.) of the whole system versus tilt angle α (in degree) from $\alpha = 0^\circ$ (parallel) to 90° (vertical to the channel axis)

Table 5. The energy barrier from minimum 2 to minimum 3 ($E_{\text{tot},71.25^\circ} - E_{\text{tot},56.2^\circ}$)

Method	AM1	B3LYP	BP86
Barrier (kcal/mol)	26.7	27.8	18.2

5.4.3.2. Geometrical aspects

In addition to approximate quantum chemical calculations, we present some simple geometrical reasoning along similar lines as in ref. [1]. The main interactions between oxonine and zeolite are $\text{NH}\cdots\text{OSi}$, $\text{CH}\cdots\text{OSi}$, $\text{CN}\cdots\text{OSi}$ and $\text{OSi}\cdots\text{HC}$. Table 6 lists the respective distances along the rotational path, shown in Fig. 10.

Table 6 shows that all distances (except may be the shortest $\text{Si}\cdots\text{H}$ ones) lie in reasonable ranges, compare the last line of table 4. Some $\text{Si}\cdots\text{H}$ distances are as short as 255 pm. Fig. 7 shows that this creates only a repulsion of a few kcal/mol that is easily counterbalanced by the other attractions. There is no geometric hindrance of free motion from 0° to 60° . The rotational barrier seems to come mainly from $\text{Si}\cdots\text{H}$ compression. Around 70° , the shortest dis-

tances are 180 pm for NH \cdots OSi, 210 pm for CH \cdots OSi, 253 pm for CN \cdots OSi and 224 pm for OSi \cdots HC. The first two interactions causing the main attraction are compressed only a little at the rotational transition state, while the nonattractive interactions are compressed by about 40 and 50 pm. From Fig. 6 and 7 we estimate energy barrier contributions for NH \cdots OSi of 2 kcal/mol, for CH \cdots OSi of 1 kcal/mol, for CN \cdots OSi of 6 kcal/mol and for OSi \cdots HC of 15 kcal/mol, summing up to over 20 kcal/mol, in agreement with the AM1 and B3LYP results above. The oxonine is too large to rotate into the $\alpha = 90^\circ$ position.

Table 6. Shortest NH \cdots OSi, CH \cdots OSi, CN \cdots OSi and OSi \cdots HC distances (in pm, numerical stability better than 1 pm) of oxonine-zeolite at axes-angles $\alpha = 0^\circ$ to 90°

α ($^\circ$)	Shortest NH \cdots OSi	Shortest CH \cdots OSi	Shortest CN \cdots OSi	Shortest OSi \cdots HC
0	244	261	>300	>300
5	218	255	>300	>300
10	219	274	>300	284
15	222	276	>300	281
20	225	287	>300	290
25	228	276	299	290
30	230	252	290	288
33	219	245	289	297
36	221	241	296	299
39	238	253	294	269
42	225	230	297	258
45	221	227	289	256
48	211	221	286	255
51	203	222	289	258
54	202	228	297	276
57	200	215	293	263
60	202	214	297	259
62.5	200	227	276	253
65	190	223	265	242
67.5	183	215	257	233
68.75	182	210	255	230
70	180	212	253	227
71.25	180	221	253	225
72.5	182	228	255	224
75	193	243	266	229
77.5	207	264	276	243
80	221	274	292	263
90	223	289	>300	>300

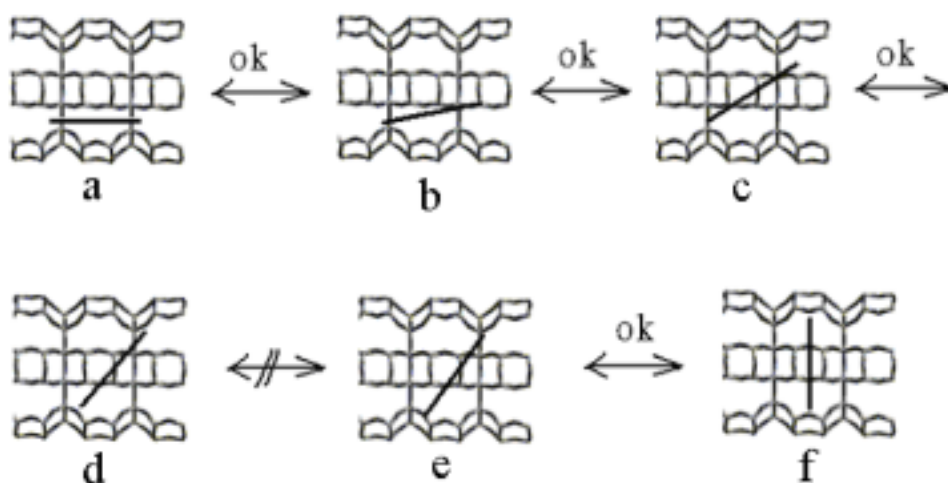


Fig. 10. Possible motions of oxonine in zeolite. \leftrightarrow means activation barrier below 8 kcal/mol, and \leftrightarrow with // means activation barrier bigger than 20 kcal/mol

5.4.4. From the calculated model to the real system

The current calculated model has some differences with the real zeolite oxonine system.

-1-) We have **cut the zeolite** and have saturated the outer parts by H atoms. Since the size of the model was taken larger than the oxonine molecule, this simplification is not expected to cause significant errors. We believe the stray fields from the edges to have minor effects on the molecule.

-2-) The real zeolite has some of the Si replaced by Al, that is zeolite is not silicon dioxide but a potassium aluminosilicate. The charge-counter-balancing **K⁺ ions** are in the zeolite channels. The K⁺ can either be replaced by oxonine⁺, or the oxonine⁺ ions can also take their counter-anions into the channels. However, since the dye molecule solution does not contain K⁺, the K⁺ should osmotically diffuse from the zeolite into the surrounding solution. Anyhow, any additional cations, anions and some **solvent molecules** (like water) were not at all included in our model. We hope that this simplification will cause only minor errors because these small particles can easily find places in the zeolite channels without perturbing the oxonine.

-3-) As mentioned, some of the silicon atoms are replaced in the zeolite at random by **aluminum atoms**. Because of the indeterminacy of the Al positions, it is not easy to create a respective unique model. It is known [9] that these aluminum atoms hardly affect the size of the channels, except creating some electric fields. Therefore including some aluminum atoms should not change the geometric situation. However, it may be that the defect anionic sites created by the Al³⁺ versus Si⁴⁺ atomic cores fix the oxonine cation positions and stabilize them.

We have designed a model to study the effect of aluminum substitution. We replace one of the four Si near to the oxonine by one Al and again optimize the structure at the AM1 level. We

do this for each of the four positions. The calculated results from this model show an α increase by 3° . It may be that oxonine prefers sites where it is in contact with more than one Al.

In summary, based on our theoretical results, $\alpha \approx 60^\circ$ is the best angle for the oxonine molecule in a real zeolite channel.

5.5. The $\pi\pi^*$ transition dipole moment of oxonine: The influence of the zeolite channel environment

5.5.1. Oxonine, a first model

The $\pi\pi^*$ transition dipole moment of oxonine is along its long axis. If there are some other molecules or ions coming close to the oxonine, its transition dipole moment can be changed. At first we test our models, the methods and the basis sets for the theoretical estimation of the experimentally detected fluorescence transition. In our test systems we position H_2O molecules, potassium cations or positive and negative point charges around the oxonine. Concerning H_2O , two of them are placed above and two below the oxonine plane, to form hydrogen bond with the amino hydrogens at a distance of 2 Å. The results are listed in table 7.

Table 7. Excitation energies ΔE (in eV), $\pi\pi^*$ transition moment squares μ^2 in dipole-length (len.) and dipole-velocity (vel.) forms (in a.u.), and angle of transition moment with respect to molecular long axis of oxonine, and of oxonine + $4\text{H}_2\text{O}$. The experimental transition energy 2.2 eV ($\lambda=560$ nm)

DF method	Basis (ECP/RI)	Ox^+ ΔE	μ^2 vel.	μ^2 len.	$\text{Ox}^++4\text{H}_2\text{O}$ ΔE	μ^2 vel.	μ^2 len.	angle len.	angle vel.
B3LYP	sdf (ECP)	2.88	6.2	10.0	2.75	7.3	11.7	2.3°	3.5°
B3LYP	SVP	2.84	8.8	10.0	2.73	10.2	11.5	2.1°	2.2°
B3LYP	TZVP	2.80	9.2	10.3	2.70	10.7	11.9	2.0°	2.1°
B3LYP	aug-cc-pVDZ	2.78	10.2	10.4	2.68	11.8	12.0	2.3°	2.3°
BP86	SVP (RI)	2.68	7.3	8.3	2.58	8.6	9.8	2.4°	2.6°
BP86	TZVP (RI)	2.65	7.8	8.7	2.55	9.1	10.1	2.2°	2.3°
BP86	TZVPP (RI)	2.64	8.5	8.6	2.54	10.0	10.1	2.5°	2.5°

Using time dependent DFT, the transition dipole moment does not exhibit a strong basis set dependency. A single polarized split valence basis already gives similar results as the large TZVPP [24, 25] or aug-cc-PVDZ [41] basis sets, in particular in the length representation (which will be used in the subsequent discussions). The length representation is often more stable for valence excitations than the velocity representation. Anyhow, both representations

give similar results already for medium basis sets. So the calculations seem reliable. The calculated excitation energy is also only slightly method-dependent and basis sets dependent. In general B3LYP gives a little larger excitation energy than BP86, but the difference of about 0.15 eV is not serious. The experimental value for the excitation energy is a few 0.1 eV lower (≈ 2.2 eV).

In summary, the SVP basis set with TD-DF is already good enough to get reasonable results for the transition dipole moment. Water molecules can rotate the transition moment by a few degrees. Preliminary test calculations at the CIS by Schwarz-Niu [42] gave less satisfactory results for energies and dipole-length-velocity agreement. The influence of point charges and K^+ ions on the transition dipole direction was found very small, but the orbital interaction with Si-O clusters was found larger.

5.5.2. Second model

Therefore we constructed a second model. The idea was to include all atoms that may have orbital interaction with the oxonine, and then to perform a TD-DF calculation with a reasonably large basis set. We take the oxonine unit and all zeolite atoms in contact at minimum position 2 (i.e. O within 280 pm of H(C), O within 280 pm of H(N) and of N, and Si within 280 pm of H(C,N)) and then all O atoms connected to the selected Si atoms. The other atoms of zeolite were discarded; the oxygen atoms were saturated by H atoms. The transition dipole moment was then calculated with TD BP86/TZVP/RI method. The excitation energy is 2.41 eV (514 nm), and the transition dipole moment deviates from the molecular long axis by 4.9 degree toward the zeolite atoms. This is a little more than for the first less realistic model and a little less than found before in ref. [42].

5.5.3. Third model

Now we take the oxonine in the large zeolite cut, as in the structure optimizations. Then a smaller basis must be taken for the TD-DF calculations.

At first we choose the B3LYP-DF. The atomic cores are approximated by ECPs. The unpolarized split valence so-called ecp-n-sdf basis sets ($n=2$ for C, N, O, $n=10$ for Si) were used. Both pure silicon zeolite and aluminum replaced zeolite models were considered. Finally the larger SVP basis sets were used. The results are listed in table 8.

Table 8. Transition energies ΔE (in eV), direction angle α of molecule in zeolite channel, deviation δ of transition moment from molecular axis, and direction θ of transition moment with respect to zeolite channel, from TD-DF calculations (B3LYP/ECP, or BP86/RI)

Zeolite model	DF(ECP)	Basis (RI)	ΔE	α	δ	θ
Pure Si	B3LYP(ECP)	sdf	2.76	56.2°	3.6°	59.8°
2 Al included	B3LYP(ECP)	sdf	2.56	59.1°	3.7°	62.8°
2 Al included	BP86	SVP (RI)	2.42	59.1°	4.2°	63.3°

The model that is closest to the experimental system in [1] is ‘aluminum included zeolite’, and it is calculated with the B3LYP/sdf and the BP86/SVP approaches. We obtain an angle θ between μ and the zeolite axis of 63° . The reliability of this value can be solidified as follows: a) The calculated excitation energy of 2.4 eV is only a little too large, the experimental value is around 2.2 eV, this is quite acceptable. b) The length and velocity representations of the transition dipole moment are quite consistent, differing in length by less than 10% and in direction by a few degrees only. c) The current calculation and the large basis sets calculation in §5.1 give consistent results.

In summary, the zeolite environment makes the transition dipole moment rotate off the molecular axis, thereby increasing the angle with the channel axis by about 4 degree. In the real zeolite there are more than 1 Al, and this may rotate the molecule also a little more off the channel axis. So an angle $\theta \sim 65^\circ$ seems most probable.

5.5.4. Explanation of the experimental findings

The calculated angle for the transition dipole moment is 63.3° , the reliability should be within a few degrees, while the experimentally derived one is $72 \pm 4 (=2\sigma)^\circ$. Thus there remains only a small unexplained discrepancy. The several degrees difference may come from the error effects mentioned at the beginning of §5.4.4.. In particular oxonine may sit at positions where it comes in contact with more than one aluminum atom, so that the molecular axis is rotated more.

5.6. Summary

The geometric reasoning in [1] arrived at an oxonine molecule - zeolite channel angle of not more than 40° . We here propose an angle of over 60° .

The position of oxonine in pure silicon zeolite was optimized with AM1 methods, and the energies were calculated at the DF level. We find three minima near 25° , 56° and 90° . The latter is the most stable one, however it cannot be reached because the barrier of rotation for the somewhat long oxonine molecule in the channel is too large, of the order of 20 to 30 kcal/mol. Therefore the second stable structure at $\alpha = 56^\circ$ is preferred. The aluminum replacement increases this angle, by a single Al near oxonine by 3° . The transition dipole moment at the best molecular position was studied by TD-DF methods. The direction of the transition moment is rotated away from the channel axis towards the channel surface by orbital interactions between the molecule and the zeolite. This change is of the order of 5° or possibly even a little larger. So there remains nearly no discrepancy with the experimental value of $72 \pm 4^\circ$.

The original discrepancy found in [1] is mainly due to choosing A(H)···B distances for (A)H···B distances in a simple geometric model. In addition, a quantum chemical model accounts for the attractive weak interactions between the molecule and the zeolite channel inner surface, for the influence on the oxonine cation by the anionic centers in the zeolite structure due to Al-for-Si replacements, and for the perturbation of the transition moment by orbital interactions within the guest-host system. The current work confirms that fluorescence microscopy is a useful method to study the orientation of molecules in hosts. However, perturbations

of transition moments by several degrees through quantum mechanical orbital interactions, though not through electrostatic Stark effects may occur even in cases where the electronic transition is still localized on the guest molecule. For hydrogen bonded and weakly electrostatically attracted molecules, the direction of the molecular transition moment is only slightly affected by a few degrees. Therefore, for such systems, the experimental determination of the direction of the transition dipole moment can indeed be taken as a rough estimate of the direction of the molecule. This result should be also valid for other weak interacting systems. However, it may not be valid any longer for those host-guest systems where the studied electronic transition comes from the contact atoms.

The present quantum chemical calculations also demonstrate that the fluorescence of absorbed molecules can be calculated theoretically rather easily with a validity that is useful for the interpretation of experimental results.

References

- [1] S.Megelski, A.Lieb, M.Pauchard, A.Drechsler, S.Glaus, C.Debus, A.J.Meixener, G.Calzaferri, *J. Chem. Phys.*, **2001**, *105*, 25.
- [2] F.Schüth, *J. Phys. Chem.*, **1992**, *96*, 7493.
- [3] M.Pauchard, A.Devaux, G.Calzaferri, *Chem. Eur. J.*, **2000**, *6*, 3456.
- [4] G.Calzaferri, *Chimia*, **1998**, *52*, 525.
- [5] H.Maas, G.Calzaferri, *Angew. Chem. Int. Ed.*, **2002**, *41*, 2284.
- [6] N.Gfeller, S.Megelski, G.Calzaferri, *J. Phys. Chem. B*, **1999**, *103*, 1250.
- [7] G.Binder, L.Scandella, J.Kritzenberger, J.Gobrecht, *J. Phys. Chem. B*, **1997**, *101*, 483.
- [8] N.Gfeller, S.Megelski, G.Calzaferri, *J. Phys. Chem. B*, **1998**, *102*, 2433.
- [9] G.Calzaferri, D.Brühwiler, S.Megelski, M.Pfenniger, M.Pauchard, B.Hennessy, H.Maas, A.Devaux, U.Graf, *Solid State Sci.*, **2000**, *2*, 241.
- [10] G.D.Stucky, J.E.MacDougall, *Science*, **1990**, *247*, 669.
- [11] J.M.Thomas, *Angew. Chem. Int. Ed.*, **1988**, *27*, 1673.
- [12] M.J.S.Dewar, E.G.Zoebisch, E.F.Healy, *J. Am. Chem. Soc.*, **1985**, *107*, 3902.
- [13] M.J.S.Dewar, *J. Comp. Chem.*, **1989**, *10*, 209; **1989**, *10*, 221.
- [14] A.D.Becke, *Phys. Rev. A*, **1988**, *38*, 3098.
- [15] J.P.Perdew, *Phys. Rev. B*, **1986**, *33*, 8822.
- [16] A.D.Becke, *J. Chem. Phys.*, **1993**, *98*, 5648.
- [17] C.Møller and M.S.Plesset, *Phys. Rev.*, **1934**, *46*, 618.
- [18] R.Bauernschmitt, M.Haeser, O.Treutler, R.Ahlrichs, *Chem. Phys. Lett.*, **1997**, *264*, 573.
- [19] R.Bauernschmitt, R.Ahlrichs, *Chem. Phys. Lett.*, **1996**, *256*, 454.
- [20] R.Bauernschmitt, R.Ahlrichs, *J. Chem. Phys.*, **1996**, *104*, 9047.
- [21] M.J.Frisch et al., *Gaussian 98, Revision A.9*, Gaussian, Inc., Pittsburgh PA, **1998**.
- [22] R.Ahlrichs et al., *TURBOMOLE 5.5*, University of Karlsruhe, Germany, **2002**.
- [23] W.Stevens, H.Basch, J.Krauss, *J. Chem. Phys.*, **1984**, *81*, 6026.
- [24] A.Schaefer, H.Horn, R.Ahlrichs, *J. Chem. Phys.*, **1992**, *97*, 2571.
- [25] A.Schaefer, C.Huber, R.Ahlrichs, *J. Chem. Phys.*, **1994**, *100*, 5829.
- [26] A.D.McLean, G.S.Chandler, *J. Chem. Phys.*, **1980**, *72*, 5639.
- [27] R.Krishnan, J.S.Binkley, R.Seeger, J.A.Pople, *J. Chem. Phys.*, **1980**, *72*, 650.
- [28] K.Eichkorn, O.Treutler, H.Oehm, H.Haeser, R.Ahlrichs, *Chem. Phys. Lett.*, **1995**, *242*, 652.
- [29] O.Treutler, R.Ahlrichs, *J. Chem. Phys.*, **1995**, *102*, 346.
- [30] K.Eichkorn, F.Weigend, O.Treutler, R.Ahlrichs, *Theor. Chem. Acc.*, **1997**, *97*, 119.
- [31] B.J.Howard, T. R. Dyke, W. Klemperer, *J. Chem. Phys.*, **1984**, *81*, 5417.
- [32] G.A.Jeffrey, W.Saenger, *Hydrogen Bonding in Biological Structures*, Springer, Berlin, **1991**.
- [33] G.H.Stout, L.H.Jensen, *X-ray structure determination: A practical guide*, McMillan, London, **1968**.
- [34] J.A.Cowan, J.A.C.Clyburne, M.G.Davidson, R.Luke, W.Harris, J.A.K.Howard, P.Küpper, M.A.Leech, S.P.Richards, *Angew. Chem. Int. Ed.*, **2002**, *14*, 1490.
- [35] N.Lebrun, F.Mahe, J.Lamiot, M.Foulon, J.C.Petit, D.Prevoist, *Acta Cryst. B*, **2001**, *57*, 27.
- [36] L.Pauling, *The Nature of the Chemical Bond*, Cornell University Press, Ithaca NY, **1939**.
- [37] A.Bondi, *J. Phys. Chem.*, **1964**, *68*, 441.
- [38] Fluck & Heumann, *Periodensystem der Elemente*, **1999**, Wiley-VCH, Weinheim.

- [39] Y.V.Zefirov, P.M.Zorky, *Zh. Strukt. Khim.*, **1974**, *15*, 118; **1976**, *17*, 745; **1980**, *21*, 150; **1986**, *27*, 74.
- [40] P.W.Atkins, *Physical Chemistry*, 2th Ed., Oxford University Press, 1982.
- [41] D.E.Woon, T.H.Dunning, *J. Chem. Phys.*, **1993**, *98*, 1358.
- [42] J.Schwarz-Niu, *Internal Report*, **2002**, Theoretische Chemie der Universität Siegen.

6. Brief Summary

Ab-initio MP2&CI and DF calculations were successfully used to study some chemical topics that involve inter- and intra-molecular so-called weak interactions.

i) Concerning the organic-chemistry topic of the rotational barrier of ethane, we support the original and intuitive viewpoint (which has very recently also been corroborated by the groups of Baerends and of Mo): the conformation of ethane is mainly determined by steric repulsions between the C-H bonds, in contrast to 'highlighted' speculations about hyperconjugation by Goodman, Weinhold, Schreiner et al..

ii) Concerning the general-chemistry topic of length expansion of covalent single bonds between two atoms both with lone pairs, we have demonstrated that the bond expansion is caused by two factors that show similar tendencies: a) the inter-atomic LP – LP repulsion mentioned in the textbooks in a qualitative fashion has been substantiated here by numerical data, b) in addition we have found a second contribution, namely the inter-atomic bond weakening between the two atoms who's hybridizations are triggered by the lone pairs to result in increased p-AO population in the bond due to absorption of s-population by the LPs.

iii) Concerning the inorganic-chemistry topic of so-called reduced nonbonded distances, we have found that most reduced distances in the literature are simply caused by the contraction of partially positively charged atoms as compared to neutral or negatively charged ones. If the ubiquitous charge dependence of effective atomic radii is accounted for, only a few really reduced distances survive. They are caused by specific orbital interactions of heavy nonmetal atoms, by specific charge attractions or by clamping bridges.

iv) Concerning the physico-chemical topic of the orientation of dye molecules in zeolite channels we have successfully explained the results of single molecule fluorescence microscopy. Geometric and quantum chemical interaction effects determine the possible positions and orientations of the guest molecules. Charge effects of the Si-Al replacement in the alumo-silicates also play a role. Orbital interactions between the molecule and the zeolite channel surface have some influence on the direction of the electronic transition dipole moment, though not so much intermolecular stark effects. If the guest-host interactions are of the 'weak interaction' type, fluorescence techniques are indeed a reasonable approach to determine the orientation of molecules, since the transition moment is still only weakly perturbed.